2023-03-24

Molecular dynamic simulations of bulk nanobubbles: Investigation of factors important to their stability

Pathirannehelage, Nihari Sathsarani Pathirannehe

UNIVERSITY OF CALGARY

Molecular dynamic simulations of bulk nanobubbles:

Investigation of factors important to their stability

by

Nihari Sathsarani Pathirannehe Pathirannehelage

A THESIS
SUBMITTED TO THE FACULTY OF GRADUATE STUDIES
IN PARTIAL FULFILMENT OF THE REQUIREMENTS FOR THE
DEGREE OF MASTER OF SCIENCE

GRADUATE PROGRAM IN CHEMISTRY

CALGARY, ALBERTA
MARCH, 2023

ABSTRACT

Nanobubbles are gas-filled bubbles in liquids with a diameter in the 100 nm range. Due to their small size and their long-term stability (up to months), there are various applications available in numerous fields, including medicine, agriculture, water remediation, washing, and mining. Although there are numerous applications and much research has been performed, there is a lack of insight into the stability of bulk nanobubbles. Since bubble pressure is an important parameter for bubble stability, in this project we have used molecular dynamics simulations to investigate nanobubbles in water and factors affecting the pressure. For all simulations, the TIP4P/2005 water model was used. A suitable method to calculate the short-range interactions in nanobubble simulations was explored and the particle mesh Ewald summation method was shown to be superior to the cut-off method. The pressure in systems with different sized nanobubbles was measured to examine whether there may be other contributions in addition to the Laplace pressure. The radii and positions of the bubbles were calculated based on the densities of slices through the systems. The results confirmed that pressure is impacted by factors other than the Laplace pressure, where long-range dipole-dipole interactions are found to play an important role. A manifestation of this was the observation that the distance between adjacent bubbles can effect the pressure**.**

Key words: bulk nanobubbles, nanobubble stability, MD simulations, short-range interaction calculations, bubble separation, pressure contributions.

PREFACE

This thesis is an original work by the author. No part of this thesis has been previously published.

ACKNOWLEDGEMENTS

My most profound appreciation goes to Professor Peter Kusalik, my M.Sc. advisors for his time, effort, and understanding in helping me succeed in my studies. His vast wisdom and wealth of experience have inspired me throughout my studies. In addition, I'd like to thank Professor Dennis Salahub and Professor Susana Kimura - Hara for their assistance throughout my research. I'd like to express my gratitude to everyone in Professor Kusalik's research group and the Center for Molecular Simulation (CMS) group for all the support and beautiful memories we had and shared. Thank you NSERC and Katal Energy Inc. for their generous support in funding the Nanobubble project and Compute Canada for supercomputer resources.

I owe my deepest gratitude to Professor Sudath Kalingamudali, Dr. Nadeesha Mathota Arachchige and my undergraduate research advisor Professor Shashikala Rajapakse from University of Kelaniya, Sri Lanka for believing in me since I was an undergraduate student. Thank you so much to all my friends, relatives who alleviated the pain of being far from home, and Sri Lankan community in Calgary for their generosity and encouragement, my time spent studying and living in Canada has been truly rewarding.

I cannot find words to thank my mother, farther, sister, brother and my niece Lisa for their support and love throughout my life. Special thanks to my husband Dimantha for being the primary driving force of my post-graduate studies. Finally, it would have been impossible to finish my studies without all unwavering support over the past few years.

To my mother and father …

TABLE OF CONTENTS

LIST OF TABLES

LIST OF FIGURES

LIST OF SYMBOLS

Symbol	Meaning / Description
A	Surface area of the bubble
a	Interface thickness of the bubble
a_i	Acceleration of the particle/atom i
BNBs	Bulk nanobubbles
C	Cubic
D	Distance from the bubble center to the selected slice
DLS	Dynamic light scattering
f_{bulk}	Volume fraction of water in the bulk liquid
F_i	Force on a particle/atom i
f_{surface}	Volume fraction of water in the bubble's surface
FTIR/IRS	Fourier transform infrared/IR spectra
g(r)	Radial distribution profiles
L	Simulation cell length
LJ	Lennard-Jones
MD	Molecular dynamics
m_i	Mass of the particle/atom i
MPa	mega Pascal
NBs	Nanobubbles
N_f	Number of final water molecules after the bubble insertion
N_{in}	Number of initial water molecules
nm	nanometer
ns	nanosecond
NTA	Nanoparticle tracking analysis
NPT	Constant (number of molecules), pressure and temperature
NVT	Constant (number of molecules), volume and temperature
PBC	Periodic boundary conditions
$P_{(\mu-\mu)}$	Pressure contribution associated with μ-μ interactions
$P_{(\mu-Q)}$	Pressure contribution associated with μ-Q interactions
P^*_{bulk}	Estimated bulk liquid pressure
P_{bulk}	Pressure arising from the water molecules in the bulk liquid
P_{inside}	Pressure generated by the content (gas and vapor molecules) of the bubble
$P_{Laplace}$	Laplace pressure

PME	Particle mesh Ewald
ps	picosecond
$P_{surface}$	Pressure contribution from water molecules in the bubble's surface
P_{system}	Total system pressure
R	Bubble radius
R_1	Radius of the selected bubble slice
RD	Rhombic dodecahedron
R_{in}	Initial bubble radius
r_i	Position of particle i
S	Distance (separation) between nearest image bubbles in PBC
SNBs	Surface nanobubbles
stdev.	Standard deviation
TM-AFM	Tapping mode atomic force microscopy
TO	Truncated octahedron
U	Potential energy
$U_{(r_{ij})}$	LJ energy associated with atoms i and j at a distance r_{ij}
V_{bubble}	Bubble volume
V_{bulk}	Volume of the bulk liquid
VMD	Visual Molecular Dynamics
$V_{surface}$	Volume of the surface of the bubble
V_{total}	Total system volume
V_{water}	Total water volume
v_i	Velocity of the particle/atom i,
γ	Surface tension
δP	Pressure difference between the system and bulk pressures
ε	Strength of the short-range interaction
σ	Particle diameter
μ-μ	Dipole-dipole interactions
µm	micrometer
μ-Q	Dipole-quadrupole interactions

Chapter 1 : INTRODUCTION

This chapter begins with an overview of nanobubbles (NBs), including their applications, and the existing experimental and simulation studies. Detection of NBs and factors affecting their stability will also be discussed. The focus will then narrow down to bulk nanobubbles (BNBs), providing background information that will help to contextualize the study objectives. Finally, this chapter will conclude with a summary and an overview of the organization of the subsequent chapters.

1.1 Overview of nanobubbles

NBs are nanoscale gas filled bubbles in solutions with diameters less than 1000 nm.[1–3] Typically, in water, the diameters are less than 200 nm.[4,5] Since they are nanoscale systems, NBs cannot be observed with the naked eye nor with microscopy.[6] Another characteristic of NBs, is their long lifetimes.[1–4] Nirmalkar et al.[4] have confirmed that aqueous NBs can have lifetimes up to several months. Therefore, NBs are considered very stable in solutions.[1–5] Due to their small size, NBs have higher surface area to volume ratios.[1,5] Therefore, NBs are efficient in gas-liquid mass transfer and chemical reactions at the gas-liquid interface leading to a larger number of possible applications.[5,6]

NBs can be found in a range of aqueous solutions from pure water[3] to seawater[7] and including solutions with numerous organic and inorganic impurities.[8] NBs have also been reported in other polar solvents (i.e., alcohols[9]) and non-polar solvents (i.e., diesel[10,11]). Furthermore, NBs have been reported to change the properties, such as density, solubilities, and reaction kinetics, in these different types of solutions.[12]

There are two primary types of NBs, bulk nanobubbles (BNBs) which are freely suspended gas bubbles in solution, and surface nanobubbles (SNBs) which are attached to a solid surface.[1,4,13] Additionally, there is a sub type of SNBs called micro pancakes, which have a pancake shape, and are much smaller than SNBs.[1,4] Figure 1.1. provides an illustration of these three different types of NBs in a solution.

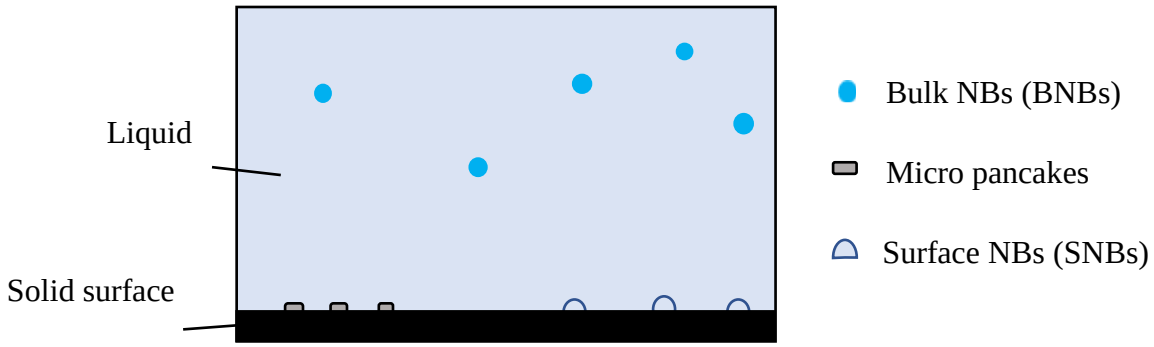

Figure 1.1: Schematic representation of BNBs, SNBs, and micro pancakes.

BNBs were first discovered by Johnson and Cooke in 1981.[7,14] They reported the earliest direct evidence of BNBs with dimensions less than 1 µm. They observed long-lived (> 22 hours) BNBs in sea water using photomicrographs.[7,14] According to their report, breaking waves in seawater might easily generate a lot of tiny bubbles that are persistent for lengthy periods of time due to the surface coatings built from naturally occurring surfactants. They showed that these enclosed bubbles contained gas, because they grew when tension (negative pressure) was provided and shrank when pressure was applied. Some of them could even be destroyed by applying positive pressure.[7] Freshwater can also contain BNBs, possibly created through turbulence caused by waves or waterfalls and stabilized due to significant levels of organic matter.[14] Interestingly, fossilised NBs coated with organic matter were discovered in Lake Kivu in the rift valley of east Africa.[15] Such coated spheres have been suggested to be the ancestors of primordial cells and may therefore be important in the formation of early life.[15]

In 1999, the first experimental evidence for SNBs was reported by Miller et al.[16] These SNBs were identified by using in-situ FTIR/IRS (Fourier Transform Infrared/IR spectra) on a hydrophobic silicon solid surface in n-butane saturated water.[16] As the normalized adsorption intensities at the surface are not constant and increase when the penetration depth is increased, Miller et al.[16] confirmed the presence of SNBs in addition to surface absorbed butane molecules. The authors observed that when the two hydrophobic surfaces (solid surface and gas bubble) approach each other, the water at the solid surface allowed the formation of SNBs.[16] Following this study, the first images of SNBs in water were taken using tapping mode atomic force microscopy (TM-AFM) in 2000.[17] Using TM-AFM, micro-pancakes were detected in a highly oriented pyrolytic graphite-water interface by Zhang et al.[18] in 2006. Unlike the cap shaped SNBs, they appeared as flat (quasi two dimensional) gas layers on the surface.[18]

NBs can be considered as efficient gas carriers in liquid systems.[1,19] Therefore, the amount of gas in a system can be increased by introducing NBs.[14] Because of this, BNBs and SNBs have found uses in numerous applications.[1–5] The following section discusses the applications of NBs.

1.2 Applications of nanobubbles

Applications of BNBs and SNBs will be discussed separately in this section. Focusing first on BNBs, applications include many different industries[3,5,6,12,20] and multiple different aspects of life[1,5]. Starting with water treatments, the removal of persistent organic pollutants (e.g., polychlorinated biphenyls and phenolic halogenated compounds) from water is important, since they can have adverse effects on wildlife, people, and the whole ecosystem.[19] The BNBs have been shown [1,2,13,19,21] to do a great job of removing organic pollutants from water through:

- improving the air flotation process to remove fats, oils, low-density organic suspended solids, and colloids;
- promoting the aeration in water to improve the conventional biodegradation processes consisting of biological activated carbon filters, activated sludge and membrane bioreactors;
- generating free radicals to oxidise and degrade organic compounds that are difficult to biodegrade. Furthermore, use of BNBs in water treatment is attractive because it is a non-reagent and cost-effective method.

As a second example, water-containing BNBs has been shown to improve the nutritional intake by plant roots and the synthesis of plant growth hormones.[13,22] This can lead to a reduction of chemical fertilizer usage, increased agricultural yields and environmental sustainability.[13,22] The healthcare sector has also found application of BNBs in ultrasound-triggered drug delivery.[5,6,23] The small size and long-term stability of BNBs allow drug delivery complexes to take advantage of enhanced permeability and retention effects.[5,23] Furthermore, BNBs are also used in several commercial applications such as cosmetics[6,24], dairy products[24], and paints[24].

In terms of SNBs, suitable gas (H_2, O_2) filled SNBs can be used to enhance reactions at the solid-liquid interface.[25–27] They can also act as a physical barrier to isolate a solid surface from the surrounding liquid.[27] Additionally, they can influence the adsorption of ions, salts, and nanoparticles to a solid surface.[27] SNBs can be applied as soft templates in producing hollow nanostructures (i.e., gold nanoparticles with optical properties), surface cleaning, and flotation.[14,27]

Although SNBs are attached to solid-liquid interfaces, the Brownian motion of BNBs allows them to easily move within a solution.[1–5] Therefore, the applications of BNBs are more diverse

compared to SNBs. To study SNBs, a complete understanding of all three phases solid, liquid and gas is required.[27] However, to study BNBs, only the liquid and gas phases are involved.[28] In this study, we have exclusively focused on BNBs. Nonetheless, there are many interesting findings, studies, and applications of SNBs, as can be found in Theodorakis and Che's review of 2019.[29]

1.3 Studies on bulk nanobubbles

After the identification of NBs in 1981[7], there have been many studies investigating BNB generation[9,30–32], detection[4,33], and stability[34,35]. In 1990, Bunkin and Bunkin[32] provided an explanation for the generation of gas bubbles with acoustic and optical cavitation methods. According to them, both acoustic fields and laser pulses can initiate the bubble nucleation process due to the mechanical and electrical properties of the bubbles.[32] In 2006 Kikuchi et al.[31] generated BNBs using electrolysis and reported that the bubbles produced at the cathode (likely to be hydrogen BNBs) were stable for at least 4 hours and that their sizes ranged from 10 - 600 nm as determined by dynamic light scattering (DLS). The diameter of the BNBs at the anode were initially 30 nm, increasing to 250 nm after 3 days and after 5 days the BNBs were not detected.[31] This work also indicated that a standard oxygen meter could not detect the oxygen in BNBs.[31] Currently, there are several different methods (i.e., acoustic, hydrodynamic, microfluids, periodic pressure changes, nanomembrane)[13] that are used to generate BNBs. Further details can be found in the review by Jadhav et al.[30]

Photomicrography was the first microbubble detection method (1981).[7] Later, atomic force microscopy (2000), and TM-AFM (2003) methods were used to detect SNBs.[14] Currently, nanoparticle tracking analysis (NTA)[33,36,37], DLS[37,38], and resonant mass measurements[33] are

common BNBs detection methods. However, many studies have been recently carried out to improve the detection of NBs and to be able to distinguish them from nanoparticles.[39]

With the detection of very stable BNBs, researchers have also tried to develop explanations for their generation and long-term stability. The Epstein Plesset hypothesis, which calculates the lifetime of a single bubble based on its radius and the solution saturation, was developed in 1950.[40] This hypothesis predicts that if the fluid is saturated with gas relative to the pressure inside the BNBs, and is in an equilibrium with the BNBs, the bubbles have infinite lifetime. However, a small change in equilibrium conditions would dramatically change the lifetime of bubbles.[14] According to the Epstein Plesset theory, the lifetime of bubbles with diameter less than 1000 nm is less than 0.02 seconds.[14] In 1997, Ljunggren and Eriksson[41] calculated how the radius of the bubble impacts the lifetime of BNBs and bubble shrinkage rate, taking gas diffusion into consideration. They reported that bubbles with radius of 10 - 100 nm should have lifetimes between 1 - 100 μs, while millimeter sized bubbles can last for months.[41] Bunkin and Bunkin[32] derived a theoretical model to describe the stability of bubbles in an electrolyte solution and reported a minimum radius and number of gas molecules required for a bubble to be stable. However, the calculated minimum radius and number of gas molecules was not universally applicable due restrictive limitations. Attard[42] analysed the thermodynamic stability of BNBs and reported that the radius of BNBs could not be accurately predicted from thermodynamic parameters. Therefore, Attard[42] was not able to explain the stability of BNBs. In view of the above, there does not seem to be a clear explanation for bubble stability.

When considering explanations for BNB stability, there are several factors that need to be examined. To stabilize a BNB, the pressure inside the bubble should balance the pressure outside

the bubble. Liquid and gas properties such as gas type[5,43], solvent type[5,43], and concentration of ions[5,43] in solutions are factors that may affect the pressure inside the BNBs and hence the stability of the BNBs. System temperature[5,43] and bubble concentration[44] may also be factors affecting BNB stability. Additionally, the BNB generation method might also be a factor.[9]

1.4 Research background

As there are numerous factors that may affect BNB stability, it is important to study each factor's effect to get a detailed understanding of its role in BNB stability. However, in an experiment isolating each factor would be challenging. One approach to simplify the study on BNB stability is to consider the mechanical equilibrium and chemical equilibrium separately.[32] The chemical equilibrium is the equilibrium of the chemical potentials between the gas molecules inside the bubble and outside the bubble (bulk solution).[45] The mechanical equilibrium is determined by the pressure balance inside and outside of the bubble.[44,45] If there is no gas inside the bubble, the chemical equilibrium can be excluded from consideration and one only need consider the mechanical equilibrium.[46] However, it is challenging to make an empty bubble in a solution in experiments, because dissolved gases in the solution will always transfer into an empty cavity. Furthermore, it is also challenging to investigate the mechanical equilibrium since it requires measuring the pressure inside BNBs.[47] To mitigate the aforementioned issues and to understand the mechanical equilibrium, molecular dynamics (MD) simulations can be a useful tool.[44,48,49] MD simulations track the movement of each atom/molecule in time based on the interatomic interactions and represent, in principle, an excellent means of probing and characterizing BNB behavior.[50] Furthermore, selecting water as the liquid for bubble simulations has an advantage in that the properties of common water models (i.e., surface tension)[46,51] required to study the mechanical equilibrium of the BNBs are well known.[52]

As noted above, to satisfy mechanical equilibrium, the pressure inside the bubble should be equal to the pressure outside the bubble.[44] The water molecules at the interface of a BNB do not experience a homogeneous environment like the bulk water molecules. On one side they have liquid water, and on the other side they have gas. As a consequence of the cohesive forces arising from the strong interactions between water molecules, interface water molecules are strongly attracted to adjacent water molecules creating a surface energy, where the surface energy per unit area is the surface tension.[48,53] This surface tension will produce a 'Laplace pressure' on the surface of the bubble, directed towards the center.[48,51] Therefore, for a gas-filled bubble, in addition to the pressure caused by the gas molecules inside the bubble, the Laplace pressure should also be accounted for.[44,46] For an empty bubble, as there are no gas molecules inside the bubble, the pressure inside the bubble should also be equal to the summation of the Laplace pressure and the pressure generated by liquid molecules in the bulk region.[44,46] The Young Laplace equation can be used to describe the pressure difference between the inside and outside of a curved surface and can be applied to calculate the Laplace pressure of a BNB.[54] However, the calculated Laplace pressure contribution to the pressure inside the bubble is very large in BNBs[55] (more than 100 times atmospheric pressure for a BNB with a 10 nm radius). Although several models have tried to explain the phenomena, the surprising long-term stability of BNBs in view of these very large pressures remains an open question. This study focuses the mechanical stability of BNBs.

Figure1.2 summarizes the organization of the research, highlighting the selection of MD simulation and an empty bubble to study the stability of BNBs.

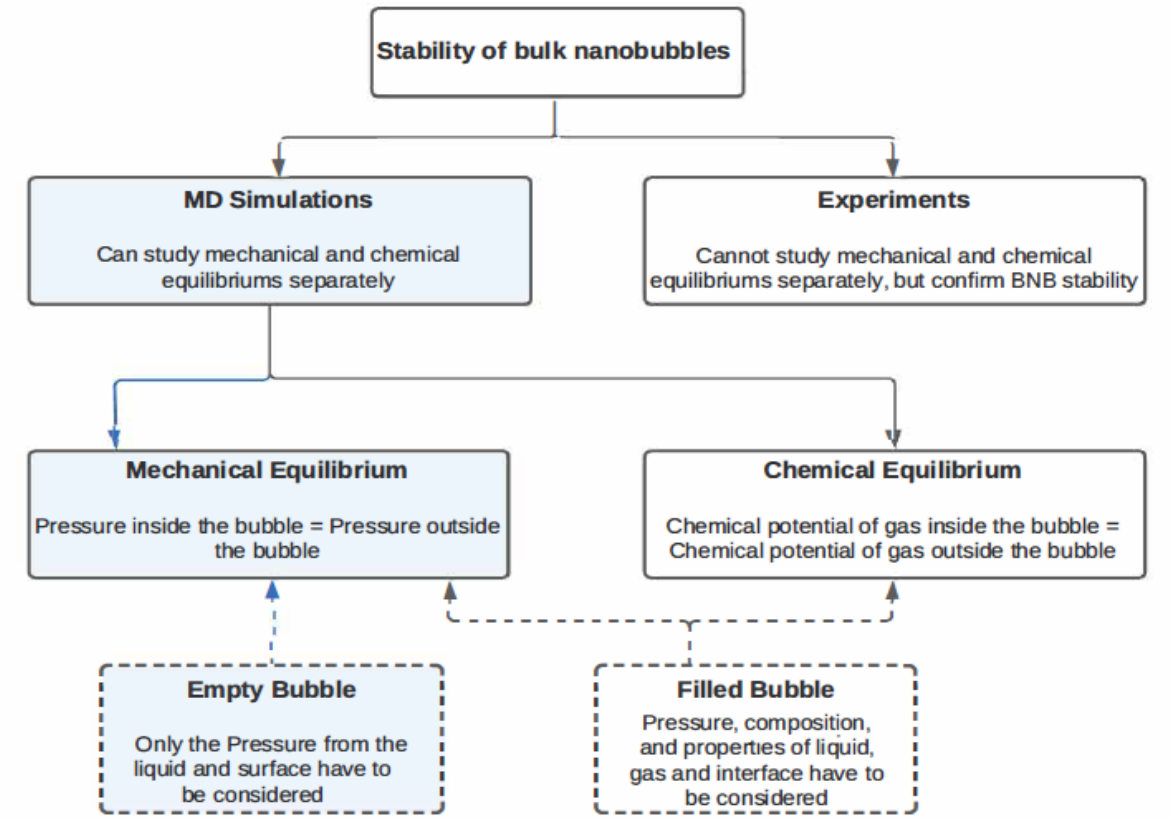

Figure 1.2: Summary of organization of the research. Selection of MD simulation and an empty bubble is highlighted.

1.5 Research objectives

Among different models recorded in the literature, the surface polarization model developed by Ghaani et al.[34] in 2020 offers a self-consistent explanation for BNB stability. Previous work has shown that water molecules will arrange themselves at the surface of BNBs causing the surface to be polarized.[32,56–59] Ghaani et al.[34] have suggested that the interaction between the surface dipoles can generate a counter pressure to stabilize the bubble. In this study, we investigate factors that may affect mechanical stability, that is the equilibrium between the pressure inside and outside the bubble, for BNBs in order to help test the surface polarization model. Figure 1.3 includes the

workflow of this study. Its main objective is to investigate factors that affect mechanical stability of BNBs. To achieve this objective three tasks were completed.

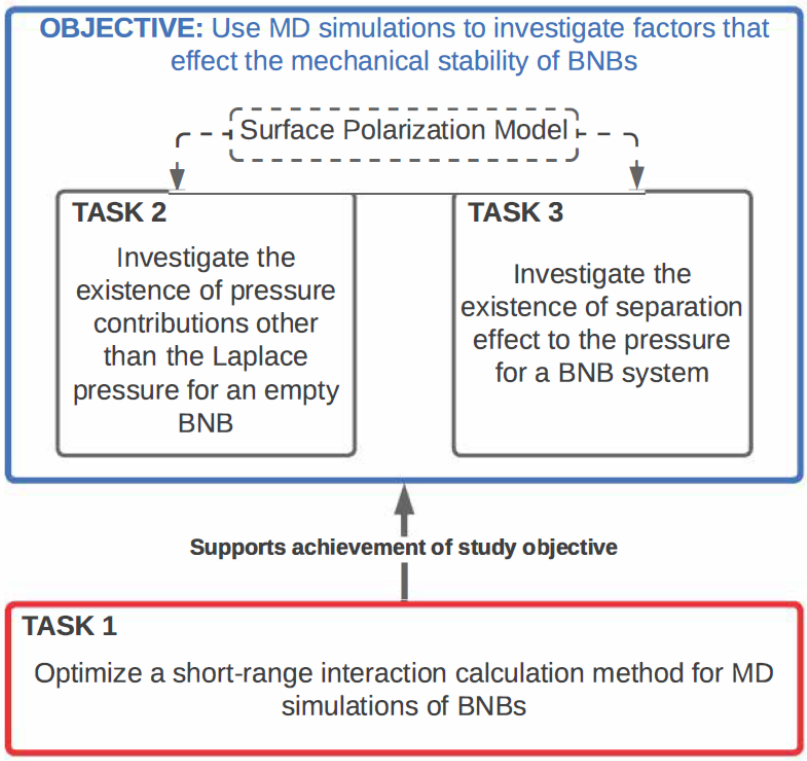

Figure 1.3: Workflow of this study which includes three main tasks. Arrows represent the connection between the tasks.

As MD simulations were used as the tool to achieve the research objective, Task 1 focused on selecting and testing a suitable MD simulation method with correct treatment of the short-range interactions. In Task 2, MD simulations were performed to measure the pressure inside the bubble and investigate whether there may be contributions in addition to the Laplace pressure. Since the interest is to identify possible factors that affect the pressure in a BNB system, the impact of bubble separation was examined in Task 3. The outcomes of both Task 2 and 3 are used to make possible connections to the surface polarization model.

Task 1. Selection of a short-range interaction calculation method for MD simulation of BNBs.

In MD simulations, it is important to select an appropriate treatment of short-range interactions as the system properties are determined based on the molecular interaction model.[60] According to the literature, to calculate the short-range interactions, use of a spherical cut-off method is a default approach.[44,46,60] However, no justification for selecting the cut-off lengths used for BNB simulations could be found. Therefore, we test a range of cut-off length values in BNB simulations. Although a spherical cut-off method has been used exclusively in BNB simulations, we show that its use can cause errors in system properties, notably the pressure, which can be remedied by employing the particle mesh Ewald (PME) method.[61] Therefore, we confirm the importance of using the PME method to calculate short-range interactions in BNB MD simulation.

Task 2. Investigate the existence of pressure contributions other than the Laplace pressure for an empty BNB.

After selecting a suitable simulation method, pressure contributions in a BNB system are determined. To calculate the Laplace pressure, the radius of the bubble is needed. Therefore, a suitable method is developed to estimate the bubble radius. By examining the relationship between the pressure in the system and the bubble radius we demonstrate that the pressure difference between inside and outside of the bubble is not equal to the Laplace pressure. According to the surface polarization model[34], dipole and quadrupole interactions between surface water molecules of the BNBs can contribute to the pressure. Therefore, the existence of dipole and quadrupole interaction effects in the pressure is confirmed.

Task 3. Investigate the existence of separation effect in the pressure for a BNB system.

Simulation results for systems of different size but with the same size of bubble suggest that there is an additional factor in the pressure. The dipole interactions between the surface water molecules of a BNB and a neighbouring bubble depend on the distance between adjacent bubbles (i.e., their separation). To determine the pressure in a BNB system, we examine the pressure in the bulk liquid and how it differs from the system pressure. The impact of bubble separation on the pressure is investigated in two set of simulations and it is confirmed that there is a separation effect.

1.6 Summary

This chapter introduced NBs, discussed applications and the history of NBs. Further, the importance of factors affecting BNB stability and previous findings from simulation and experimental studies exploring BNB behaviour were reviewed to provide a background for this study. Based on the current understanding of BNBs, the selected objectives were discussed.

1.7 Organization of the chapters

In Chapter 2, we will review the relevant literature for this study, including factors that may affect BNB behaviour, different models developed to try to explain BNB stability, and previous MD simulations of BNBs. Chapter 3 will describe the simulation methodology and analysis methods followed in this study according to its 3 primary tasks. In Chapter 4, we will present and discuss the results obtained from the simulations and analyses conducted. In the final chapter, Chapter 5, we will summarize our findings and discuss possible future work. A summary is included for chapters 2 to 4, and the relevant references are included at the end of each chapter.

1.8 References

1. Atkinson, A. J.; Apul, O. G.; Schneider, O.; Garcia-Segura, S.; Westerhoff, P. Nanobubble Technologies Offer Opportunities to Improve Water Treatment. *Acc Chem Res* **2019**, *52* (5), 1196–1205. https://doi.org/10.1021/acs.accounts.8b00606.
2. Wu, Y.; Tian, W.; Zhang, Y.; Fan, W.; Liu, F.; Zhao, J.; Wang, M.; Liu, Y.; Lyu, T. Nanobubble Technology Enhanced Ozonation Process for Ammonia Removal. *Water (Switzerland)* **2022**, *14* (12). https://doi.org/10.3390/w14121865.
3. Lee, J. il; Kim, J. M. Influence of Temperature on Bulk Nanobubble Generation by Ultrasonication. *Colloids and Interface Science Communications* **2022**, *49*. https://doi.org/10.1016/j.colcom.2022.100639.
4. Nirmalkar, N.; Pacek, A. W.; Barigou, M. On the Existence and Stability of Bulk Nanobubbles. *Langmuir* **2018**, *34* (37), 10964–10973. https://doi.org/10.1021/acs.langmuir.8b01163.
5. Meegoda, J. N.; Aluthgun Hewage, S.; Batagoda, J. H. Stability of Nanobubbles. *Environ Eng Sci* **2018**, *35* (11), 1216–1227. https://doi.org/10.1089/ees.2018.0203.
6. Park, Y.; Shin, S.; Shukla, N.; Kim, K.; Park, M. H. Effects of Nanobubbles in Dermal Delivery of Drugs and Cosmetics. *Nanomaterials* **2022**, *12* (19). https://doi.org/10.3390/nano12193286.
7. Johnson, B. D.; Cooke, R. C. *Generation of Stabilized Microbubbles in Seawater*; 1981; Vol. 213, pp 209–211. http://www.jstor.org/stable/1687157 (accessed 2023-02-12).
8. Senthilkumar, G.; Rameshkumar, C.; Nikhil, M. N. V. S.; Kumar, J. N. R. An Investigation of Nanobubbles in Aqueous Solutions for Various Applications. *Applied Nanoscience (Switzerland)* **2018**, *8* (6), 1557–1567. https://doi.org/10.1007/s13204-018-0831-8.
9. Ji, Y.; Guo, Z.; Tan, T.; Wang, Y.; Zhang, L.; Hu, J.; Zhang, Y. Generating Bulk Nanobubbles in Alcohol Systems. *ACS Omega* **2021**, *6* (4), 2873–2881. https://doi.org/10.1021/acsomega.0c05222.
10. Sharif, P. M.; Aziz Hairuddin, A.; As'Arry, A.; Rezali, K. A. M.; Noor, M. M.; Norhafana, M.; Shareef, S. M. Nano Gas Bubbles Dissolve in Gasoline Fuel and Its Influence on Engine Combustion Performance. In *IOP Conference Series: Materials Science and Engineering*; Institute of Physics Publishing, 2019; Vol. 469. https://doi.org/10.1088/1757-899X/469/1/012062.
11. Nakatake, Y.; Kisu, S.; Shigyo, K.; Eguchi, T.; Watanabe, T. Effect of Nano Air-Bubbles Mixed into Gas Oil on Common-Rail Diesel Engine. *Energy* **2013**, *59*, 233–239. https://doi.org/10.1016/j.energy.2013.06.065.
12. Wu, Y.; Huang, M.; He, C.; Wang, K.; Nhung, N. T. H.; Lu, S.; Dodbiba, G.; Otsuki, A.; Fujita, T. The Influence of Air Nanobubbles on Controlling the Synthesis of Calcium Carbonate Crystals. *Materials* **2022**, *15* (21), 7437. https://doi.org/10.3390/ma15217437.

13. Marcelino, K. R.; Ling, L.; Wongkiew, S.; Nhan, H. T.; Surendra, K. C.; Shitanaka, T.; Lu, H.; Khanal, S. K. Nanobubble Technology Applications in Environmental and Agricultural Systems: Opportunities and Challenges. *Crit Rev Environ Sci Technol* **2022**, 1–26. https://doi.org/10.1080/10643389.2022.2136931.

14. Alheshibri, M.; Qian, J.; Jehannin, M.; Craig, V. S. J. A History of Nanobubbles. *Langmuir* **2016**, *32* (43), 11086–11100. https://doi.org/10.1021/acs.langmuir.6b02489.

15. Degens, E. T.; von Herzen, R. P.; Wong, H. K.; Deuser, W. G.; Jannasch, H. W. Lake Kivu: Structure, Chemistry and Biology of an East African Rift Lake. *Geologische Rundschau* **1973**, *62* (1), 245–277. https://doi.org/10.1007/BF01826830.

16. Miller, J. D.; Hu, Y.; Veeramasuneni, S.; Lu, Y. *In-Situ Detection of Butane Gas at a Hydrophobic Silicon Surface*; 1999; Vol. 154.

17. Lou, S.-T.; Ouyang, Z.-Q.; Zhang, Y.; Li, X.-J.; Hu, J.; Li, M.-Q.; Yang, F.-J. Nanobubbles on Solid Surface Imaged by Atomic Force Microscopy. *Journal of Vacuum Science & Technology B: Microelectronics and Nanometer Structures* **2000**, *18* (5), 2573. https://doi.org/10.1116/1.1289925.

18. Zhang, X. H.; Zhang, X.; Sun, J.; Zhang, Z.; Li, G.; Fang, H.; Xiao, X.; Zeng, X.; Hu, J. Detection of Novel Gaseous States at the Highly Oriented Pyrolytic Graphite-Water Interface. *Langmuir* **2007**, *23* (4), 1778–1783. https://doi.org/10.1021/la062278w.

19. Lyu, T.; Wu, S.; Mortimer, R. J. G.; Pan, G. Nanobubble Technology in Environmental Engineering: Revolutionization Potential and Challenges. *Environmental Science and Technology*. American Chemical Society July 2, 2019, pp 7175–7176. https://doi.org/10.1021/acs.est.9b02821.

20. Sharif, P. M.; Aziz Hairuddin, A.; As'Arry, A.; Rezali, K. A. M.; Noor, M. M.; Norhafana, M.; Shareef, S. M. Nano Gas Bubbles Dissolve in Gasoline Fuel and Its Influence on Engine Combustion Performance. In *IOP Conference Series: Materials Science and Engineering*; Institute of Physics Publishing, 2019; Vol. 469. https://doi.org/10.1088/1757-899X/469/1/012062.

21. Wu, J.; Zhang, K.; Cen, C.; Wu, X.; Mao, R.; Zheng, Y. Role of Bulk Nanobubbles in Removing Organic Pollutants in Wastewater Treatment. *AMB Express*. Springer Science and Business Media Deutschland GmbH December 1, 2021. https://doi.org/10.1186/s13568-021-01254-0.

22. Wang, Y.; Wang, S.; Sun, J.; Dai, H.; Zhang, B.; Xiang, W.; Hu, Z.; Li, P.; Yang, J.; Zhang, W. Nanobubbles Promote Nutrient Utilization and Plant Growth in Rice by Upregulating Nutrient Uptake Genes and Stimulating Growth Hormone Production. *Science of the Total Environment* **2021**, *800*. https://doi.org/10.1016/j.scitotenv.2021.149627.

23. Batchelor, D. V. B.; Abou-Saleh, R. H.; Coletta, P. L.; McLaughlan, J. R.; Peyman, S. A.; Evans, S. D. Nested Nanobubbles for Ultrasound-Triggered Drug Release. *ACS Appl Mater Interfaces* **2020**, *12* (26), 29085–29093. https://doi.org/10.1021/acsami.0c07022.

24. *Nanobubbles Applications - Bauer Nanobubbles*. https://www.nanobubbles.com/what-are-nanobubbles/nanobubbles-applications/ (accessed 2023-01-23).

25. Zhou, L.; Wang, X.; Shin, H. J.; Wang, J.; Tai, R.; Zhang, X.; Fang, H.; Xiao, W.; Wang, L.; Wang, C.; Gao, X.; Hu, J.; Zhang, L. Ultrahigh Density of Gas Molecules Confined in Surface Nanobubbles in Ambient Water. *J Am Chem Soc* **2020**, *142* (12), 5583–5593. https://doi.org/10.1021/jacs.9b11303.

26. Kashiwagi, K.; Hattori, T.; Samejima, Y.; Kobayashi, N.; Nakabayashi, S. Hydrogen Nanobubbles at Roughness-Regulated Surfaces: Why Does the Standard Hydrogen Electrode Need a Platinized Platinum Electrode? *Journal of Physical Chemistry C* **2019**, *123* (12), 7416–7424. https://doi.org/10.1021/acs.jpcc.8b11648.

27. Zhang, X.; Lohse, D. Perspectives on Surface Nanobubbles. *Biomicrofluidics* **2014**, *8* (4). https://doi.org/10.1063/1.4891097.

28. Aluthgun Hewage, S.; Meegoda, J. N. Molecular Dynamics Simulation of Bulk Nanobubbles. *Colloids Surf A Physicochem Eng Asp* **2022**, *650*, 129565. https://doi.org/10.1016/j.colsurfa.2022.129565.

29. Theodorakis, P. E.; Che, Z. Surface Nanobubbles: Theory, Simulation, and Experiment. A Review. **2019**. https://doi.org/10.1016/j.cis.2019.101995.

30. Generation of Bulk Nanobubbles Using a High-Shear Rotor-Stator Device. *Ind Eng Chem Res* **2021**, *60* (23), 8597–8606. https://doi.org/10.1021/acs.iecr.1c01233.

31. Kikuchi, K.; Tanaka, Y.; Saihara, Y.; Maeda, M.; Kawamura, M.; Ogumi, Z. Concentration of Hydrogen Nanobubbles in Electrolyzed Water. *J Colloid Interface Sci* **2006**, *298* (2), 914–919. https://doi.org/10.1016/j.jcis.2006.01.010.

32. Bunkin, N. F.; Bunkin, F. v. Bubbstons: Stable Microscopic Gas Bubbles in Very Dilute Electrolytic Solutions. *Amarican Institute of Physics* **1992**, 271–278.

33. Eklund, F.; Alheshibri, M.; Swenson, J. Differentiating Bulk Nanobubbles from Nanodroplets and Nanoparticles. *Current Opinion in Colloid and Interface Science*. Elsevier Ltd June 1, 2021. https://doi.org/10.1016/j.cocis.2021.101427.

34. Ghaani, M. R.; Kusalik, P. G.; English, N. J. Massive Generation of Metastable Bulk Nanobubbles in Water by External Electric Fields. *Sci Adv* **2020**, *6* (14). https://doi.org/10.1126/sciadv.aaz0094.

35. Vehmas, T.; Makkonen, L. Metastable Nanobubbles. *ACS Omega* **2021**, *6* (12), 8021–8027. https://doi.org/10.1021/acsomega.0c05384.

36. Ma, X. tong; Li, M. bo; Sun, C. Measurement and Characterization of Bulk Nanobubbles by Nanoparticle Tracking Analysis Method. *Journal of Hydrodynamics* **2022**. https://doi.org/10.1007/s42241-022-0077-5.

37. Jadhav, A. J.; Barigou, M. Bulk Nanobubbles or Not Nanobubbles: That Is the Question. *Langmuir* **2020**, *36* (7), 1699–1708. https://doi.org/10.1021/acs.langmuir.9b03532.

38. Nirmalkar, N.; Pacek, A. W.; Barigou, M. On the Existence and Stability of Bulk Nanobubbles. *Langmuir* **2018**, *34* (37), 10964–10973. https://doi.org/10.1021/acs.langmuir.8b01163.

39. Ma, T.; Kimura, Y.; Yamamoto, H.; Feng, X.; Hirano-Iwata, A.; Niwano, M. Characterization of Bulk Nanobubbles Formed by Using a Porous Alumina Film with Ordered Nanopores. *Journal of Physical Chemistry B* **2020**, *124* (24), 5067–5072. https://doi.org/10.1021/acs.jpcb.0c02279.

40. Epstein, P. S.; Plesset, M. S. On the Stability of Gas Bubbles in Liquid-Gas Solutions. *J Chem Phys* **1950**, *18* (11), 1505–1509. https://doi.org/10.1063/1.1747520.

41. Ljunggren, S.; Eriksson, J. C. *COLLOIDS A The Lifetime of a Colloid-Sized Gas Bubble in Water and the Cause of the Hydrophobic Attraction1*; ELSEVIER, 1997; Vol. 129.

42. Attard, P. The Stability of Nanobubbles. *Eur Phys J Spec Top* **2014**, *223* (5), 893–914. https://doi.org/10.1140/epjst/e2013-01817-0.

43. Zhou, Y.; Han, Z.; He, C.; Feng, Q.; Wang, K.; Wang, Y.; Luo, N.; Dodbiba, G.; Wei, Y.; Otsuki, A.; Fujita, T. Long-Term Stability of Different Kinds of Gas Nanobubbles in Deionized and Salt Water. *Materials* **2021**, *14* (7). https://doi.org/10.3390/ma14071808.

44. Hong, S. N.; Choe, S. H.; Jong, U. G.; Pak, M. S.; Yu, C. J. The Maximum Interbubble Distance in Relation to the Radius of Spherical Stable Nanobubble in Liquid Water: A Molecular Dynamics Study. *Fluid Phase Equilib* **2019**, *487*, 45–51. https://doi.org/10.1016/j.fluid.2019.01.014.

45. Koshoridze, S. I.; Levin, Yu. K. ON THE DYNAMIC EQUILIBRIUM OF NANOBUBBLES IN WATER. *Nanoscience and Technology: An International Journal* **2018**, *9* (1), 1–8. https://doi.org/10.1615/nanoscitechnolintj.2018025819.

46. MATSUMOTO, M. Surface Tension and Stability of a Nanobubble in Water: Molecular Simulation. *Journal of Fluid Science and Technology* **2008**, *3* (8), 922–929. https://doi.org/10.1299/jfst.3.922.

47. Shi, X.; Xue, S.; Marhaba, T.; Zhang, W. Probing Internal Pressures and Long-Term Stability of Nanobubbles in Water. *Langmuir* **2021**, *37* (7), 2514–2522. https://doi.org/10.1021/acs.langmuir.0c03574.

48. Matsumoto, M.; Tanaka, K. Nano Bubble-Size Dependence of Surface Tension and inside Pressure. *Fluid Dyn Res* **2008**, *40* (7–8), 546–553. https://doi.org/10.1016/j.fluiddyn.2007.12.006.

49. Lu, Y.; Yang, L.; Kuang, Y.; Song, Y.; Zhao, J.; Sum, A. K. Molecular Simulations on the Stability and Dynamics of Bulk Nanobubbles in Aqueous Environments. *Physical Chemistry Chemical Physics* **2021**, *23* (48), 27533–27542. https://doi.org/10.1039/d1cp03325e.

50. Hollingsworth, S. A.; Dror, R. O. Molecular Dynamics Simulation for All. *Neuron* **2018**, *99* (6), 1129–1143. https://doi.org/10.1016/j.neuron.2018.08.011.

51. Vega, C.; de Miguel, E. Surface Tension of the Most Popular Models of Water by Using the Test-Area Simulation Method. *Journal of Chemical Physics* **2007**, *126* (15). https://doi.org/10.1063/1.2715577.

52. Vega, C.; Abascal, J. L. F.; Nezbeda, I. Vapor-Liquid Equilibria from the Triple Point up to the Critical Point for the New Generation of TIP4P-like Models: TIP4P/Ew, TIP4P/2005, and TIP4P/Ice. *Journal of Chemical Physics* **2006**, *125* (3). https://doi.org/10.1063/1.2215612.

53. Rezaei Nejad, H.; Ghassemi, M.; Mirnouri Langroudi, S. M.; Shahabi, A. A Molecular Dynamics Study of Nano-Bubble Surface Tension. *Mol Simul* **2011**, *37* (1), 23–30. https://doi.org/10.1080/08927022.2010.513007.

54. Goldman, S. Generalizations of the Young-Laplace Equation for the Pressure of a Mechanically Stable Gas Bubble in a Soft Elastic Material. *Journal of Chemical Physics* **2009**, *131* (18). https://doi.org/10.1063/1.3259973.

55. Chen, C.; Li, J.; Zhang, X. The Existence and Stability of Bulk Nanobubbles: A Long-Standing Dispute on the Experimentally Observed Mesoscopic Inhomogeneities in Aqueous Solutions. *Communications in Theoretical Physics*. IOP Publishing Ltd March 1, 2020. https://doi.org/10.1088/1572-9494/ab6183.

56. Menzl, G.; Gonzalez, M. A.; Geiger, P.; Caupin, F.; Abascal, J. L. F.; Valeriani, C.; Dellago, C. Molecular Mechanism for Cavitation in Water under Tension. *Proc Natl Acad Sci U S A* **2016**, *113* (48), 13582–13587. https://doi.org/10.1073/pnas.1608421113.

57. Wang, S.; Zhou, L.; Gao, Y. Can Bulk Nanobubbles Be Stabilized by Electrostatic Interaction? *Physical Chemistry Chemical Physics* **2021**, *23* (31), 16501–16505. https://doi.org/10.1039/d1cp01279g.

58. Tan, B. H.; An, H.; Ohl, C. D. How Bulk Nanobubbles Might Survive. *Phys Rev Lett* **2020**, *124* (13). https://doi.org/10.1103/PhysRevLett.124.134503.

59. Matyushov, D. v. Electrophoretic Mobility without Charge Driven by Polarisation of the Nanoparticle-Water Interface. *Mol Phys* **2014**, *112* (15), 2029–2039. https://doi.org/10.1080/00268976.2014.882521.

60. Yonetani, Y. Liquid Water Simulation: A Critical Examination of Cutoff Length. *Journal of Chemical Physics* **2006**, *124* (20). https://doi.org/10.1063/1.2198208.

61. Luty, B. A.; Davis, M. E.; Tironi, I. G.; van Gunsteren, W. F. A Comparison of Particle-Particle, Particle-Mesh and Ewald Methods for Calculating Electrostatic Interactions in Periodic Molecular Systems. *Mol Simul* **1994**, *14* (1), 11–20. https://doi.org/10.1080/08927029408022004.

Chapter 2 : LITERATURE REVIEW AND RESEARCH BACKGROUND

This chapter focuses on reviewing the relevant literature and background related to my study. First, the long term stability of BNBs, factors that affect behavior of BNBs, and some of the explanations developed to account for the stability of BNBs are discussed. Next, the literature on MD simulations of BNBs is reviewed. Finally, the methodologies that have been followed for the analysis of BNB radius and position during MD simulation studies are discussed.

2.1 Literature on bulk nanobubble stability

As mentioned in Chapter 1, due to the many factors that appear to affect the nature and stability of BNBs, there has been a large number of studies reported. Since it is important to understand the effects of the various factors on BNBs, the next section will provide a detailed discussion of these. Then, based on studies of these factors, researchers have developed models to explain the stability of BNBs. These models are discussed in section 2.1.2.

2.1.1 Stability of bulk nanobubbles

Although BNBs are long-lived stable bubbles[1–4], there is still limited understanding of the origin of their stability.[5,6] The stability of BNBs can be considered from thermodynamic and kinetic perspectives.[2,7] According to the Young Laplace equation, the pressure difference between the inside and outside for a 100 nm bubble is ~3 MPa.[7–9] More details on this pressure difference, $\Delta P_{Laplace}$ will be discussed later in this chapter. Further, according to Henry's law [7–9], the partial pressure of gas inside BNBs should be proportional to the concentration of dissolved gas in solution. For a pressure of ~3 MPa, a very high gas concentration in solution is required to reach equilibrium between the bubble and the solution. An analysis of the equilibrium[2,7] predicts that

even if the gas distribution between inside and outside of the BNBs reaches a balance, it will in fact be unstable. If the BNB shrinks slightly (e.g., due to fluctuations) the slightly elevated internal pressure will cause some of the gas in the bubble to diffuse out and lead to further shrinkage of the bubble. Such a mechanism should cause bubbles to shrink quickly, leading to the disappearance of the BNBs.[7,8] On the other hand, if the BNB expands slightly, the pressure in the BNB will drop, leading to unbounded bubble growth. Therefore, this analysis predicts that BNBs cannot be stable in an open system from the view of thermodynamics.[7–9] However, BNBs are found to be very stable and can be considered to represent a metastable state, which is a local free energy minimum.[3,9,10] Kinetic stability refers to situations where changes in the system are kinetically impeded. The Epstein Plesset equation[11] provides an estimate for the dynamic evolution of BNBs, considering liquid properties (i.e, density, viscosity, surface tension), bubble size and pressure difference between bubble and the liquid. According to Epstein Plesset equation[11] the time required for complete dissolution of a BNB to be less than 0.02 s.[7] Therefore, analyses based both on thermodynamic and kinetic factors predict the instability of BNBs.

To study BNB stability, changes in bubble size (diameter) and number density (number of BNBs per unit volume) over time have been investigated by several groups.[2,3,7,12,13] Factors that appear to change the bubble number density can be considered as possibly important to bubble stability.[5,6,14,15] However, for BNBs to be stable they should be in equilibrium with the surrounding solution, and hence any factor that affects the BNBs-solution equilibrium, may change the nature (i.e., size, number density) of BNBs.[6,12] For example, the generation methodology could impact the nature of BNBs.[16,17] Consequently, results are often found to be inconsistent between various studies.

The effect of generation method on BNB number density and size was analyzed by Ji et al.[16] using BNBs produced by acoustic cavitation, pressurization-depressurization, and vibration (using a vortex oscillator[18]) methods. The generation method can affect the number density of BNBs in solution, as each method has a different capacity for mixing gas with liquids and promoting bubble nucleation.[19] For a propanol solution, Ji et al.[16] obtained the highest number density of BNBs by the acoustic cavitation method, and found that changes in the parameters of the generation methods, including the frequency of the ultrasound generator, the rate of pressurization-depressurization and the vibration time, can change the BNBs size and number density.[16] Ananda et al.[20] worked on BNB generation using a high-shear rotor-stator device and noticed the rotor speed and operating time effect the size and bubble number density. However, optimum energy input appropriate for bubble generation may vary with the utilized gas and the solution as the energy required for nucleation of different gas bubbles is different.[19] Other than the generation method, the solution and gas properties are also important for BNBs.[5,6]

In terms of the effect of temperature, the dependance of BNB number density and size changes with increasing and decreasing temperature was analyzed by Li et al.[13] They concluded that heating and cooling in the range of 10˚C to 70˚C does not impact the apparent stability of air BNBs in pure water. They reported that although bubble sizes were found to change with the temperature, their number density was relatively steady.[13] The effect of temperature on BNBs generated by ultrasonication was examined by Lee and Kim.[21] In their study, they examined the BNB number density at three different temperatures (25˚C, 50˚C and 75˚C) in DI water. According to their results, stable BNBs were found at all three temperatures and the highest BNB number density was reported for 75˚C. However, the mean diameter of the BNBs decreased with increasing

temperature. They explained their observations by noting that the dissolved gas concentration in DI water is higher at low temperatures than at high temperatures. Therefore, at low temperatures bubble growth is facilitated by diffusion resulting in larger bubbles.[21] According to both studies by Li et al.[13] and Lee and Kim[21] BNBs are relatively stable for a wide range of temperature.

The possible influence of liquid properties, such as carbon chain length[16], liquid polarity[16], impurity levels/ions concentration,[6,12] and pH[6,12] on BNB stability have been evaluated by several recent studies. Ji et al.[16] analyzed BNB number density in different alcoholic solutions (methanol, ethanol, propanol, butanol, pentanol and hexanol) with different lengths of carbon chains, and therefore different polarities. Of these six alcohols, the highest number density of BNBs was recorded in propanol. As all the solutions are alcohols, and only the lengths of the carbon chain were different, these authors concluded that solvent properties are important for BNB stability.[16] Further, they claimed that since BNBs were recorded in all six alcohols, BNBs are very stable not only in water, but in other polar organic solvents.[16]

The effect of the pH of the solution on the stability of BNBs was analyzed by Nirmalkar et al.[12] Beacuse pH is a measurement of H^+ ion concentration in solutions, changing pH may affect the surface charge of BNBs and other surface properties.[12] According to Nirmalkar et al.'s[12] study, they found stable BNBs over a large range of pH (3-10). However, they found that changes in solution pH affect both number density and size of the BNBs. Further, they also studied the effect of surfactants (anionic, cationic, and non-ionic) on BNB stability, and reported stable bubbles in solutions with different concentrations. Similar to the effect of surfactants, they examined the effect of ion concentration on bubble number density and size. They reported stable BNBs in both NaCl and CaI_2 solutions, with concentrations from 0 to 200 mM. However, they did not study the

bubble number density changes over time with either surfactants or ions.[12] We recall that stable BNBs were detected in sea water for more than 22 hours, apparently confirming that BNBs are very stable even in solutions with different ions and surfactants.[22] There are many studies reported[5,12,14,23] investigating the effect of pH, surfactant and ion concentration on BNBs. According to this literature, although the BNB number density and bubble mean diameter varies with pH, surfactant and ion concentration, BNBs remain relatively stable.[7,12–14,23] However, in reviewing the literature on the effects of different factors on BNB stability, we noted that several of these studies considered the stability of BNBs as simply detecting BNBs at different conditions, rather than detecting persistent BNBs over long periods of time under different conditions.

The stability of different gas filled BNBs in DI water was analysed by Zhou et al.[14] They examined air, N_2, O_2, CO_2 and Ar with 8% H_2 gas filled bubbles and noted their lifetime in days in DI water. All BNBs except CO_2 were stable in DI water for at least 60 days. They found that CO_2 BNBs were stable only for 5 days. However, they further examined the stability of these five types of BNBs in 1mM of NaCl, CaCl, and $AlCl_3$ solution and reported all these bubbles were stable for at least 60 days confirming the long-term stability of BNBs.[14]

Nirmalkar et al.[6] analyzed the changes in bubble number density and size over time in water with different initial bubble number densities and reported BNB lifetime of more than 150 days. Further, during that period bubble sizes were relatively unchanged. In their study, they compared the use of NTA and DLS for their size distribution measurements and reported that DLS is biased towards large bubble sizes as DLS measurements are based on the intensity of the scattered light. As NTA tracks Brownian motion (random displacement in a solution) of the BNBs, NTA measurements are claimed to be more reliable than DLS.[6] Moreover, it is important to use an

accurate method for BNBs detection, as it may not be possible to differentiate BNBs and nanoparticles, and both may contribute to number density and size results. There are many studies reviewing the reliability and accuracy of different instrumentation and methods for BNB detection in the literature.[6,24,25]

According to the discussion above, although bubble number density and size may change with numerous factors, very stable BNBs can be found in broad range of solutions and conditions. Studies on BNBs become complicated as these factors are often difficult to analyze separately. For an example, with different gas species, both bubble number density and size may change together.[14] Therefore, it is hard to distinguish whether a gas species directly affects the bubble lifetime, or changes in number density and size effect the bubble lifetime. Therefore, although there have been many experimental (and some simulation) studies investigating factors affecting BNB stability, none have yet provided a consistent and widely accepted explanation for the stability of BNBs and their observed long lifetimes. However, if different factors could be isolated and tested, it would be helpful in understanding their effects upon the stability of BNBs.

It is important to point out that to stabilize a BNB, the pressure inside the bubble should balance the pressure outside the bubble. Therefore, any factor that changes the pressure inside the bubble may affect the stability of BNBs. Since both liquid and gas properties may affect the interface properties of a bubble, the pressure may also change. Consequently, the pressure inside the bubble can change thereby affecting the nature and lifetimes of BNBs.

2.1.2. Bulk nanobubble stability models

Through a variety of studies, several theories have been developed that look to explain the stability of BNBs considering different factors. In this section, some of the key models are discussed,

including the thermodynamic[3], diffusive shielding[26], DLVO[14], electrostatic repulsion[27], and surface polarization[10] models.

Thermodynamic stability model for BNBs

Beyond investigations focused on the mechanical and chemical stability of BNBs, some studies have explicitly focused on the thermodynamic stability of BNBs. The thermodynamic stability of BNBs was evaluated by Vehmas and Makkonen[3] with the help of previous studies [2,15,28]. Because the Gibbs free energy is the crucial factor understanding the spontaneity of a process, they looked to evaluate the overall Gibbs free energy change during the BNB dissolution process.[3] According to their model, dissolution of a BNB with diameter below 180 nm is not a spontaneous process and requires an activation free energy to initiate the process.[3] However, the authors do not provide a physical explanation for the origins of this behavior.

Diffusive shielding model for BNB stability

Joost et al.[26] proposed the effect of diffusive shielding to account for BNB stability. According to them, BNBs in a solution can be considered as a cluster of similar sized bubbles. The BNBs in the cluster are stabilized by the surrounding similar sized BNBs.[26,29] The distance between these bubbles must be small enough (about ten times the bubble radius) so the bubbles can (locally) saturate the surrounding liquid with gas. When a bubble cluster is stable, changes in solution is prevented and the bubbles survive indefinitely unless they merge. This stabilization of BNBs as a cluster is known as the diffusive shielding of BNB stability.[26] However, BNBs show Brownian motion.[29–31] Due to Brownian motion, bubbles can move apart or might collide and merge with neighbouring bubbles leading different sized bubbles, breaking the stable bubble cluster.[26]

DLVO model for BNB stability

The DLVO theory[14] (named after Derjaguin, Landau, Verwey and Overbeek) can quantitatively explain the stability of colloids in aqueous solutions and describes the forces between charged surfaces interacting in a liquid medium. It has been suggested[9,12] the DLVO theory may also used to explain the interactions between BNBs in electrolyte solution. According to the DLVO theory, colloids are stabilized by balancing the attractive van der Waals and repulsive electric double layer interactions.[9,12] As van der Waals forces are effective over only a short range, when two colloidal particles approach each other, van der Waals attractive forces become more important.[14] Therefore, the separation between interfaces is an important factor for the total free energy. Although changes in the ionic strength of the liquid affect the range of the electric double layer interactions, the van der Waals forces are not affected.[32] Therefore, this model may explain the apparent stability of BNBs in pure water and solutions with low ionic strength, however it does not explain the relative stability of BNBs in solutions with high ionic strength.[32] Further, DLVO theory is only a good estimate for surface separations down to about 5 nm.[32] The study on BNB stability by Attard [2] stated that there may be additional unidentified forces that stabilize BNBs other than the van der Waals and repulsive electric double layer interactions.

Electrostatic repulsion model for BNB stability

The Electrostatic repulsion model assumes the accumulation of negative ions on the surface of BNBs, consistent with the negative values measured for their zeta potentials.[27,33] The electrostatic repulsion between the negative ions on the BNB surface, if present, will cause a counter pressure (electrostatic stress) to balance the Laplace pressure.[33,34] Although many researchers have claimed the possible source of the negative ions is OH^- ions,[33,35] from water auto-ionization, the concentration of OH^- ions in pure water is negligible (10^{-7} mol/L).[36] Therefore, this model is

challenged to explain the stability of BNBs in pure water. Wang et al.[27] looked to extend this model and claimed the contribution of ions to the pressure inside a BNB in water includes two pressure contributions:

- The pressure arising from the mutual repulsions of the ions attached to the surface (surface ions) of the BNB;
- The pressure arising from the attractive forces due to the counter ions in the diffusive layer associated with the surface ions.

Wang et al.[27] observed that the contribution of counter ions has not been considered in previous studies. To estimate the effects of both the factors noted above, they calculated the electrostatic pressure arising from surface charges when the surrounding medium is a dielectric material, and the electrostatic contribution to the pressure when the double layer in an electrolyte solution is also considered. Comparing the ratio between the electrostatic pressure and the Laplace pressure, which was founded to be much less than 0.01, these authors concluded that the electrostatic interactions arising from ions cannot be the primary factor which effectively balances the Laplace pressure.[27] They suggest that non-electrostatic repulsive interactions may help to stabilize the BNBs, but did not clarify how these might arise.

Surface polarization model for BNB stability

The surface polarization model assumes that when water is in contact with air or a hydrophobic solute, it results in the spontaneous polarization of the interface. Matyushov[37] considered a similar electrostatic model and investigated how the surface polarization of nanoparticles can be applied as a possible explanation for BNBs stability. He argued that when the surface polarization couples with a uniform external field, it can lead to a non-zero force acting on the particle/bubble, even

though the particle/bubble does not possess a net charge. The direction and strength of the force is governed by the first order (dipole) and second-order (quadrupole) orientation parameters of the interfacial water molecules.[37] This theory predicts that the quadrupole effect is negligible for particles/bubbles whose sizes exceed a few nanometers. Hence the dipole contribution of the surface polarization is expected to dominate for larger sizes and is predicted to govern the zero-charge mobility of submicron particles or bubbles.

The surface polarization model is supported by numerous experimental and simulation studies which consistently report the polarization of the air-water interface.[10,38] For example, Vácha et al.[39] carried out ab initio MD simulations to probe the charge transfer between interfacial water molecules. They were able to demonstrate the instantaneous asymmetric hydrogen bonding at the water surface, and connected it to apparent charge transfer at the water-vapor interface. Using a simple continuum model, the charge transfer (or surface polarization) was shown to give rise to a negative zeta potential which supports the conclusions of Matyushov's[37] study of surface polarization. Thus, while a negative zeta potential is usually considered by many studies as evidence for accumulation of negative ions[5,21] on the surface of BNBs (i.e., electrostatic repulsion model), polarization of the gas-water interface is a sufficient condition for explaining the zeta potential.[10]

Ghaani et al.[10] studied the impact of surface polarization as an explanation for the stability of BNBs. They demonstrated that for BNBs, the interactions between surface dipoles can produce a repulsive force to counter the Laplace pressure effect. This dipole-dipole repulsion results in a pressure contribution that is opposite to the Laplace pressure and also inversely proportional to the radius of the bubble. These authors also performed simulations of BNBs in a uniform electric field,

as discussed in Matyushov's[37] study, and observed movement of the bubbles. To explain their simulation results they conjectured that it is non-linear polarization of a BNB's interface that results in the movement of bubble in the electric field, analogous to a phenomenon known as dielectrophoresis.[10] Thus, according to this model, only the surface polarization is needed to account for both bubble stability and mobility.[10] Beacuse this model relies on a known property of the air/water interface and can be used to successfully explain experimental observations of BNBs, we will focus on this model. Even though several explanations for stability of BNBs have been put forwarded, as discussed above, there is still needed to test and improve these models. Therefore, this study focusses on obtaining key results from simulations of the BNBs focused on factors that may affect their stability. Before moving into these details, it is first important to establish an understanding of the contribution to the pressure inside the bubble arising from the Laplace pressure.

As mentioned in Chapter 1, the Laplace pressure acts on the surface of the bubble, towards its center. If bubble has radius *R*, the Laplace pressure ($\Delta P_{Laplace}$) can be represented by the Young Laplace equation[30,40]

$$\Delta P_{Laplace} = \frac{2\gamma}{R}. \tag{2.1}$$

For liquid water at 1 bar and 298 K, the surface tension (γ) is about 0.073 N/m.[8,31,41] If we assume the surface tension of water and require *R* to have units of nm, then eqn. 2.1 becomes

$$\Delta P_{Laplace} = \frac{1460}{R} \text{ bar}. \tag{2.2}$$

From eqn. 2.2, it is clear that the Laplace pressure is very large for small (i.e., nm scale) bubbles and will increase with decreasing bubble size. For a bubble with *R*=10 nm, the Laplace pressure

contribution to the pressure inside the bubble is 146 bar, and significantly larger than the atmospheric pressure. Therefore, to balance such a large pressure and to stabilize a BNB, a counter pressure to the Laplace pressure is required, such as the contribution identified in the surface polarization model discussed above.[10]

Clearly there is need to model BNB systems and to determine various properties, notably the pressure contributions inside BNBs. Recall, MD simulations represent a useful tool for this purpose. While it may be challenging to limit nanoscale impurities and to measure the pressure inside a BNB in an experiment,[24,42] MD simulations are well suited for this purpose. Therefore, MD simulation studies of BNB will now be reviewed.

2.2 Molecular dynamics simulations

MD simulation is considered a very powerful tool for probing the dynamics of a microscopic system, and have been used previously in several BNB simulation studies.[29,41,43–46] MD simulation is a computer simulation method in which the physical movement of atoms and molecules within a system are numerically modeled to study equilibrium and dynamic properties.[47,48] Within a MD simulation, the chemical and mechanical equilibrium of BNBs can be tracked and analysed. More details on MD simulations can be found in any MD simulation textbook[47,49] for example "The Art of Molecular Dynamics Simulation" by Rapaport[50].

The basis of a MD simulation is Newton's equations of motion, here expressed as

$$F_i = m_i a_i \,, \tag{2.3}$$

where F_i is the force on a particle/atom i, m_i and a_i are mass and acceleration of the particle/atom i, respectively. The acceleration can be written as a change in the velocity v_i,

$$a_i = \frac{dv_i}{dt}\,, \tag{2.4}$$

and eqn. 2.3 becomes

$$F_i = m_i \frac{dv_i}{dt}\,. \tag{2.5}$$

a_i can be further written as a 2nd order differential of the position of particle r_i, and eqn.2.5 becomes

$$F_i = m_i \frac{d^2 r_i}{dt^2}\,. \tag{2.6}$$

As eqn. 2.6 is a 2nd order differential equation, it requires two conditions to be solved, the initial position vector, and initial velocity. In a molecular system, the force F_i on the i^{th} atom at a given time can be calculated from the gradient of the potential energy U,

$$F_i = -\nabla_i U\,. \tag{2.7}$$

Combining eqns. 2.6 and 2.7 we get

$$F_i = -\nabla_i U = m_i \frac{d^2 r_i}{dt^2}\,. \tag{2.8}$$

Based on eqn. 2.8, in MD simulation to solve the equations of motion for different particles in a system, the potential energies as a function of positions should be known.

If the initial state of a system is known, theoretically, its state at any other time can be predicted by solving the Newtonian equations of motion.[50] However, if there are many particles in the system, it is impossible to solve the equations of motion analytically. Therefore, a numerical

algorithm (e.g., the Leap Frog algorithm[51]) must be used to integrate the equations of motion for the particles assuming the time interval for the numerical integration is very short such that the force on the particle i is essentially constant over that time interval. Once the forces acting on the particles are calculated, the initial velocities and positions can be used to calculate the new positions and velocities. With the movement of the particles, positions and forces are then updated accordingly. The final resultant trajectory of the simulation includes all the positions and the velocities of the particles from which the average system properties can be extracted.[50]

2.2.1. Simulation parameters

MD simulations can be performed by any one of several standard software packages currently available. In this section, selection of suitable simulation parameters will be discussed. The following three aspects are critical for any MD simulation:[47]

- Selection of a suitable numerical algorithm to integrate the equations of motion;
- Selection of a model to describe the inter and intra particle interactions;
- Selection of appropriate method for evaluating energy and forces.

<u>The numerical algorithm to integrate the equations of motion</u>

The Leap Frog algorithm is one of the commonly used algorithms to integrate the equations of motion and generate MD trajectories.[51] The Leap Frog algorithm uses Taylor expansions of positions and velocities,[51] and is a time reversible and second order integration method. Other than the Leap Frog algorithm, there are other algorithms available.[51,52] A discussion comparing several numerical integration methods can be found in the study of Gunsteren and Berendsen.[51]

Inter and intra particle interactions

To represent interactions, an empirical force field is typically used in atomistic MD simulations. The force field is a representation of all bonded and non-bonded interactions in the system. Bonded interactions consist of bond stretching, bending and dihedral interaction terms. Non-bonded interactions can be divided into van der Waals and electrostatic interactions. It is important to select a suitable model for calculating both inter and intra particle interactions in a simulation study. There are many force fields available for MD simulations[47–49], including standard force field such as Amber[53], CHARMM[54], and OPLS-AA[53]. More details on different force fields can be found in standard references such as "The Art of Molecular Dynamics Simulation" by Rapaport.[50]

Method for determining energy and forces

Periodic boundary conditions (PBC) are commonly used in MD simulations, where the systems approximated by PBC consist of an infinite number of replicas of the simulation cells.[49] PBC will be discussed further in section 2.3.3. In an infinite system, it is necessary to approximate the long-range electrostatic interactions. One approach is to introduce a cut-off radius, also known as a cut-off length.[55] In this approach interactions only within a particular cut-off radius around each atom are considered. The truncation of the interactions beyond the cut-off distance can be corrected by adding a tail correction. However, selecting the most suitable cut-off length is important as it can impact important properties of the systems, including the system energy, pressure, and surface properties. MD simulation studies with cut-off lengths in the range of 1 - 2 nm are common.[30,31,56]

Once these essential parameters have been selected, the simulation can be performed using a suitable molecular model and a software package. The process of an MD simulation for a BNB system consists of the following three basic steps to obtain results:[48,49]

- Structure preparation (includes structural processing for placing all molecules into the simulation box);
- Perform the MD simulations (including energy minimization and equilibration);
- Analyze the trajectory (including finding bubble position, average pressure and density calculations).

In previous BNB studies, researchers have used a variety of molecular models, software packages and simulation methodologies to achieve the above three steps.[47,48] These will now be discussed in sections 2.2.2 and 2.2.3.

2.2.2 Simulation software

There are numerous software packages available for performing MD simulations including Gromacs[57], Packmol[58], NAMD[59], CHARMM[54], and AMBER[53]. Based on the application and accessibility, a suitable software package can be selected. Gromacs[57] is a free and open-source software package which can be used for high-performance MD simulations and for the analysis of results. This is user-friendly with freely available tutorials. The initial system preparation, MD simulations (energy minimization, equilibration and production) and trajectory analysis can all be done using Gromacs.[57] Packmol[58] is also freely available software, which can be used to set up the systems by packing the molecules into a simulation box to minimize molecular overlaps that could otherwise disrupt the simulation.[58]

Once the simulation software package is selected, a suitable visualization software can be used to observe the structure and properties of the system. VMD[60] (Visual Molecular Dynamics) is a molecular visualization program for displaying, animating, and analyzing systems using 3D graphics and built-in scripting.[60] This software is useful for observing the bubble

behavior/movement in the system. To obtain average system properties over time, the Grace software[61] package can be used. Grace is a user friendly, 2D plotting tool.[61]

2.2.3 Water model

After selecting appropriate software packages for performing the MD simulation and analysis, suitable models for each chemical species in the system should be selected for the simulation. Since the physical properties of water are well known[62], and as water is the most studied BNBs containing liquid [62], a model water system will be the liquid phase in this study. Additionally, the focus of this study will be on an empty BNB in pure water. Hence the only chemical species in systems is water. There are several standard water models (i.e., SPC, SPC/E, TIP3P, TIP4P, TIP4P/2005, TIP5P etc.) available for simulations.[63,64]

The TIP4P/2005 model is a four-site, rigid, and non-polarisable water model.[65] Since TIP4P/2005 is a rigid model, it does not change its bond lengths or angles during a simulation, and so reduces the computational cost (by allowing for a large time step to be used). Among empirical force field models, the TIP4P/2005 water model is one of the best atomistic models, having been shown to reproduce very well the properties of liquid water under the ambient conditions.[65] Therefore, the TIP4P/2005 water model was selected for this study. A detailed comparison of water models can be found in the paper of Alkhwaji et al.[63] study. Ghaani et al.[10] also used the TIP4P/2005 water model, while Hewage et al.[46] and Bird et al.[66] used the SPC/E model in their studies. The TIP4P/ICE model was used by Lu et al.[56] for their methane water systems.

2.3. Simulation setup

Any simulation also includes several important selections that require careful consideration (i.e., size of the system, length of the simulation) as they may impact the quality of the results obtained. Several of these are part of the simulation setup, and include simulation system preparation, selecting a suitable interaction calculation methodology. These important initial steps of a MD simulation study are discussed in sections 2.3.1 to 2.3.3.

2.3.1 Simulation system

An MD simulation of a BNB first requires the setting up of the simulation system. The simulation system, also known as a simulation cell, is defined as the smallest repeated unit of the system within PBC.[67] In a BNB simulation, the cell is usually initially filled with the water and the BNB is then inserted at the center of the cell. Selecting a suitable simulation cell shape, cell size and bubble size is important, as these choices define the system and directly impact the computational cost.[67] Another important consideration is whether to fill the bubble, as some previous studies have used filled bubbles[46,56] while others have started with an empty cavity.[30,31]

In simulations of BNBs, cubic cells have been commonly used. Cubic simulation cells are easy to deal with as they have a simple symmetry (cell dimensions and angles (90^0) are all the same) and are widely used systems.[67] For example, in their simulation, Hong et al.[30] used different cubic systems with L = 5, 8, 10, 12, 15 nm, and in their study of spontaneous cavitation Min and Berkowitz[68] used cubic boxes with L = 3.5, 4.0, 4.5, and 5.0 nm. However, there are system shapes other than cubic, such as rectangular, rhombic dodecahedron (RD), or truncated octahedron (TO), that can be used as systems.[67] In their BNB simulation, Ghaani et al.[10] used a rectangular system to accommodate their methane and propane bubbles. For their two methane BNB simulations Lu

and coworkers[56] employed a rectangular shape system, while for the single methane BNB simulations, they used a cubic system.

The RD and TO systems specifically, can be more (computationally) cost effective[67] than cubic systems due to their efficiency in accommodating a spherical BNB. Based on the size of the bubble and the inter-bubble (i.e., periodic image) distance desired, an appropriate box length (L) should be selected. So, if the bubble is large, it will require a larger system with more liquid molecules, but the computational cost also increases with the system's size. An approach that can be used to accommodate a larger bubble efficiently is to change the system's shape. Rather than using a cubic system, a RD system (twelve-sided rhombus) or TO can be used.[67] Such system shapes will support the introduction of larger bubbles with considerably smaller system volumes, and corresponding numbers of liquid molecules. For example, the volume of a RD system is $L^3/\sqrt{2}$, which is about 71% of the volume of a cube with length L.[67] For a RD system, *L* is defined as the nearest image distance (or simulation cell length). Among cubic, RD, and TO shapes, RD has the smallest volume and is the most spherical simulation cell. Thus, RD systems can be used to significantly reduce computational costs (by about 29%).[67] Figure 2.1 shows a bubble inside a cubic and a RD system, where the greater efficiency of the RD is immediately apparent.

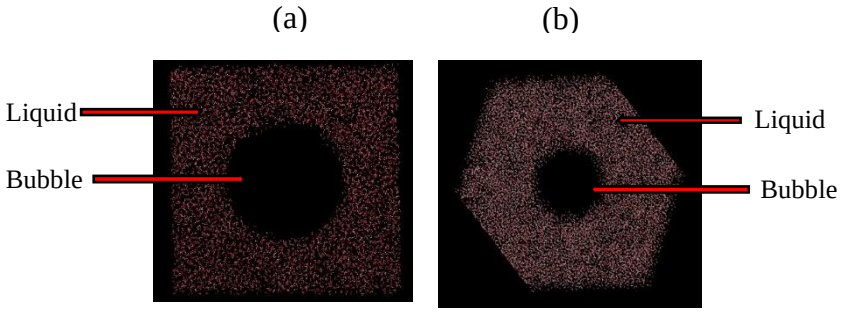

Figure 2.1: A bubble inside (a) a cubic and (b) a RD simulation cell, where the middle vacant space indicates the bubble. Slices through the systems are shown.

Experiments have typically reported sizes of BNBs varying from 50 nm to 500 nm.[46] In MD simulations, simulating a 50 nm BNB would represent an enormous computational cost. For example, a cubic system with L = 100 nm for a 50 nm diameter bubble surrounded by water at ambient conditions would require about 30,000,000 water molecules in the system. Consequently, in the literature, the diameters of the bubbles typically used in MD simulations are in the range of 5 to 10 nm. To simulate a 5 nm bubble in a L = 10 nm cubic box then requires about 31,200 water molecules. Therefore, MD simulations, at least at present, are limited to bubbles smaller than those seen in experiments.

In terms of the gas inside the bubble, some studies have filled bubbles with gases such as methane[10,56], propane[10], O_2[46] or N_2[66]. Other studies have started with just an empty cavity.[30,31] However, with time a small number of liquid molecules will evaporate into the empty cavity, so the cavity can be seen to be filled by gas[31] according to the vapor pressure of the liquid phase. Since the water vapor pressure at room temperature is quite small[65], it is rare to find vapor phase molecules inside the bubble in simulations at room temperature. Hence, these vapor phase molecules can be reasonable ignored.

2.3.2. Simulation methodologies

Different BNB simulation studies have followed somewhat different methodologies to introduce the bubble into the system and then to simulate the system. However, these choices of methodologies are usually related to the focus of the study (i.e., formation of a bubble[68]/ spontaneous cavitation[68], behavior of a stable bubble[56], etc.) and system details such as whether the bubble is filled or a cavity.

In order to achieve bubble formation, Matsumoto and Tanaka[31], applied a repulsive force to the center of an equilibrated system to make a cavity with a desired radius. Once the cavity was formed and system equilibrated, the force was removed. In Matsumoto's[69] simulation study of BNBs, water molecules were removed from a spherical region at the center of the system to make the cavity. Hong et al.[30] also made a cavity at the center of the simulation cell by removing water molecules corresponding to roughly the required bubble sizes. In Hewage et al.[46] study on the behavior of oxygen BNBs, they deleted the water molecule at the center of a sphere and replaced them with an appropriate number of O_2 molecules.

Once the required bubble is made, before observing bubble behavior and measuring properties such as pressure, the system should first be appropriately equilibrated, which may require simulation times in the 1 - 200 ns range.[56] If the bubble is an empty cavity, it requires only mechanical equilibration. However, if the bubble is filled with a gas, it requires both mechanical and chemical equilibration. Usually, the time taken to reach mechanical equilibrium is shorter (it is a faster process) compared to chemical equilibrium (a much slower process). Therefore, systems with filled bubbles require longer times to equilibrate compared to systems with cavity bubbles.[56,69]

For system equilibration, both constant volume and temperature conditions (NVT, which is also called the canonical ensemble) or constant pressure and temperature conditions (NPT) can be used depending on whether the bubble is filled or not.[31,46] If simulating a cavity bubble, one cannot use NPT conditions to equilibrate a bubble containing system because at any positive pressure the liquid molecules will simply move to fill the cavity space and the bubble/cavity will disappear. So, such a cavity system can only be stabilized under constant volume conditions. However, if the

bubble is filled with sufficient gas, so as to give a positive pressure, a NPT simulation can be performed. Thus, if the bubble is filled, it is possible to carried out either NPT and NVT simulations.[5]

2.3.3 Truncation of interactions and periodic boundary conditions

In order to get reasonably accurate and reliable values for system properties, it is important to carefully evaluate all the molecular interactions in the system. For a system in a PBC (as discuss further below) this may include interactions out to infinity, but due to computational resource implications, one typically limits the interactions that are considered in determining the forces during the simulation. Luty et al.[70] performed a detailed analysis and comparison of various approaches for modelling interactions in molecular systems. According to them, one option is to introduce a boundary for the system and assume that the system is surrounded by a vacuum. However, if we assume a surrounding vacuum (i.e., a finite system), the atoms or molecules at the boundary will experience unbalanced forces and this will directly affect the system properties. Therefore, rather than assume a finite system, computational chemists have developed various techniques to model infinite system interactions.[70] Recall, a well-known and common approach is to assume a system is surrounded by an infinite number of replicas of itself is known as PBC. PBC are extremely effective at reducing the effects of boundaries. The impact of PBC on BNB simulations will be discussed later in this section. Within PBC, the interactions within the system become, in principle, infinite.[70]

Recall that the interactions in a simulation system can be divided into two categories, namely bonded and non-bonded interactions. The non-bonded interactions can be further divided into subcategories of long-range and short-range interactions.[49] As will be discussed below, long-range

interactions arise from coulombic interactions and typically require special care. Short-range interactions, sometimes known as van der Waals interactions, include a component to account for dispersion and a repulsive term (due to the overlapping of the electron clouds). The Lennard-Jones (*LJ*) potential is one very commonly used form for short-range non-bonded interactions.[49] The *LJ* energy associated with atoms i and j at a distance r_{ij} can be written as

$$U_{(r_{ij})} = 4\varepsilon \{(\frac{\sigma}{r_{ij}})^{12} - (\frac{\sigma}{r_{ij}})^{6}\} \ , \tag{2.9}$$

where ε is the strength of the short-range interaction, and σ is the particle diameter at which the potential energy given by eqn. 2.9 is zero. In eqn. 2.9, $(\frac{\sigma}{r_{ij}})^6$ is the dispersive interaction term, while $(\frac{\sigma}{r_{ij}})^{12}$ is the repulsive term.[49]

To calculate short-range interactions, a cut-off length is usually introduced, where the interactions of a particular atom are truncated (i.e., set to zero) beyond the cut-off distance. To help correct for this truncation, a tail correction is frequently added to the energy and pressure. Selecting a suitable cut-off length is important as it can impact important properties of the system, including the system energy, pressure, and surface properties.[70] However, a range of cut-off length values are reported in the literature for BNB simulations (i.e., 0.9 nm[66], 1.0 nm[68], 1.1 nm[10] , 1.2 nm[30,31] , 1.6 nm[69]), where none of these previous studies appear to provide a clear justification and validation for the particular cut-off value they used. In order to investigate the possible influence of the short-range cut-off length value, it is important to have done a cut-off length optimization as a preliminary step prior to performing simulations of BNBs.

In homogeneous systems, such as for a bulk liquid water system, the use of cut-off lengths and appropriate tails corrections are found to give consistent and reasonably accurate results for properties such as the pressure.[70] However, a system containing a BNB is no longer homogeneous. Figure 2.2 features the heterogenous environment around the molecule *j* at the bubble surface. Therefore, the use of standard cut-off schemes with tail corrections will become problematic for BNBs in solution. It is important to realize that there is an alternative approach to spherical cut-offs of the inter-molecular interactions that is suitable for a non-homogenous system, namely the PME summation.[70]

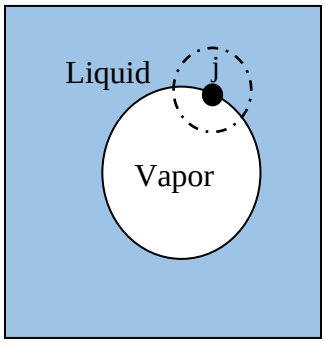

Figure 2.2: Schematic of a BNB system where the interface molecule j experiences a heterogenous environment. The dashed line represents the short-range cut-off radius for molecule j.

The long-range interactions in a system arise from coulombic interactions (i.e., due to atomic charges or molecular dipoles). However, in an infinite system it is not possible to directly evaluate all the electrostatic interactions. As truncation of these coulombic interactions can give rise to significant errors, Ewald summation is commonly used to calculate the long-range interactions. In Ewald summation, the interactions are split into short-range and long-range terms. The shape of the short-range interaction is modified, through inclusion of a screening term, where the complementary function is introduced to the long-range component.[70] One widely used implementation of Ewald summation is the PME method, as discussed in detailed by Luty et al.[70]

As described by these authors, when applied to the coulombic interaction between point charges, the PME method introduces a shielding charge distribution (of equal magnitude) that is subtracted from the original point charge. The resulting interaction from the combination of the point charge and shielding charge is a short-range function which is easily handled by a direct summation over near neighbors.[70] Effects of the shielding charges, which are long-range, but which will be of a much smoother nature than those of the original point charges, are then evaluated using Fourier methods. It is important to point out that Ewald summations, and the PME method in particular, can be applied to other interactions, including the dispersion interaction term. By evaluating dispersion interactions with the PME method one is able to avoid the use of an interaction cut-off, and hence, should be better able to obtain accurate system properties for a BNB containing system. The PME method can improve both the accuracy of the electrostatic energy calculations and simulation time.[70] Therefore, in BNB simulations, most studies have used PME for evaluating the long-range interaction.[10,56,68] However, for PME, one does need to choose the parameters within the algorithm, such as PME order and Fourier spacing, (see section 4.1.2) to be appropriate for the system requirements. In the study of Bird et al.[66] they have used Wolf summation in their simulations of coalescence of BNBs, where their system contained more than 10 000 000 water molecules, which is much larger compared to the other BNB simulations.[66]

PBC are typically used in simulations of most systems including those with BNBs. PBC can be applied to all three x, y, and z directions, or any combination of interest.[67] However, it is also important to realize the potential impacts of PBC in simulations of BNBs. Figure 2.3(a) shows a simulation system containing a BNB. Figure 2.3(b) shows the same system, but now includes 3 of the image systems that are present in PBC, each containing a BNB. It should then be noted that

PBC will repeat the simulation cell in all three x, y and z directions, and in principle there are an infinite number of these replica cells.

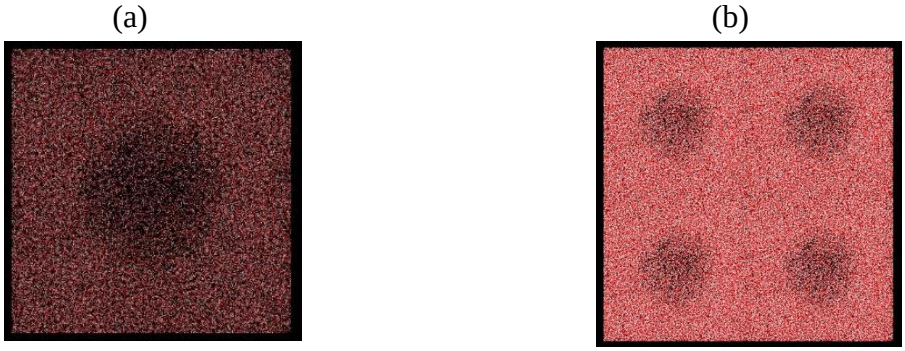

Figure 2.3: (a) Basic simulation cell containing a BNB; (b) Simulation cell along with 3 of its images (in PBC).

Although PBC are important, as they approximate an infinite bulk system, there is an unavoidable issue that occurs. One of these arises because of interactions between images, as will be discussed below. Another is associated with bubble movement. As BNBs will exhibit Brownian motion[4,30], with the movement of a bubble, all image bubbles also move identically. One can expect that the movement of a bubble will produce a hydrodynamic flow of the liquid molecules around it, where this flow will be in the opposite direction. Clearly the flows from neighboring bubbles may interact and effect the bubble's normal (expected) behavior[67]. Thus, if the mobility of a BNB is measured during the study, without sufficient separation between a BNB and all its images, such effects may cause systematic errors in the results.

2.4 Analysis

Once the system setup is selected and simulation is completed, the system/bubble behavior and properties can be analysed. However, it is important to develop a suitable method to calculate each average system property appropriately and carefully. This section discusses the behavior of BNBs

and different methodologies that previous studies have followed to obtain average system properties.

2.4.1. System changes upon bubble insertion

In a majority of the simulation studies to date, the bubble is initially placed at the center of the system.[30,56,69] For both filled and cavity bubbles, the system undergoes changes upon insertion of the bubble to establish a new equilibrium. If one generates an empty bubble in the system by removing some liquid molecules, the remaining liquid molecules will want to fill the cavity, and the bubble can be expected to shrink slightly.[30,69] As a result, the surrounding bulk liquid will tend to be stretched (at constant volume conditions), or equivalently to experience a negative pressure.[29] This behavior can also be seen as arising from the interfacial surface tension wanting to reduce the surface area by collapsing the bubble.[29] While a small number of liquid molecules may evaporate and appear inside the bubble, the liquid molecules resist filling the vacant volume because of their strong intermolecular interactions.[69] When the pressure in the bulk liquid is balanced by the forces acting on the interface and the pressure of any gas inside the bubble, the bubble will have attained an equilibrium and its volume no longer changes.[29] Consistent with this behavior, Hewage and Meegoda[46] noted that their initial 10 nm bubble became a stable 9 nm bubble during their simulation. Hong et al.[30] noted the change of the bubble radius during their simulation, and they observed that the bubble shrank within the first 200 ps before attaining a stable size. However, their 5.22 nm and 5.24 nm bubbles were observed to completely collapse after 500 ps and 4 ns, respectively. Therefore, not all bubbles are able to achieve a balance of the forces required for stability, i.e., the cohesive forces within the bulk liquid are not sufficiently strong to resist the collapse of the bubble.[30] From the analysis of Matsumoto and Tanaka[31], it is clear that the initial bubble size relative to the overall system size is an important factor for achieving a stable unfilled

bubble (or cavity). Further, another mechanism by which bubbles may disappear is through fusion with a neighbouring bubble.[56,66] Through a coalescence process, it is possible to form a larger, more stable bubble. Bird et al.[66] have examined bubble coalescence in water in their simulations with very large systems.

As discussed above, the initial bubble is likely to undergo changes as the system relaxes towards an equilibrium. Therefore, it is important to study the equilibrated system properties, including the bubble size and position. Once the simulation is completed, system properties can be evaluated by separate analysis. In the next section, methodologies that previous studies have used to analyse the bubble radius and position are given.

2.4.2. Bubble radius and position analysis

Since BNBs are very small, the method for calculating their radii needs to be very accurate as even a small error in the bubble diameter calculation will make a significant large percentage error. This problem is further compounded by the fact that the surfaces of BNBs exhibit fluctuations, and their surfaces are not uniform.[56,69] Therefore, special care is needed when calculating the bubble size.

Another important factor that needs to be considered during bubble size analysis is the movement of the BNBs. Recall, from both experimental and simulation results it has been confirmed that BNBs exhibit Brownian motion[5,46,69]. Therefore, the position of the bubble needs to be tracked during a simulation to allow for the calculation of bubble size.

To find the position of the bubble, Matsumoto and Tanaka[31] divided the system into meshes of about 0.05 nm cubes and consider the vacant mesh points as belonging to the bubble. The average position of the vacant cubes is then taken as the center of the bubble. Assuming a spherical shape for the bubble, the density profile of the system was then fitted with a hyperbolic function.[31] Although it is possible to count the vacant mesh points to get the size of the bubble, it does not give an accurate bubble size, as cubes cannot fit into a sphere. Therefore, this may cause an error in calculating the volume of the BNBs. In the case of gas filled bubbles, one can determine the position and size of the bubble from the positions of the gas molecules inside it. Lu et al.[3] calculated the size of their methane bubble by averaging the largest distance between two methane molecules in the interface. They also confirmed the selected methane molecules are in the bubble interface by counting the number of water molecules around the selected methane molecules.[56]

As mentioned earlier, by monitoring the position of a BNB during a simulation trajectory, one finds that the bubble exhibits random displacements. Snapshots examined in the work of Hong et al[30] confirmed similar Brownian motion of BNBs. The study of Lu and coworkers[56] investigated the bubble dynamics of two methane BNBs in a system. They used a system with two 5 nm or two 10 nm methane bubbles, where a coarse-grained force field was employed to improve the computational efficiency. At the beginning of the simulation, the two bubbles were at 20 nm distance. The 5 nm bubbles took about 721 ns for coalescence while the 10 nm bubbles took about 353 ns. However, from the given snapshots, it is clear that the larger bubbles moved directly towards each other, while the small bubbles showed a ‘close-away-close’ movement (i.e., not directly towards the adjacent bubble) for some time. Also, these authors examined the diffusion of BNBs and confirmed that the smaller BNBs have greater self diffusion via Brownian motion.[56] In

the simulation literature, they consistently conclude that the BNBs show Brownian motion in their solutions, which is in agreement with experimental studies.[4,5,46,56]

Ghaani, et al.[10] studied the displacement of BNBs under a uniform electric field for propane and methane BNBs in water. They have calculated the drift velocity (the net velocity due to the electric field) as a function of the applied field strength, where they have varied the applied filed from 0 to 1.4 V/nm. They compared drift velocities for small (2.5 nm) and big (5 nm) bubbles and the results suggest that a larger (5 nm) bubble is needed for physical realism. These results confirm that for mobility of BNBs in an electric field, a surface charge is not required and surface polarization at gas-water interface is sufficient.[10]

2.4.3. Bubble surface thickness

Although BNBs are usually taken as perfect spheres, snapshots of BNBs in MD simulations clearly show the bubble surface is not uniform.[56,69] Additionally, it has been confirmed previously that the bubble surface has a finite thickness.[31,69] To find the thickness of the BNB interface, radial distribution profiles have been commonly used.[31,69] Matsumoto and Tanaka[31]and Hewage et al.[46] have reported the radial distribution profiles from the bubble center, and the interface thickness can be found from the width of the sigmoidal graphs. To obtain the radial distribution profile, a reference point is required, and therefore it is important to know the position of the center of the bubble. Visualization techniques, such as with VMD[60], can be useful for finding the center and size of a bubble, and the interface thickness.

2.5 Summary

In this chapter, the research background and previous MD simulation studies of BNBs were presented. From this discussion, we can summarize that BNBs are very stable, multi-purpose, and environmentally friendly solution nano-structures that are widely used in various fields such as medicine, agriculture, and chemistry. The focus on BNBs has not only been on their applications, but also on understanding their unexpected long-term stability. As the main focus of this study is to identify the factors that contribute to the mechanical stability of BNBs, this chapter reviewed previous MD simulation studies that have been performed. Based on the previous work, we have conducted simulations and developed suitable analysis approaches for the BNB systems of interest. Details for the simulation methodologies will now be discussed in the next chapter.

2.6 References

1. Zhou, Y.; Han, Z.; He, C.; Feng, Q.; Wang, K.; Wang, Y.; Luo, N.; Dodbiba, G.; Wei, Y.; Otsuki, A.; Fujita, T. Long-Term Stability of Different Kinds of Gas Nanobubbles in Deionized and Salt Water. *Materials* **2021**, *14* (7). https://doi.org/10.3390/ma14071808.
2. Attard, P. The Stability of Nanobubbles. *Eur Phys J Spec Top* **2014**, *223* (5), 893–914. https://doi.org/10.1140/epjst/e2013-01817-0.
3. Vehmas, T.; Makkonen, L. Metastable Nanobubbles. *ACS Omega* **2021**, *6* (12), 8021–8027. https://doi.org/10.1021/acsomega.0c05384.
4. Alheshibri, M.; Qian, J.; Jehannin, M.; Craig, V. S. J. A History of Nanobubbles. *Langmuir* **2016**, *32* (43), 11086–11100. https://doi.org/10.1021/acs.langmuir.6b02489.
5. Meegoda, J. N.; Aluthgun Hewage, S.; Batagoda, J. H. Stability of Nanobubbles. *Environ Eng Sci* **2018**, *35* (11), 1216–1227. https://doi.org/10.1089/ees.2018.0203.
6. Nirmalkar, N.; Pacek, A. W.; Barigou, M. On the Existence and Stability of Bulk Nanobubbles. *Langmuir* **2018**, *34* (37), 10964–10973. https://doi.org/10.1021/acs.langmuir.8b01163.
7. Chen, C.; Li, J.; Zhang, X. The Existence and Stability of Bulk Nanobubbles: A Long-Standing Dispute on the Experimentally Observed Mesoscopic Inhomogeneities in Aqueous Solutions. *Communications in Theoretical Physics*. IOP Publishing Ltd March 1, 2020. https://doi.org/10.1088/1572-9494/ab6183.

8. Wang, S.; Liu, M.; Dong, Y. Understanding the Stability of Surface Nanobubbles. *Journal of Physics Condensed Matter* **2013**, *25* (18). https://doi.org/10.1088/0953-8984/25/18/184007.

9. Zhang, H.; Guo, Z.; Zhang, X. Surface Enrichment of Ions Leads to the Stability of Bulk Nanobubbles. *Soft Matter* **2020**, *16* (23), 5470–5477. https://doi.org/10.1039/d0sm00116c.

10. Ghaani, M. R.; Kusalik, P. G.; English, N. J. Massive Generation of Metastable Bulk Nanobubbles in Water by External Electric Fields. *Sci Adv* **2020**, *6* (14). https://doi.org/10.1126/sciadv.aaz0094.

11. Epstein, P. S.; Plesset, M. S. On the Stability of Gas Bubbles in Liquid-Gas Solutions. *J Chem Phys* **1950**, *18* (11), 1505–1509. https://doi.org/10.1063/1.1747520.

12. Nirmalkar, N.; Pacek, A. W.; Barigou, M. Interpreting the Interfacial and Colloidal Stability of Bulk Nanobubbles. *Soft Matter* **2018**, *14* (47), 9643–9656. https://doi.org/10.1039/c8sm01949e.

13. Li, M.; Ma, X.; Eisener, J.; Pfeiffer, P.; Ohl, C. D.; Sun, C. How Bulk Nanobubbles Are Stable over a Wide Range of Temperatures. *J Colloid Interface Sci* **2021**, *596*, 184–198. https://doi.org/10.1016/j.jcis.2021.03.064.

14. Zhou, Y.; Han, Z.; He, C.; Feng, Q.; Wang, K.; Wang, Y.; Luo, N.; Dodbiba, G.; Wei, Y.; Otsuki, A.; Fujita, T. Long-Term Stability of Different Kinds of Gas Nanobubbles in Deionized and Salt Water. *Materials* **2021**, *14* (7). https://doi.org/10.3390/ma14071808.

15. Zargarzadeh, L.; Elliott, J. A. W. Thermodynamics of Surface Nanobubbles. *Langmuir* **2016**, *32* (43), 11309–11320. https://doi.org/10.1021/acs.langmuir.6b01561.

16. Ji, Y.; Guo, Z.; Tan, T.; Wang, Y.; Zhang, L.; Hu, J.; Zhang, Y. Generating Bulk Nanobubbles in Alcohol Systems. *ACS Omega* **2021**, *6* (4), 2873–2881. https://doi.org/10.1021/acsomega.0c05222.

17. Jadhav, A. J.; Barigou, M. Bulk Nanobubbles or Not Nanobubbles: That Is the Question. *Langmuir* **2020**, *36* (7), 1699–1708. https://doi.org/10.1021/acs.langmuir.9b03532.

18. Fang, Z.; Wang, X.; Zhou, L.; Zhang, L.; Hu, J. Formation and Stability of Bulk Nanobubbles by Vibration. *Langmuir* **2020**, *36* (9), 2264–2270. https://doi.org/10.1021/acs.langmuir.0c00036.

19. Gent, A. N.; Tompkins, D. A. Nucleation and Growth of Gas Bubbles in Elastomers. *J Appl Phys* **1969**, *40* (6).

20. Generation of Bulk Nanobubbles Using a High-Shear Rotor-Stator Device. *Ind Eng Chem Res* **2021**, *60* (23), 8597–8606. https://doi.org/10.1021/acs.iecr.1c01233.

21. Lee, J. il; Kim, J. M. Influence of Temperature on Bulk Nanobubble Generation by Ultrasonication. *Colloids and Interface Science Communications* **2022**, *49*. https://doi.org/10.1016/j.colcom.2022.100639.

22. Johnson, B. D.; Cooke, R. C. *Generation of Stabilized Microbubbles in Seawater*; 1981; Vol. 213, pp 209–211. http://www.jstor.org/stable/1687157 (accessed 2023-02-12).

23. Ma, X.; Li, M.; Xu, X.; Sun, C. Coupling Effects of Ionic Surfactants and Electrolytes on the Stability of Bulk Nanobubbles. *Nanomaterials* **2022**, *12* (19). https://doi.org/10.3390/nano12193450.

24. Eklund, F.; Alheshibri, M.; Swenson, J. Differentiating Bulk Nanobubbles from Nanodroplets and Nanoparticles. *Curr Opin Colloid Interface Sci* **2021**, *53*. https://doi.org/10.1016/j.cocis.2021.101427.

25. Ljunggren, S.; Eriksson, J. C. COLLOIDS A The Lifetime of a Colloid-Sized Gas Bubble in Water and the Cause of the Hydrophobic Attraction1. *Colloids and Surfaces SURFACES A: Physicochemical and Engineering Aspects* **1997**, *129*, 151–155.

26. Weijs, J. H.; Seddon, J. R. T.; Lohse, D. Diffusive Shielding Stabilizes Bulk Nanobubble Clusters. *ChemPhysChem* **2012**, *13* (8), 2197–2204. https://doi.org/10.1002/cphc.201100807.

27. Wang, S.; Zhou, L.; Gao, Y. Can Bulk Nanobubbles Be Stabilized by Electrostatic Interaction? *Physical Chemistry Chemical Physics* **2021**, *23* (31), 16501–16505. https://doi.org/10.1039/d1cp01279g.

28. Manning, G. S. On the Thermodynamic Stability of Bubbles, Immiscible Droplets, and Cavities. *Physical Chemistry Chemical Physics* **2020**, *22* (31), 17523–17531. https://doi.org/10.1039/d0cp02517h.

29. Gao, Z.; Wu, W.; Sun, W.; Wang, B. Understanding the Stabilization of a Bulk Nanobubble: A Molecular Dynamics Analysis. *Langmuir* **2021**, *37* (38), 11281–11291. https://doi.org/10.1021/acs.langmuir.1c01796.

30. Hong, S. N.; Choe, S. H.; Jong, U. G.; Pak, M. S.; Yu, C. J. The Maximum Interbubble Distance in Relation to the Radius of Spherical Stable Nanobubble in Liquid Water: A Molecular Dynamics Study. *Fluid Phase Equilib* **2019**, *487*, 45–51. https://doi.org/10.1016/j.fluid.2019.01.014.

31. Matsumoto, M.; Tanaka, K. Nano Bubble-Size Dependence of Surface Tension and inside Pressure. *Fluid Dyn Res* **2008**, *40* (7–8), 546–553. https://doi.org/10.1016/j.fluiddyn.2007.12.006.

32. Israelachvili, J. N. Chapter 14 - Electrostatic Forces between Surfaces in Liquids. In *Intermolecular and Surface Forces (Third Edition)*; Israelachvili, J. N., Ed.; Academic Press: San Diego, 2011; pp 291–340. https://doi.org/https://doi.org/10.1016/B978-0-12-375182-9.10014-4.

33. Satpute, P. A.; Earthman, J. C. Hydroxyl Ion Stabilization of Bulk Nanobubbles Resulting from Microbubble Shrinkage. *J Colloid Interface Sci* **2021**, *584*, 449–455. https://doi.org/10.1016/j.jcis.2020.09.100.

34. Bunkin, N. F.; Bunkin, F. v. Bubbstons: Stable Microscopic Gas Bubbles in Very Dilute Electrolytic Solutions. *Amarican Institute of Physics* **1992**, 271–278.

35. Jin, F.; Li, J.; Ye, X.; Wu, C. Effects of PH and Ionic Strength on the Stability of Nanobubbles in Aqueous Solutions of α-Cyclodextrin. *Journal of Physical Chemistry B* **2007**, *111* (40), 11745–11749. https://doi.org/10.1021/jp074260f.

36. Botti, A.; Bruni, F.; Imberti, S.; Ricci, M. A.; Soper, A. K. Solvation Shell of OH- Ions in Water. *J Mol Liq* **2005**, *117* (1–3), 81–84. https://doi.org/10.1016/j.molliq.2004.08.013.

37. Matyushov, D. v. Electrophoretic Mobility without Charge Driven by Polarisation of the Nanoparticle-Water Interface. *Mol Phys* **2014**, *112* (15), 2029–2039. https://doi.org/10.1080/00268976.2014.882521.

38. Martins-Costa, M. T. C.; Ruiz-Lopez, M. F. Solvation Effects on Electronic Polarization and Reactivity Indices at the Air–Water Interface: Insights from a Theoretical Study of Cyanophenols. *Theor Chem Acc* **2015**, *134* (2). https://doi.org/10.1007/s00214-014-1609-z.

39. Vácha, R.; Marsalek, O.; Willard, A. P.; Bonthuis, D. J.; Netz, R. R.; Jungwirth, P. Charge Transfer between Water Molecules as the Possible Origin of the Observed Charging at the Surface of Pure Water. *Journal of Physical Chemistry Letters* **2012**, *3* (1), 107–111. https://doi.org/10.1021/jz2014852.

40. Goldman, S. Generalizations of the Young-Laplace Equation for the Pressure of a Mechanically Stable Gas Bubble in a Soft Elastic Material. *Journal of Chemical Physics* **2009**, *131* (18). https://doi.org/10.1063/1.3259973.

41. Rezaei Nejad, H.; Ghassemi, M.; Mirnouri Langroudi, S. M.; Shahabi, A. A Molecular Dynamics Study of Nano-Bubble Surface Tension. *Mol Simul* **2011**, *37* (1), 23–30. https://doi.org/10.1080/08927022.2010.513007.

42. Shi, X.; Xue, S.; Marhaba, T.; Zhang, W. Probing Internal Pressures and Long-Term Stability of Nanobubbles in Water. *Langmuir* **2021**, *37* (7), 2514–2522. https://doi.org/10.1021/acs.langmuir.0c03574.

43. Menzl, G.; Gonzalez, M. A.; Geiger, P.; Caupin, F.; Abascal, J. L. F.; Valeriani, C.; Dellago, C. Molecular Mechanism for Cavitation in Water under Tension. *Proc Natl Acad Sci U S A* **2016**, *113* (48), 13582–13587. https://doi.org/10.1073/pnas.1608421113.

44. Yamamoto, T.; Ohnishi, S. Molecular Dynamics Study on Helium Nanobubbles in Water. *Physical Chemistry Chemical Physics* **2011**, *13* (36), 16142–16145. https://doi.org/10.1039/c1cp22018g.

45. Maheshwari, S.; van der Hoef, M.; Zhang, X.; Lohse, D. Stability of Surface Nanobubbles: A Molecular Dynamics Study. *Langmuir* **2016**, *32* (43), 11116–11122. https://doi.org/10.1021/acs.langmuir.6b00963.

46. Aluthgun Hewage, S.; Meegoda, J. N. Molecular Dynamics Simulation of Bulk Nanobubbles. *Colloids Surf A Physicochem Eng Asp* **2022**, *650*, 129565. https://doi.org/10.1016/j.colsurfa.2022.129565.

47. Tuckerman, M. E.; Martyna, G. J. Understanding Modern Molecular Dynamics: Techniques and Applications. *Journal of Physical Chemistry B* **2000**, *104* (2), 159–178. https://doi.org/10.1021/jp992433y.

48. Hollingsworth, S. A.; Dror, R. O. Molecular Dynamics Simulation for All. *Neuron* **2018**, *99* (6), 1129–1143. https://doi.org/10.1016/j.neuron.2018.08.011.

49. Braun, E.; Gilmer, J.; Mayes, H. B.; Mobley, D. L.; Monroe, J. I.; Prasad, S.; Zuckerman, D. M. Best Practices for Foundations in Molecular Simulations [Article v1.0]. *Living J Comput Mol Sci* **2019**, *1* (1). https://doi.org/10.33011/livecoms.1.1.5957.

50. Rapaport D.C. *The Art of Molecular Dynamics Simulation, 2nd Ed.*; Cambridge University Press: Cambridge, 2004.

51. van Gunsteren, W. F.; Berendsen, H. J. C. A Leap-Frog Algorithm for Stochastic Dynamics. *Mol Simul* **1988**, *1* (3), 173–185. https://doi.org/10.1080/08927028808080941.

52. Hedman, F.; Stockholms universitet. Avdelningen för fysikalisk kemi. *Algorithms for Molecular Dynamics Simulations : Advancing the Computational Horizon*; Department of Physical, Inorganic and Structural Chemistry, Stockholm University, 2006.

53. Ponder, J. W.; Case, D. A. Force Fields for Protein Simulations. In *Protein Simulations*; Advances in Protein Chemistry; Academic Press, 2003; Vol. 66, pp 27–85. https://doi.org/https://doi.org/10.1016/S0065-3233(03)66002-X.

54. Brooks, B. R.; Brooks, C. L.; Mackerell, A. D.; Nilsson, L.; Petrella, R. J.; Roux, B.; Won, Y.; Archontis, G.; Bartels, C.; Boresch, S.; Caflisch, A.; Caves, L.; Cui, Q.; Dinner, A. R.; Feig, M.; Fischer, S.; Gao, J.; Hodoscek, M.; Im, W.; Kuczera, K.; Lazaridis, T.; Ma, J.; Ovchinnikov, V.; Paci, E.; Pastor, R. W.; Post, C. B.; Pu, J. Z.; Schaefer, M.; Tidor, B.; Venable, R. M.; Woodcock, H. L.; Wu, X.; Yang, W.; York, D. M.; Karplus, M. CHARMM: The Biomolecular Simulation Program. *J Comput Chem* **2009**, *30* (10), 1545–1614. https://doi.org/10.1002/jcc.21287.

55. Sun, S.; Poudel, P.; Alexov, E.; Li, L. Electrostatics in Computational Biophysics and Its Implications for Disease Effects. *Int J Mol Sci* **2022**, *23* (18). https://doi.org/10.3390/ijms231810347.

56. Lu, Y.; Yang, L.; Kuang, Y.; Song, Y.; Zhao, J.; Sum, A. K. Molecular Simulations on the Stability and Dynamics of Bulk Nanobubbles in Aqueous Environments. *Physical Chemistry Chemical Physics* **2021**, *23* (48), 27533–27542. https://doi.org/10.1039/d1cp03325e.

57. Abraham, M. J.; Murtola, T.; Schulz, R.; Páll, S.; Smith, J. C.; Hess, B.; Lindah, E. Gromacs: High Performance Molecular Simulations through Multi-Level Parallelism from Laptops to Supercomputers. *SoftwareX* **2015**, *1–2*, 19–25. https://doi.org/10.1016/j.softx.2015.06.001.

58. Martinez, L.; Andrade, R.; Birgin, E. G.; Martínez, J. M. PACKMOL: A Package for Building Initial Configurations for Molecular Dynamics Simulations. *J Comput Chem* **2009**, *30* (13), 2157–2164. https://doi.org/10.1002/jcc.21224.

59. Phillips, J. C.; Hardy, D. J.; Maia, J. D. C.; Stone, J. E.; Ribeiro, J. v.; Bernardi, R. C.; Buch, R.; Fiorin, G.; Hénin, J.; Jiang, W.; McGreevy, R.; Melo, M. C. R.; Radak, B. K.; Skeel, R. D.; Singharoy, A.; Wang, Y.; Roux, B.; Aksimentiev, A.; Luthey-Schulten, Z.; Kalé, L. v.; Schulten, K.; Chipot, C.; Tajkhorshid, E. Scalable Molecular Dynamics on CPU and GPU Architectures with NAMD. *Journal of Chemical Physics* **2020**, *153* (4). https://doi.org/10.1063/5.0014475.

60. Humphrey, W.; Dalke, A.; Schulten, K. VMD – Visual Molecular Dynamics. *J Mol Graph* **1996**, *14*, 33–38.

61. *Grace - Free Software Directory*. https://directory.fsf.org/wiki/Grace#tab=Overview (accessed 2023-02-11).

62. Vega, C.; de Miguel, E. Surface Tension of the Most Popular Models of Water by Using the Test-Area Simulation Method. *Journal of Chemical Physics* **2007**, *126* (15). https://doi.org/10.1063/1.2715577.

63. Alkhwaji, A.; Elbahloul, S.; Fadzli Bin, K.; Bakar, A.; Abdullah, Z. The Comparison Between Water Models In Predicting Water Thermal And Dynamic Properties From Molecular Dynamics. *INTERNATIONAL JOURNAL OF SCIENTIFIC & TECHNOLOGY RESEARCH* **2020**, *9* (08), 511–516.

64. Topsoe, H.; Dumesic, J. A.; Derouane, E. G.; Kusalik, P. G.; Svishchev, I. M. *Helpful Discussions with The Spatial Structure in Liquid Water*; Kiuwer Academic, 1993; Vol. 2.

65. Vega, C.; Abascal, J. L. F.; Nezbeda, I. Vapor-Liquid Equilibria from the Triple Point up to the Critical Point for the New Generation of TIP4P-like Models: TIP4P/Ew, TIP4P/2005, and TIP4P/Ice. *Journal of Chemical Physics* **2006**, *125* (3). https://doi.org/10.1063/1.2215612.

66. Bird, E.; Smith, E.; Liang, Z. Coalescence Characteristics of Bulk Nanobubbles in Water: A Molecular Dynamics Study Coupled with Theoretical Analysis. *Phys Rev Fluids* **2021**, *6* (9). https://doi.org/10.1103/PhysRevFluids.6.093604.

67. Wassenaar, T. A.; Mark, A. E. The Effect of Box Shape on the Dynamic Properties of Proteins Simulated under Periodic Boundary Conditions. *J Comput Chem* **2006**, *27* (3), 316–325. https://doi.org/10.1002/jcc.20341.

68. Min, S. H.; Berkowitz, M. L. Bubbles in Water under Stretch-Induced Cavitation. *Journal of Chemical Physics* **2019**, *150* (5). https://doi.org/10.1063/1.5079735.

69. MATSUMOTO, M. Surface Tension and Stability of a Nanobubble in Water: Molecular Simulation. *Journal of Fluid Science and Technology* **2008**, *3* (8), 922–929. https://doi.org/10.1299/jfst.3.922.

70. Luty, B. A.; Davis, M. E.; Tironi, I. G.; van Gunsteren, W. F. A Comparison of Particle-Particle, Particle-Mesh and Ewald Methods for Calculating Electrostatic Interactions in Periodic Molecular Systems. *Mol Simul* **1994**, *14* (1), 11–20. https://doi.org/10.1080/08927029408022004.

Chapter 3 : SIMULATION AND ANALYSIS METHODOLOGIES

This chapter will provide a detailed discussion of the simulation and analysis methodologies followed in this study to complete each of the three tasks outlined in Chapter 1. Starting with the selection of a short-range interaction calculation method, this chapter will include the methodologies followed for determining the bubble sizes and positions, interface thickness, and pressure contributions from BNB simulations.

3.1. Task 1: Selection of a short-range interaction calculation method for MD simulation of BNBs.

This section discusses selection of simulation systems, including system size, bubble size, number of water molecules, and simulation time for each simulation. Furthermore, the simulation methodology, which includes system equilibration and bubble insertion will be discussed. Recall from section 2.3.3 that a suitable short-range interaction calculation method is essential for BNB simulations. To compare the effect of using a cut-off length and the PME method for short-range interaction calculations, the average system pressures were obtained and compared for the same system. Additionally, the impact of different cut-off lengths and different values for selected parameters in the PME method were evaluated.

3.1.1 Selecting primary systems

As discussed in section 2.3.1, there are two shapes of systems used in the simulations of this study, namely cubic (C) and rhombic dodecahedron (RD). Although cubic systems are easy to simulate, for larger systems the RD shape was used almost exclusively to reduce the computational cost. The primary set of systems studied included two cubic (C1 and C2) and six RD systems (RD1 –

RD6). However, additional systems were built in subsequent stages of this project based on the specific needs (i.e., for separation analysis and the bulk liquid density). Table 3.1 includes the systems prepared, including the number of water molecules before and after the bubble insertion, as well as the initial bubble radius. The number of water molecules were calculated using a molecular number density (N/V) of 33.4 molecules/nm^3 which corresponds to liquid water at room temperature (298 K) and 1 bar pressure.[5] The equations used for determining the values in Table 3.1 and sample calculations are given in Appendix A.

Table 3.1: Key parameters used for simulation of primary system set. The table displays the simulation cell length L, volume, number of initial water molecules N_{in}, initial bubble radius $R_{in,}$ number of final water molecules after the bubble insertion N_f for each system.

System label	L (nm)	System volume (nm^3)	N_{in}	R_{in} (nm)	N_f
C1	10.5	1160.6	38660	2.8	35600
C2	13.5	2460.4	82180	4.0	73230
RD1	11.0	941.2	31430	2.8	28360
RD2	13.0	1553.5	51890	4.0	42930
RD3	15.0	2398.9	79710	4.0	70760
RD4	17.0	3480.8	116030	5.2	96390
RD5	20.0	5656.9	188940	6.4	152260
RD6	23.0	8603.4	287350	7.6	225940

The R_{in} values selected for this study were generally larger than most values (1.1 - 3.5 nm)[6,7] previously reported. The L values were selected to always have a large bulk liquid volume compared to the BNB volume in each system. Recall, since increasing L will increase the computational cost, the largest system of this study was limited to L = 23 nm. However, these

systems are larger compared to most of the systems previously used in the literature (L = 5 to 15 nm).[6,7]

3.1.2 System preparation

Using the values of L and N_{in} given in Table 3.1, all C and RD systems were prepared using Gromacs-2022.4[1] software. After the energy minimization step, the systems were equilibrated for 1 ns at a pressure of 1 bar and a temperature of 298 K (NPT simulation). These conditions were selected as we are interested in BNB behavior at ambient conditions. There was no change in the average systems properties (i.e., density of the system) during the last 500 ps of the trajectory confirming that the systems were well equilibrated. The relevant em.mdp and npt.mdp files used for these simulations are given in Appendix D.

3.1.3 Insertion of the BNB and simulation

Using the final configurations of water molecules from the equilibrated liquid water systems, a cavity, with radius R_{in} given in Table 3.1, was made at the center of the box using Packmol[2] software. Once the bubble (cavity) was made, the systems were then simulated under constant volume and temperature condition (NVT simulation) for at least 20 ns using Gromacs-2022.4[1] software. The relevant input file for bubble insertion and the nvt.mdp file used for bubble simulations are given in Appendix D. Considering the system sizes and computational cost, the simulation times given in Table 3.2 were selected for each system. These selected simulation times were sufficient to provide average system pressure values better than ± 1 bar.

Table 3.2: Simulation times selected for primary systems based on the system size.

System label	Simulation time (ns)
C1	40
C2	30
RD1	40
RD2	40
RD3	30
RD4	20
RD5	20
RD6	20

3.1.4 Truncation of short-range interactions (cut-off length selection)

To find a suitable cut-off length for the dispersive term of the short-range interactions (see eqn. 2.9), the influence of cut-off length was examined. For this purpose, the smallest cubic system (C1) was selected to reduce computational cost. A set of NVT simulations were carried out for 10 ns using 1.0, 1.2, 1.4, 1.6, 1.8 and 2.0 nm cut-off lengths and values for the system pressure were compared. From this comparison, a suitable cut-off length for this study was selected based on the apparent error in the average system pressure values and computational cost. These results will be discussed in section 4.1.1. Once the cut-off length was selected, the simulations listed in Table 3.1 were then performed under NVT conditions.

3.1.5 Effect of using the PME for short-range interactions

Simulations of all the systems in Table 3.1 were repeated using the PME method for the short-range interaction calculation (instead of a short-range cut-off). These simulations were performed to determine the impact of using the PME method on average system properties, specifically the

pressure. Testing of the various parameters within the PME method was also performed. Section 4.1.2 will provide a detailed discussion on these parameters and the comparison. The average system pressure values obtained for a C1 system with the selected values for parameters in PME method were compared with those of the different cut-off lengths. Based on this comparison, based on the accuracy of the average system pressure and computational cost, a PME method with suitable values for selected parameters was chosen. The simulations in Table 3.1 were then repeated with the chosen PME parameter values.

3.2 Task 2: Investigate the existence of pressure contributions other than the Laplace pressure in an empty BNB

In order to complete Task 2, pressure contributions for bubble containing systems need to be obtained. Within this task, this will be done using the average system pressure. To compare with the Laplace pressure value obtained from the Young Laplace equation[7], the radius of the bubble is required; therefore, a suitable methodology for finding the bubble radius was developed. Using values for the radius, the Laplace pressure and system pressure were then compared to confirm whether or not they were in agreement.

3.2.1 Pressure contributions in a BNB

In this study, a BNB in a water system was simulated as a cavity. To stabilize the bubble, there should be no net force on the bubble interface. In other words, the interface should be in mechanical equilibrium. Figure 3.1 illustrates the pressure contributions in (a) an empty and (b) a filled BNB in water. P_{bulk} is the pressure arising from the water molecules in the bulk liquid (white arrow). Since BNB's surface is a liquid-gas interface, the pressure difference, the Laplace pressure, $\Delta P_{Laplace}$, will act on the interface of the bubble towards the bubble center (blue arrow).[7] P_{inside} is

the pressure generated by the content (gas and vapor molecules) of the bubble (black arrow). In this schematic of filled bubble P_{bulk} and $\Delta P_{Laplace}$ are acting towards the center of the bubble, and P_{inside} acting outward from the center.

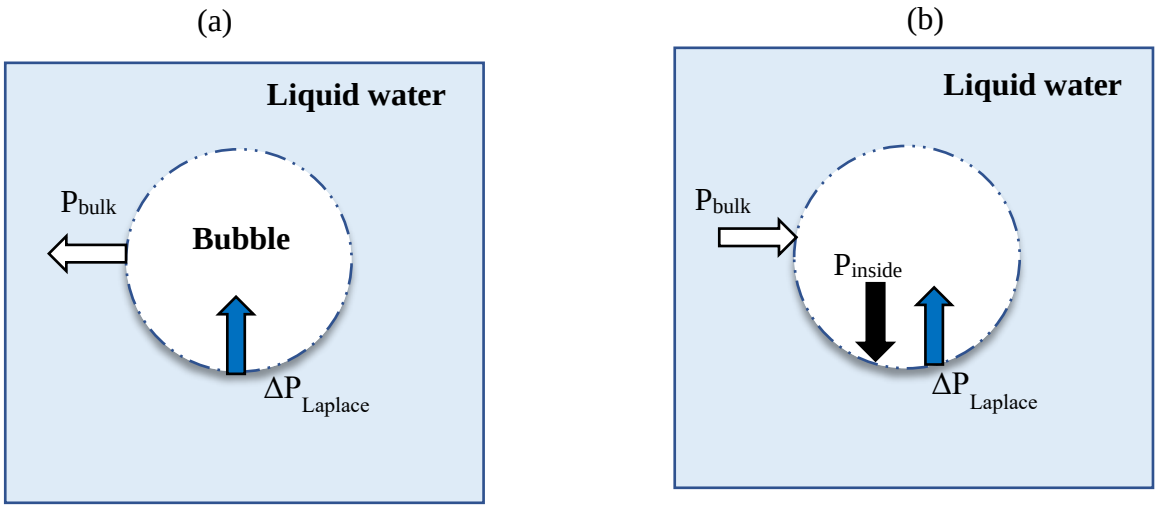

Figure 3.1: Pressure contributions of (a) an empty BNB and (b) filled BNB in a liquid water system

Therefore, considering the filled bubble we have that,

$$P_{bulk} + \Delta P_{Laplace} = P_{inside} \, . \tag{3.1}$$

Although we started with a cavity, with time a few water molecules from the liquid will evaporate and form a vapor inside the cavity. For the TIP4P/2005 water model, its vapor pressure at 300 K is 0.00778 bar.[3] From eqn. 2.2, we see that the Laplace pressure contribution for the bubbles examined in this study will be at least 150 bar. Therefore, the water vapor pressure can be safely ignored for all the systems in this study and P_{inside} assumed equal to zero. Therefore, eqn. 3.1 becomes

$$P_{bulk} = - \Delta P_{Laplace} \, . \tag{3.2}$$

Recall that $\Delta P_{Laplace}$ can be written using the surface tension of water (γ) and bubble radius (R) as described in section 2.1.2. Then using eqn. 2.1, eqn. 3.2 can be written as

$$P_{bulk} = -\frac{2\gamma}{R}. \tag{3.3}$$

It is typical in BNB simulations to assume that the value for P_{bulk} is reasonably given by the total system pressure (P_{system}).[7,8] (We will examine the validity of this assumption later in this chapter). Subject to this assumption eqn. 3.3 becomes

$$P_{system} = -\frac{2\gamma}{R}. \tag{3.4}$$

According to eqn. 3.1, the negative sign of P_{system} in eqn. 3.4 indicates that P_{bulk} is directed opposite to $\Delta P_{Laplace}$. Once water molecules have been removed during the BNB insertion, the remaining water molecules will experience a balance between the forces due to the bubble wanting to collapse and the cohesive forces between water molecules. Therefore, water molecules will experience a tension, and this is manifested as a negative pressure.

To investigate the impact of the Laplace pressure on the pressure inside the bubble, and to confirm the relationship between P_{system} and R, graphs of P_{system} vs $1/R$ can be used for primary analysis. If the system pressure data is found to agree with eqn. 3.4, the slope of the graph of P_{system} vs $1/R$ should be about 1434 bar nm^{-1}, where the surface tension of the TIP4P/2005 water model at 298 K has been used.[9] Alternatively, the product $P_{system} \times R$ should give the same constant value. However, to evaluate eqn. 3.4, radii of the bubbles are needed. The methodology for radius determination is given in the next section.

3.2.2 Finding the bubble radius

Although other methods have been used in previous studies to estimate bubble radii in BNB simulations[8,10,11] as discussed in Chapter 2, the following method was used to find the radii of empty BNBs in this study. The average densities in narrow slices (here 0.2 nm is used) through the system were determined along the x, y and z directions and the average density of each slice plotted verses its position in the system. Figure 3.2 shows a schematic representation of (a) a BNB containing system and three slices taken through it and (b) cross-sections of these slices.

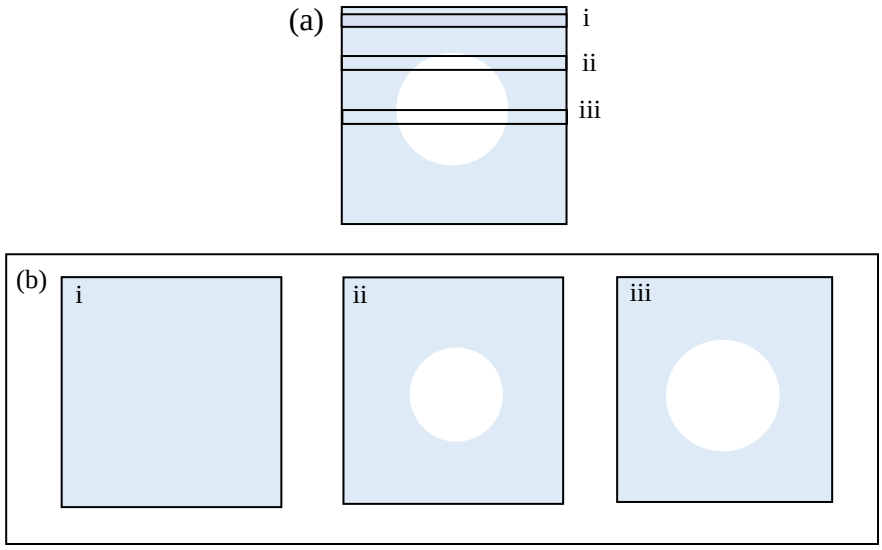

Figure 3.2: Bubble contributions to various slices through the cell. In (a) 3 different slices are labelled as i, ii and iii and in (b), the cross-sections of the three slices corresponding to i - bulk region, ii - edge of the bubble, and iii - center of the bubble, are shown.

Since the bubble is an empty region, the slices taken through the bubble region will have a lower average density compared to the slices in the bulk liquid region. Figure 3.3 shows (a) the corresponding slices along the bubble system, and (b) the resulting density profile. The density profile has a parabolic shape in the region of the bubble, and the plateau regions in Figure 3.3 (b)

correspond to regions that contain only the bulk liquid. The diameter of the bubble can then be calculated from the width of the parabolic section of the density profile.

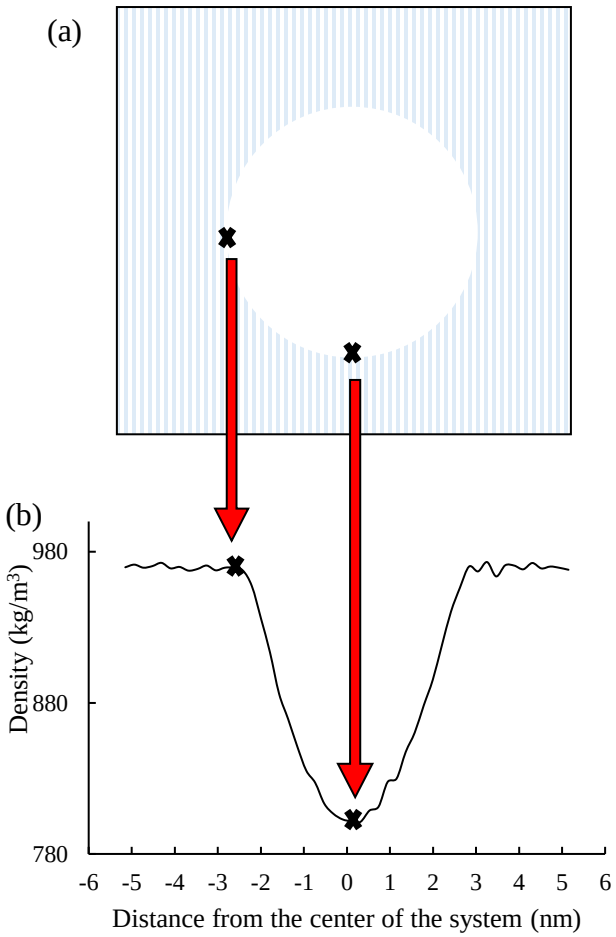

Figure 3.3: (a) Slices through the bubble containing system and (b) average density along each slice. Cross marks and arrows represent each slice and their average density values.

In order to reduce the error caused by the bubble movement, bubble interface distortions, and to improve the accuracy of the data, it is necessary to determine appropriate time averages to obtain suitable density profiles from which bubble radii can be determined. From a simulation trajectory of a C1 system, 200 ps, 250 ps, and 400 ps time average density profiles along the three directions were generated at 1 ns, 2 ns and 3 ns. By comparing the shifts in profiles for the 200 ps, 250 ps and 400 ps data, the time average which gives the smallest shift between the density profiles was

selected for finding the BNB position, and the one giving the smoothest parabola was selected for determining the bubble radius. These results are presented in Chapter 4 in Figure 4.2.

As the next step, to calculate the bubble radius, 400 ps time average density profiles along x, y and z axes at 1, 3, 5, 7 and 9 ns were analyzed (the selection of 400 ps averaging is discussed in section 4.2.2). The density profile obtained from a C1 system at 1 ns through the y-z plane is shown in Figure 3.4. The width of the parabola - the distance between the two intercepts of the parabola with the plateau region (blue arrow) - represents the bubble diameter. To get the average diameter, and so the radius, 15 data sets (5-time intervals in 3 directions) were used, where standard deviations were also calculated.

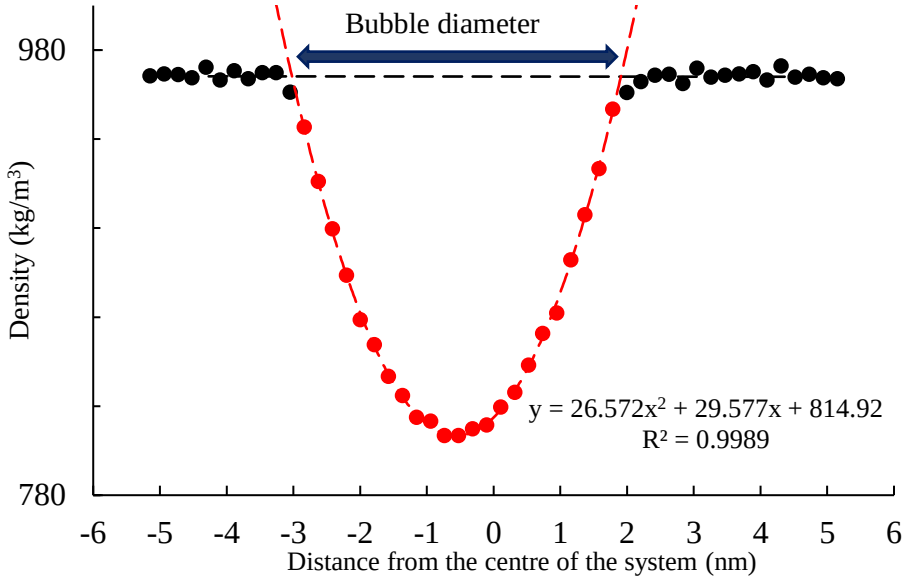

Figure 3.4: Density profile obtained from a C1 system at 1 ns through the y-z plane with separate trend lines for the plateau (black) and parabolic (red) regions.

During this analysis, it was noted that the specific choice of data for fitting the parabola could influence the quality of the fit, particularly points near the top of the parabola. To improve the accuracy of parabolic fit and hence the radius calculation, it is important to consider the data

selection. The strategy used was to find the best parabolic fit, through the data while also maximized the number of data points used. Curves were then fit to data sets that constituted about 60%, 70%, 80%, 90% and 100% of the data points of the parabola, where the lowest were retained. The R^2 values of these parabolas (indicating how precisely data points agree with the parabolic fit) were compared. Figure 3.5 shows an example of the changes in intercept points with selected data point range. The blue arrow and the blue parabolic fit corresponding to the full set of data points associated with the parabola. The red arrow and the red parabolic fit show data points corresponding to ~ 75% of the total and its parabolic fit. Clearly, the widths of the blue and red parabola fits are somewhat different. Therefore, the parabola width and so the bubble radius will also be affected. The parabolic fit which gives the highest R^2 value and uses the maximum number of data points was selected to draw the parabolic fit and so to obtain the bubble radius.

To confirm the appropriateness of a parabolic fit for calculating the BNB's radius, a simple geometric model for the bubble volume in each slice has been examined (see Appendix B). In this geometric model, we assume that the bubble volume in each slice can be represented as a cylindrical slab and find that this volume depends on $(R^2 - D^2)$, where D is the distance from the bubble center to the selected slice. Because the volume of the slab will clearly go to zero when $D = R$, the width of the resulting parabola should equal the diameter of the bubble. We can also see that the assumption of a cylindrical slab will not work well near the edge of the bubble, hence the quality of the parabolic fit can be expected to degrade for data points near the top of the parabola.

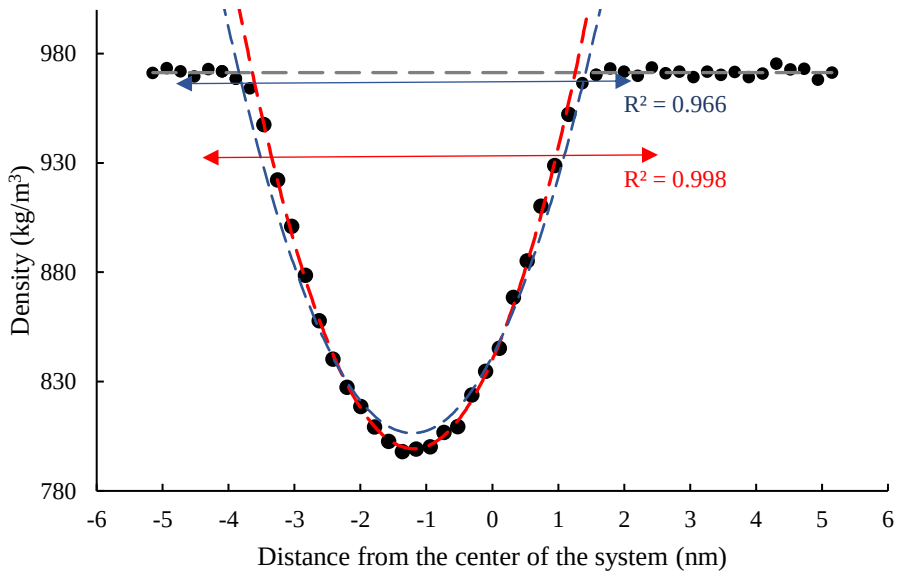

Figure 3.5: Changes in intercept points with selection of different data sets for fitting of the parabola. Blue parabolic fit was drawn taking all the data points in the parabola up to blue arrow and the red parabolic fit was drawn taking all the data points in the parabola up to red arrow.

3.2.3 Finding the bubble position

The center of the bubble can be found from the position of the slice with the lowest average density, which should be the midpoint of the parabola. The positions in the x, y and z directions were obtained from 200 ps time average density profiles (the selection of 200 ps will be discussed in section 4.2.2).

3.3 Task 3: Investigate the existence of separation effect in the pressure for a BNB system

Task 3 focuses on the effect of distance between the bubbles on the pressure in the BNB system. As will be discussed in this section, the impact of the interface and the importance of measuring the pressure in the bulk liquid region are key aspects of this analysis.

3.3.1 Effect of separation on the pressure in a BNB system

After confirming that the average system pressure (refer to eqn. 3.4) is not given solely by the Laplace pressure, the possible effect of the distance (separation) between nearest image bubbles in PBC to the pressure was investigated. For this separation analysis, bubbles with radii ≈2.5 nm and ≈3.75 nm were considered in different size simulation cells. By increasing L, the length of the simulation cell, the separation was correspondingly increased. The average system pressure was obtained from simulations using both a 1.6 nm cut-off and the PME method for the short-range interactions. The results were then analyzed to determine whether there is a separation dependence.

In the separation analysis of this study, the initial separation was calculated as the difference between the system length, L, and the initial bubble radius, R_{in}. For these simulations, the same procedure was followed as given in sections 3.1.1- 3.1.3 with both the 1.6 nm cut-off and the PME method for the systems described in Table 3.3 - 3.6. The systems with L <13.5 nm was simulated for 40 ns, while systems with L= 13.5 nm for 30 ns, and L >13.5 nm for 20 ns. These simulation times were sufficient to provide average pressure values to better than ± 1 bar and while maintaining a reasonable computational cost. Table 3.3 and 3.4 summarizes the systems with R ≈2.5 nm bubble. Table 3.5 and 3.6 summarizes the systems with R ≈3.75 nm bubble.

Table 3.3: Key parameters of systems prepared for separation analysis using a 1.6 nm cut-off method for a R ≈2.5 nm bubble. The table displays the simulation cell length L, number of initial water molecules N_{in}, number of final water molecules after the bubble insertion N_f, initial bubble radius R_{in}, and initial separation for each system.

System label	L (nm)	N_{in}	N_f	R_{in} (nm)	Initial separation (nm)
10.5 C	10.5	38660	35426	2.85	7.65
11.5 C	11.5	50800	47030	3.00	8.50
13.5 C	13.5	82180	77592	3.20	10.30
16.5 C	16.5	150040	143356	3.63	12.87
11RD	11.0	31430	28360	2.80	8.20
13RD	13.0	51890	48110	3.00	10.00
15RD	15.0	79710	75124	3.20	11.80
17RD	17.0	116030	110772	3.35	13.65

Table 3.4: Key parameters of systems prepared for separation analysis using the PME method for a R ≈2.5 nm bubble. The table displays the simulation cell length L, number of initial water molecules N_{in}, number of final water molecules after the bubble insertion N_f, initial bubble radius R_{in}, and initial separation for each system.

System label	L (nm)	N_{in}	N_f	R_{in} (nm)	Initial separation (nm)
10.5C	10.5	38660	35253	2.90	7.60
11.5C	11.5	50800	47100	2.98	8.52
13.5C	13.5	82180	77595	3.20	10.3
16.5C	16.5	150040	143620	3.58	12.92
11RD	11.0	31430	28360	2.80	8.20
13RD	13.0	51890	48290	2.95	10.05
15RD	15.0	79710	75336	3.15	11.85

Table 3.5: Key parameters of systems prepared for separation analysis using a 1.6 nm cut-off data for a R ≈3.75 nm bubble. The table displays the simulation cell length L, number of initial water molecules N_{in}, number of final water molecules after bubble insertion N_f, initial bubble radius R_{in}, and initial separation for each system.

System label	L (nm)	N_{in}	N_f	R_{in} (nm)	Initial separation (nm)
13.5 C	13.5	82180	73230	4.00	9.50
16.5 C	16.5	150040	139680	4.20	12.30
13RD	13.0	51890	43270	3.95	9.05
15RD	15.0	79710	70760	4.00	11.00
17RD	17.0	116030	106010	4.15	12.85
20RD	20.0	188940	177815	4.30	15.70
23RD	23.0	2873350	274304	4.50	18.50

Table 3.6: Key parameters of systems prepared for separation analysis using the PME data for a R ≈3.75 nm bubble. The table displays the simulation cell length L, number of initial water molecules N_{in}, number of final water molecules after bubble insertion N_f, initial bubble radius R_{in}, and initial separation for each system.

System label	L (nm)	N_{in}	N_f	R_{in} (nm)	Initial separation (nm)
13.5 C	13.5	82180	73230	4.00	9.50
16.5 C	16.5	150040	139680	4.20	12.30
13RD	13.0	51890	43588	3.90	9.10
15RD	15.0	79710	70760	4.00	11.00
17RD	17.0	116030	106738	4.05	12.95
20RD	20.0	188940	178200	4.25	15.75

3.3.2 Bubble interface thickness

As discussed in section 3.2.1, it is typical for simulations of BNBs to assume that the average system pressure reasonably represents the pressure in the bulk liquid region. Yet, from Figure 3.1 we can see that some of the molecules are near the surface of the bubble and hence may experience a pressure different from the bulk liquid. We will then distinguish between the molecules at the surface of the BNB, surface molecules, and molecules away from the BNB's surface, bulk liquid molecules. To consider the effect of surface and bulk liquid molecules on the system pressure, the surface thickness of the BNB is required. The surface thickness of the BNB can be determined from radial distribution profiles, which measure the average density as a function of the distance from the center of the bubble (where the center of the BNB was taken as the position of the bubble for that time window). Radial distribution profiles were obtained from 400 ps time averages to improve the precision of the data. Figure 3.6 shows a radial distribution profile for a L=11 nm RD system with a $R \approx$2.5 nm BNB. The thickness of the bubble interface is the width of the sigmoidal region of the graph (the black arrow in Figure 3.6).

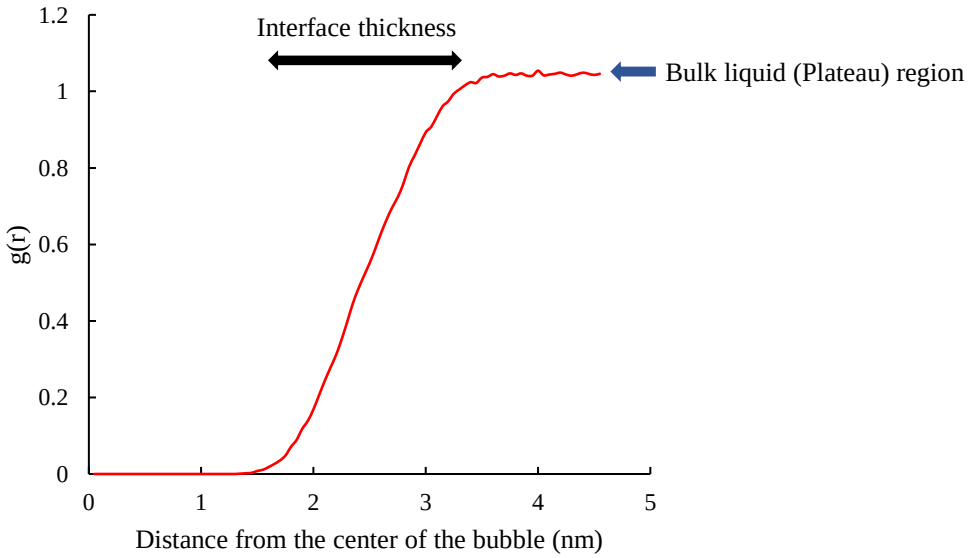

Figure 3.6: Radial distribution profile, g(r), for a R ≈2.5 nm BNB in a L=11 nm RD system. The black arrow shows the interface thickness of the BNB. The blue arrow shows the bulk liquid region.

3.3.3 Effect of separation on bulk liquid pressure

It was noted above in section 3.3.2 that the average system pressure will have contributions from both surface and bulk liquid water molecules. In the analysis below, the pressure contributions from the surface and bulk water molecules will be considered separately in a relationship for the total system pressure. We will then consider how this relationship simplifies for systems with BNBs of the same size.

Before moving into the formal development, it will be useful to define the following symbols.

V_{water} - total water volume

V_{bubble} - bubble volume (which is calculated using radius of the bubble)

V_{bulk} - volume of the bulk liquid (water not belonging to the bubble's surface)

$V_{surface}$ - volume of the surface of the bubble (with radius R and thickness α)

V_{total} - total system volume

P_{bulk} - bulk water pressure (pressure arising from the water within the bulk liquid)

$P_{surface}$ - pressure contribution from water molecules in the bubble's surface

f_{bulk} - volume fraction of water in the bulk liquid

f_{surface} - volume fraction of water in the bubble's surface

We can then start by expressing the average system pressure in terms of bulk and surface contributions,

$$P_{system} = (P_{bulk} \times f_{bulk}) + \left(P_{surface} \times f_{surface}\right). \quad (3.5)$$

From the definitions above it immediately follows that

$$V_{total} = V_{bubble} + V_{surface} + V_{bulk}\,, \quad (3.6)$$

and

$$V_{water} = V_{surface} + V_{bulk}\,. \quad (3.7)$$

It also follows that

$$f_{bulk} = \frac{V_{bulk}}{V_{water}}\,, \quad (3.8)$$

and

$$f_{surface} = \frac{V_{surface}}{V_{water}}\,. \quad (3.9)$$

While P_{system} is measured directly in the simulation, the bulk water pressure, P_{bulk}, can be found from the density of the bulk water. First, a calibration curve for the dependence of the density of bulk water systems (i.e., without a bubble) under different pressure conditions is required (see section 4.3.5). Then from radial distribution profiles (see Figure 3.6 - plateau region), the average density of the bulk water region can be determined for each BNB system. This density value can be then used with the calibration curve to find the P_{bulk} for each system.

Assuming P_{system} and P_{bulk} are known, eqn. 3.5 can be simplified using eqns. 3.8 and 3.9, yielding

$$P_{system} \times V_{water} = (P_{bulk} \times V_{bulk}) + (P_{surface} \times V_{surface}), \quad (3.10)$$

and substituting from eqn. 3.7 becomes,

$$P_{system} \times V_{water} = P_{bulk}\left(V_{water} - V_{surface}\right) + \left(P_{surface} \times V_{surface}\right). \quad (3.11)$$

We can then rearrange to obtain

$$P_{system} \times V_{water} = (P_{bulk} \times V_{water}) + V_{surface}\,(P_{surface} - P_{bulk}) \ . \quad (3.12)$$

To further simplify eqn. 3.12, we introduce δP,

$$\delta P \ = \ P_{system} - \ P_{bulk} \ , \quad (3.13)$$

from which it follows that

$$V_{water} \times \delta P = V_{surface}\,(P_{surface} - P_{bulk}) . \quad (3.14)$$

Assuming the surface volume of the bubble can be estimated as

$$V_{surface} = a \times A \ , \quad (3.15)$$

where α is the interface thickness and A is the surface area of a BNB with radius R

$$A = 4\pi \times R^2 \ , \quad (3.16)$$

the eqn. 3.14 becomes

$$V_{water} \times \delta P = a \times 4\pi \times R^2\left(P_{surface} - P_{bulk}\right). \quad (3.17)$$

For systems with bubbles of the same size, $V_{surface}$ (which is $a \times 4\pi \times R^2$) is a constant and $\left(P_{surface} - P_{bulk}\right)$ should also be a constant.[12] Therefore, the right-hand side of eqn. 3.17 should

give a constant value for bubbles of the same size. This then implies that $(V_{water} \times \delta P)$ should be a constant. If $(V_{water} \times \delta P)$ is not a constant, it suggests that there is an additional contribution to the pressure that depends on system size, or the bubble separation.

For analysis of $(V_{water} \times \delta P)$ values, new systems were prepared with R ≈2.5 nm bubbles in different sized cubic and RD systems using the PME method. The system parameters used for the bulk liquid density calculations are given in Table 3.7. From the resultant system volumes and radii values, V_{water} can be obtained. To determine the P_{bulk} and $P_{surface}$, the average system pressure and the average density data are needed. Section 3.3.4 discusses the methodology used to find P_{bulk} and $P_{surface}$ using average density values.

Table 3.7: Key parameters of the systems prepared for bulk liquid density calculations using the PME method for a R ≈2.5 nm bubble. The table displays the simulation cell length L, number of initial water molecules N_{in}, number of final water molecules after the bubble insertion N_f, initial bubble radius R_{in}, for each system.

System label	***L* (nm)**	N_{in}	N_f	R_{in} **(nm)**
10.5C	10.5	38660	35253	2.90
11.5C	11.5	50800	47100	2.98
13.5C	13.5	82180	77595	3.20
16.5C	16.5	150040	143620	3.58
13RD	13.0	51890	48290	2.95
15RD	15.0	79710	75336	3.15

3.3.4 Finding the bulk liquid density of BNB systems

Recall, the plateau region (Figure 3.6 - blue arrow) of the radial distribution profiles can be used to calculate the bulk water density. In this study, an average of plateau values from 10 windows (1 - 10 ns) were taken to improve the accuracy of the data. A sample calculation of the bulk liquid density from the average g(r) value of the plateau region is given in Appendix C. It should be noted that care was required to ensure a sufficiently long plateau region was sampled to provide sufficiently accurate results. To generate the required calibration plot of average density of bulk water vs system pressure, five C1 systems without a cavity (bubble) were simulated for 10 ns under different constant pressures (-200, -300, -400, -500 and -600 bar) and at 298 K. The average system density was directly obtained from the simulation as the system is homogenous. Even though a constant system pressure was set, there is a small difference with the measured system pressure from the simulation. To avoid errors cause by this small pressure difference, the final system average pressure was used for the calibration plot.

Finally, P_{bulk} was obtained for all the systems in Table 3.7 using the average density of the bulk liquid regions obtained from the g(r) value of the plateau region and the pressure-density calibration curve. From the values of P_{system} and P_{bulk}, $P_{surface}$ was calculated and the accuracy of the $(V_{water} \times \delta P)$ statement examined (see section 4.3.5).

3.4 Simulation details

For all MD simulations performed in this study, the Gromacs 2020.4[1] and Packmol[2] software packages, and the TIP4P/2005[3] water model were used with 0.002 ps time step. The Nosé–Hoover thermostat[4] and the Berendsen barostat[4] was used to control the temperature and the pressure of

the systems, respectively. Examples of topology (.top) and MD parameter (.mdp) files, along with a Packmol input file are included in Appendix D.

3.5 Summary

In Chapter 3, we have described the MD simulations performed during this study. In order to achieve the three main tasks listed in Chapter 1, the methodologies developed to analyze and improve the simulation results were discussed. Also, the reasons for each selection were reviewed. In Chapter 4, the results obtained from these simulations will be examined.

3.6 References

1. Abraham, M. J.; Murtola, T.; Schulz, R.; Páll, S.; Smith, J. C.; Hess, B.; Lindah, E. Gromacs: High Performance Molecular Simulations through Multi-Level Parallelism from Laptops to Supercomputers. *SoftwareX* **2015**, *1–2*, 19–25. https://doi.org/10.1016/j.softx.2015.06.001.
2. Martinez, L.; Andrade, R.; Birgin, E. G.; Martínez, J. M. PACKMOL: A Package for Building Initial Configurations for Molecular Dynamics Simulations. *J Comput Chem* **2009**, *30* (13), 2157–2164. https://doi.org/10.1002/jcc.21224.
3. Vega, C.; Abascal, J. L. F.; Nezbeda, I. Vapor-Liquid Equilibria from the Triple Point up to the Critical Point for the New Generation of TIP4P-like Models: TIP4P/Ew, TIP4P/2005, and TIP4P/Ice. *Journal of Chemical Physics* **2006**, *125* (3). https://doi.org/10.1063/1.2215612.
4. Braun, E.; Gilmer, J.; Mayes, H. B.; Mobley, D. L.; Monroe, J. I.; Prasad, S.; Zuckerman, D. M. Best Practices for Foundations in Molecular Simulations [Article v1.0]. *Living J Comput Mol Sci* **2019**, *1* (1). https://doi.org/10.33011/livecoms.1.1.5957.
5. *Scaling in Density Introduction*. https://www.astro.princeton.edu/~dns/teachersguide/ScDensInt.html (accessed 2023-02-11).
6. MATSUMOTO, M. Surface Tension and Stability of a Nanobubble in Water: Molecular Simulation. *Journal of Fluid Science and Technology* **2008**, *3* (8), 922–929. https://doi.org/10.1299/jfst.3.922.

7. Hong, S. N.; Choe, S. H.; Jong, U. G.; Pak, M. S.; Yu, C. J. The Maximum Interbubble Distance in Relation to the Radius of Spherical Stable Nanobubble in Liquid Water: A Molecular Dynamics Study. *Fluid Phase Equilib* **2019**, *487*, 45–51. https://doi.org/10.1016/j.fluid.2019.01.014.

8. Matsumoto, M.; Tanaka, K. Nano Bubble-Size Dependence of Surface Tension and inside Pressure. *Fluid Dyn Res* **2008**, *40* (7–8), 546–553. https://doi.org/10.1016/j.fluiddyn.2007.12.006.

9. Vega, C.; de Miguel, E. Surface Tension of the Most Popular Models of Water by Using the Test-Area Simulation Method. *Journal of Chemical Physics* **2007**, *126* (15). https://doi.org/10.1063/1.2715577.

10. Lu, Y.; Yang, L.; Kuang, Y.; Song, Y.; Zhao, J.; Sum, A. K. Molecular Simulations on the Stability and Dynamics of Bulk Nanobubbles in Aqueous Environments. *Physical Chemistry Chemical Physics* **2021**, *23* (48), 27533–27542. https://doi.org/10.1039/d1cp03325e.

11. Aluthgun Hewage, S.; Meegoda, J. N. Molecular Dynamics Simulation of Bulk Nanobubbles. *Colloids Surf A Physicochem Eng Asp* **2022**, *650*, 129565. https://doi.org/10.1016/j.colsurfa.2022.129565.

12. Yamamoto, T.; Ohnishi, S. Molecular Dynamics Study on Helium Nanobubbles in Water. *Physical Chemistry Chemical Physics* **2011**, *13* (36), 16142–16145. https://doi.org/10.1039/c1cp22018g.

Chapter 4 : RESULTS AND DISCUSSION

This chapter presents the results obtained from the simulations performed and their analysis according to the methodologies discussed in Chapter 3. The chapter is divided into three sections based on the tasks identified in Chapter 1. The results obtained in each of the tasks will be discussed in detail.

4.1 Task 1: Selection of a short-range interaction calculation method for MD simulation of BNBs.

The selected short-range interaction calculation method in a simulation impacts the system properties. As we are interested in the average system pressure, the pressure dependence on short-range interaction calculation methods will be evaluated in this section using different cut-off lengths and the PME method. Recall, no clear justification is given in the literature for the different cut-off lengths previously used for short-range interaction calculations in BNB simulations. Therefore, the pressure dependence on the commonly use cut-off length range will be analysed first. Then the use of the PME method for the short-range interaction calculation for BNB simulations will be investigated, and the selected PME parameters within the algorithm will be evaluated.

4.1.1 Cut-off length selection

The average system pressures obtained for a C1 system with cut-off lengths of 1.0, 1.2, 1.4, 1.6, 1.8 and 2.0 nm are given in the Table 4.1, along with the approximate time taken for a 10 ns simulation. The standard deviations for the average pressure values were always less than ±1 bar.

Recall, the negative average pressure values represent the tension in the system after the bubble insertion.

Table 4.1: Average pressures, and approximate time taken for simulation of a C1 systems for 10 ns using cut-off lengths of 1.0, 1.2,1.4,1.6,1.8 and 2.0 nm.

Cut-off length (nm)	Average pressure (bar)	Approximate time taken (hrs)
1.0	-712.7	6
1.2	-631.2	12
1.4	-587.2	12
1.6	-562.7	12
1.8	-550.4	18
2.0	-544.6	20

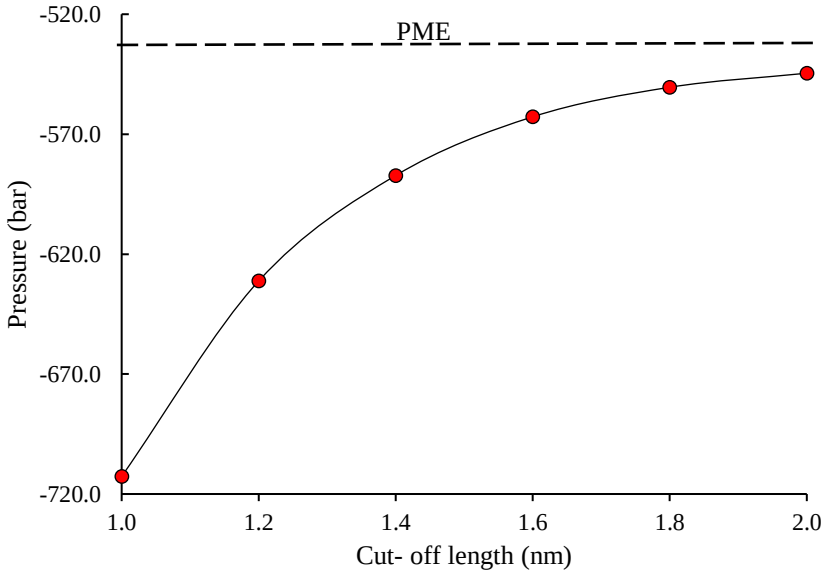

Figure 4.1: The system pressure dependence on the short-range cut-off length for a C1 system with R ≈2.5 nm bubble at 298 K. The pressure obtained from the PME method for same system is shown in the dashed line.

From the results in Table 4.1, the average system pressure vs cut-off length used was plotted in Figure 4.1, where it can be seen that with increasing cut-off length the magnitude of the system pressure decreases quite significantly. For example, the differences found for standard cut-off

length of 1.0 or 1.2 nm are rather large (i.e.,> 80 bar). It is also apparent from Figure 4.1 that the system pressure is asymptotically approaching a value with increasing cut-off length. However, it is also important to note that with increasing cut-off length, the number of interactions considered in simulation increase substantially. As can also be seen from Table 4.1, the time taken for the simulation (the computational cost) increases considerably for longer cut-off lengths. Therefore, while a longer cut-off length of at least 2.0 nm appears desirable a value of 1.6 nm was selected as the longest short-range cut-off length with an acceptable computational cost and average pressure value close to the asymptotic value. It was used for the simulations reported below.

4.1.2 Selections in the PME method

Simulations were carried out to evaluate suitable values for the parameters Fourier spacing, PME order and Ewald-rtol-lj, and use of dispersion correction for the PME method. Table 4.2 gives the results obtained from 40 ns simulations of a C1 system using the PME method. In the PME method, the charges are assigned to grid points. The Fourier spacing parameter identifies the maximum spacing between these grids for the fast Fourier transformation, or in other words the minimum number of grid points in Fourier space. In general, a PME order of 4 to 6 is commonly used for most systems, but higher orders may be needed for more complex systems.[1] The PME order four is considered as cubic interpolation and it is recommended.[2] The Ewald-rtol-lj is applied to control the relative strength of the dispersion potential at the short-range cut-off. Although Ewald-rtol-lj of 1×10^{-3} is commonly used in simulations,1×10^{-5} was selected since decreasing Ewald-rtol-lj value increases the accuracy of the results.[1,3] From Table 4.2 it can be seen that the variations of these values have apparently negligible effect on the system pressure. Therefore, considering the reliability of the average system pressure, and the computational cost, a Fourier spacing of 1.2 nm, a PME order of 4, and Ewald-rtol-lj of 1×10^{-5} were selected. Further, the impact of adding a

dispersion correction which is commonly use with cut-off method was analysed, and we found no difference in the average system pressure. Therefore, no dispersion correction was added. The selected parameters used for all PME method simulations are highlighted in Table 4.2. Further, the pressure obtained from using the above selected values is marked in Figure 4.1, and it extrapolates the pressures obtained from cut-off method confirming the accuracy of the choice. It is important to point out that simulations using the above parameters in the PME method run roughly 22% faster than simulations using the 1.6 nm cut-off. Additionally, we have also tested the PME parameters for the electrostatic interactions and confirmed that our choice does not change the results. However, this chapter includes the results obtained for both 1.6 nm cut-off method and the PME method to provide the complete picture of the study.

Table 4.2: Average system pressures and time taken for simulations of C1 systems for 40 ns using different parameters - Fourier spacing, PME order, Ewald-rtol-li and with/without dispersion correction of the PME method.

Fourier spacing (nm)	0.16	0.16	0.12	0.12
PME order	4	4	4	4
Ewald-rtol-lj	1×10^{-5}	1×10^{-4}	1×10^{-5}	1×10^{-5}
Dispersion correction	Yes	Yes	Yes	No
Approximate time taken (hrs)	46	65	39	39
Average pressure (bar)	-527.4	-529.2	-530.1	-529.4

4.2 Task 2: Investigate the existence of pressure contributions other than the Laplace pressure in an empty BNB.

To investigate other factors that might affect the pressure in a BNB system, the Laplace pressure contribution was evaluated. If there is a difference between the Laplace pressure and the measured pressure due to the BNB, it suggests that other pressure contributions may present.

4.2.1 Average system pressure

Once the simulations of the primary systems with a 1.6 nm cut-off and the PME method were completed, values for the average system pressures were directly obtained from the standard output for the simulation runs. Table 4.3 includes these average pressure values. It is again notable that the standard deviations of the average pressure values for all the systems were less than ±1 bar.

Table 4.3: Average system pressures obtained for primary systems using a 1.6 nm cut-off length and the PME method for evaluating the short-range interactions.

System label	Average pressure (bar)	
	1.6 nm cut-off length	**PME**
C1	-565.1	-529.4
C2	-383.4	-348.7
RD1	-549.5	-518.6
RD2	-368.1	-339.8
RD3	-381.5	-341.8
RD4	-295.5	-258.0
RD5	-244.5	-208.9
RD6	-209.9	-174.2

According to the results in Table 4.3, the negative system pressure values obtained from the PME method were consistently smaller in magnitude than the 1.6 nm cut-off length values for similar size bubbles. Clearly the selected short-range interaction calculation method affects the average system pressure values even for larger bubbles. Moreover, other properties may also be affected by the interaction calculation method. In terms of computational cost, for a C1 system the PME method took only about 40 hrs, while the 1.6 nm cut-off method took 48 hrs to complete the 40 ns simulation, again demonstrating the PME method's greater efficiency. Further it is clear that the different size bubbles in different systems give different average pressure values.

4.2.2 Finding the bubble radius and position

For our analysis of pressure contributions in BNB systems, values for the average bubble radius are required. For this study we developed and tested a suitable method to calculate the bubble radius in our systems. It was also important to confirm the accuracy of the method. The following seven sections will discuss each aspect of the radius calculation method development and testing.

i. Selection of suitable time average

For finding the bubble radius, one needs to select a suitable time window for averaging the density profiles. Figure 4.2 shows density profiles drawn through the x-y plane (i.e., along the z axis) for a C1 system at 1 ns. Careful examination of the density profiles at 1, 2 and 3 ns reveal the effect of bubble movement (shifts in the red and black parabola in Figure 4.2) is less apparent for 200 ps average profiles, compared to the 250 ps and 400 ps average density profiles. This trend was consistent for all directions and at different time intervals. Based on these results, 200 ps time average density profile (i.e., averaging configurations over 200 ps) was selected to find the position of the bubble. Figure 4.3 compares density profiles plotted for (a) 200 ps and (b) 400 ps time average profiles through the y-z plane (along the x axis) at (i) 1 ns, (ii) 2 ns and (iii) 3 ns during the simulation of a C1 system. As the parabolas were generally smoother for 400 ps time average density profiles, they were used for all radius calculations.

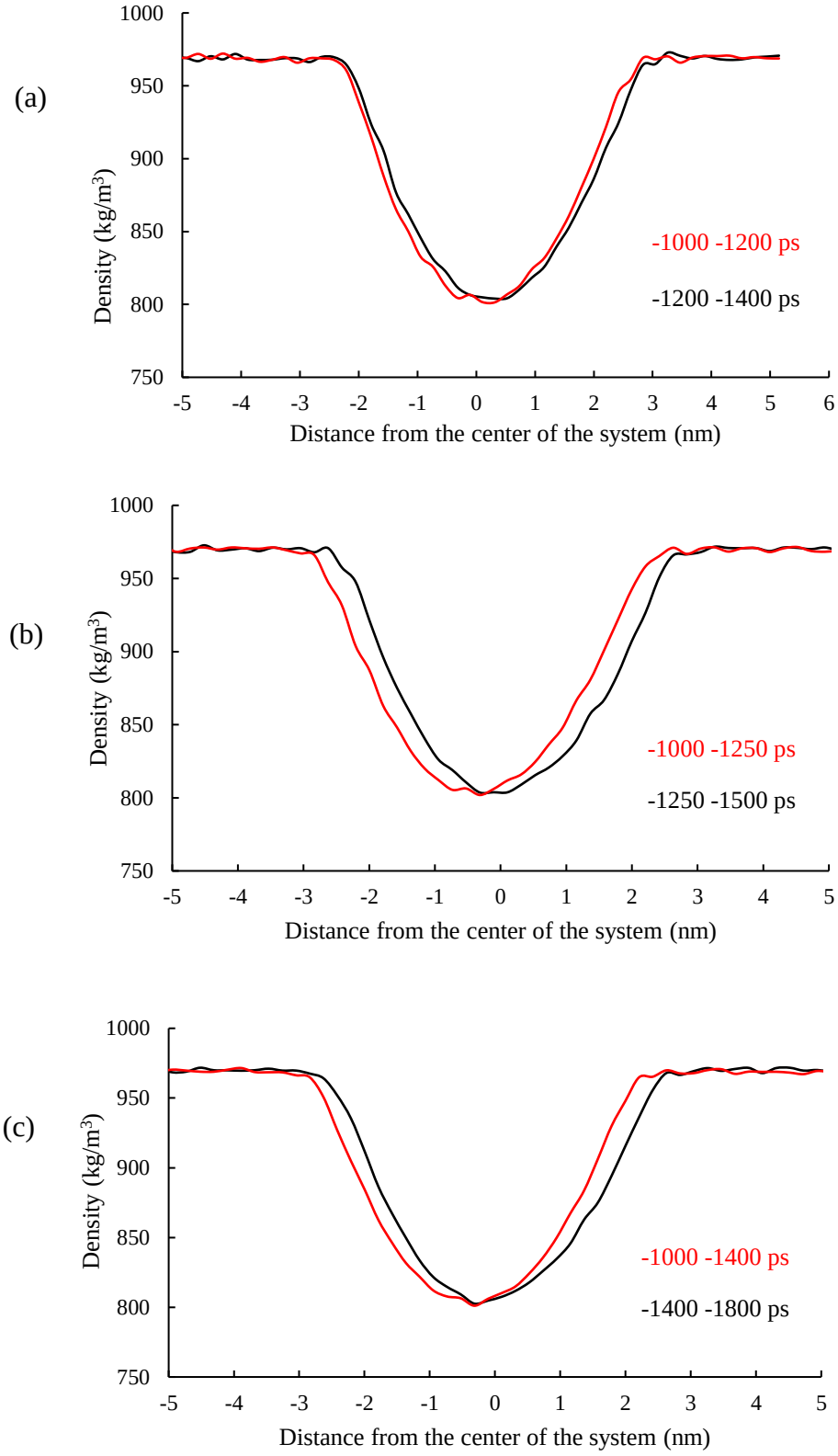

Figure 4.2: Comparison of two consecutive density profiles through the x-y planes for a C1 system with a R ≈2.5 nm bubble at 1 ns where profiles have been averaged over (a) 200 ps, (b) 250 ps and (c) 400 ps.

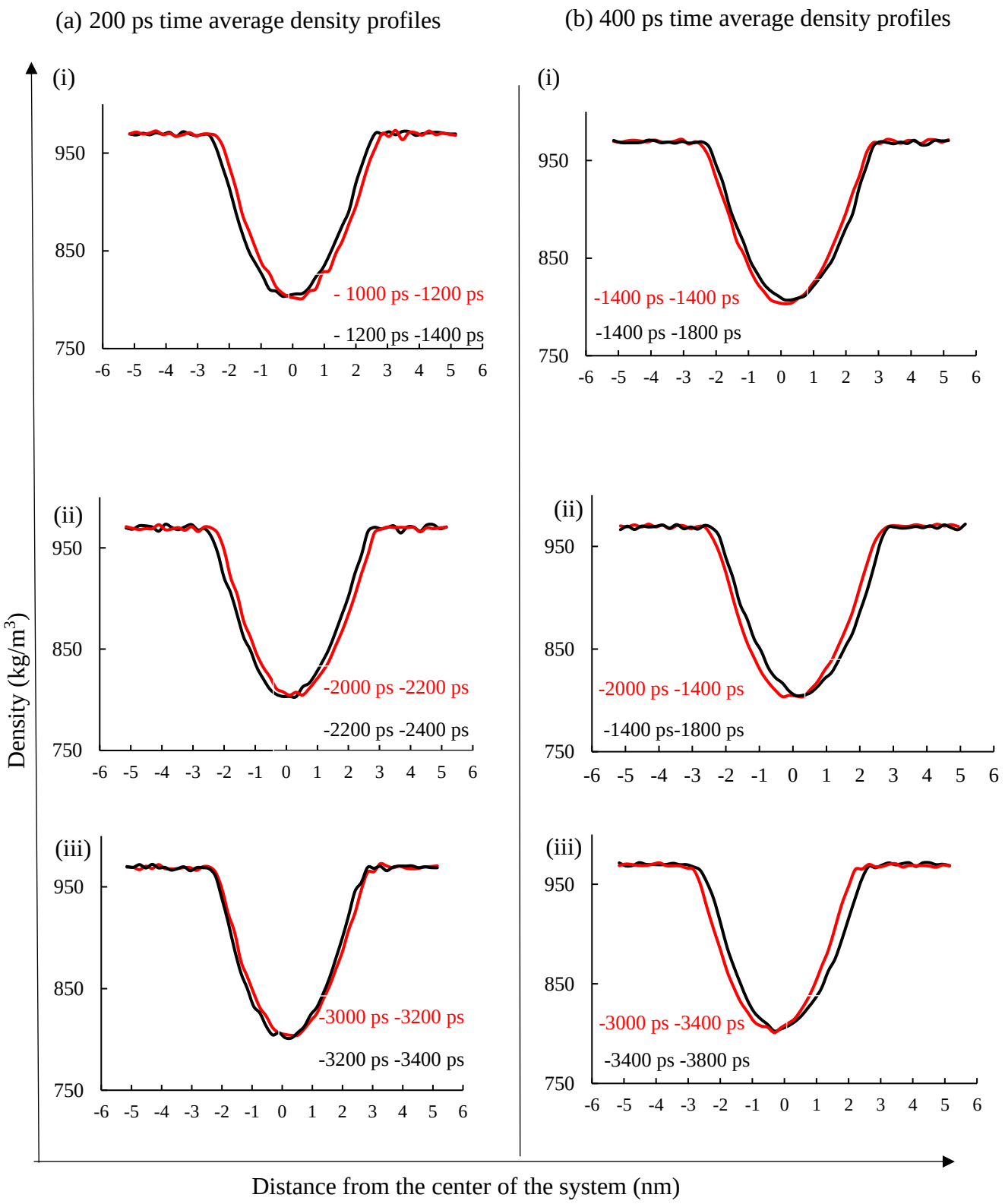

Figure 4.3: Comparison of two consecutive density profiles through the y-z planes for a C1 system with a R ≈2.5 nm bubble at (i) 1 ns, (ii) 2 ns and (iii) 3 ns where profiles have been averaged over (a) 200 ps and (b) 400 ps.

ii. Selecting the suitable trend line for parabola

As was discussed in section 3.2.2, because a BNB's interface has a finite thickness and because the limited applicability of a parabola to describe the density profiles, special care should be taken at the edge of the parabola when determining the bubble diameter. We proceed by drawing separate trend lines for both plateau regions and the parabola, and then identify the intersection points to determine the bubble diameter. In terms of selecting the data points for fitting the parabola, we selected the suitable range for the data considering the maximum range that provides the best R^2 value for the fit, where the lower most points were retained. Figure 4.4 shows the separate trend lines drawn for the bulk and bubble regions of the density profile through the x-z plane for a C1 system at 1 ns.

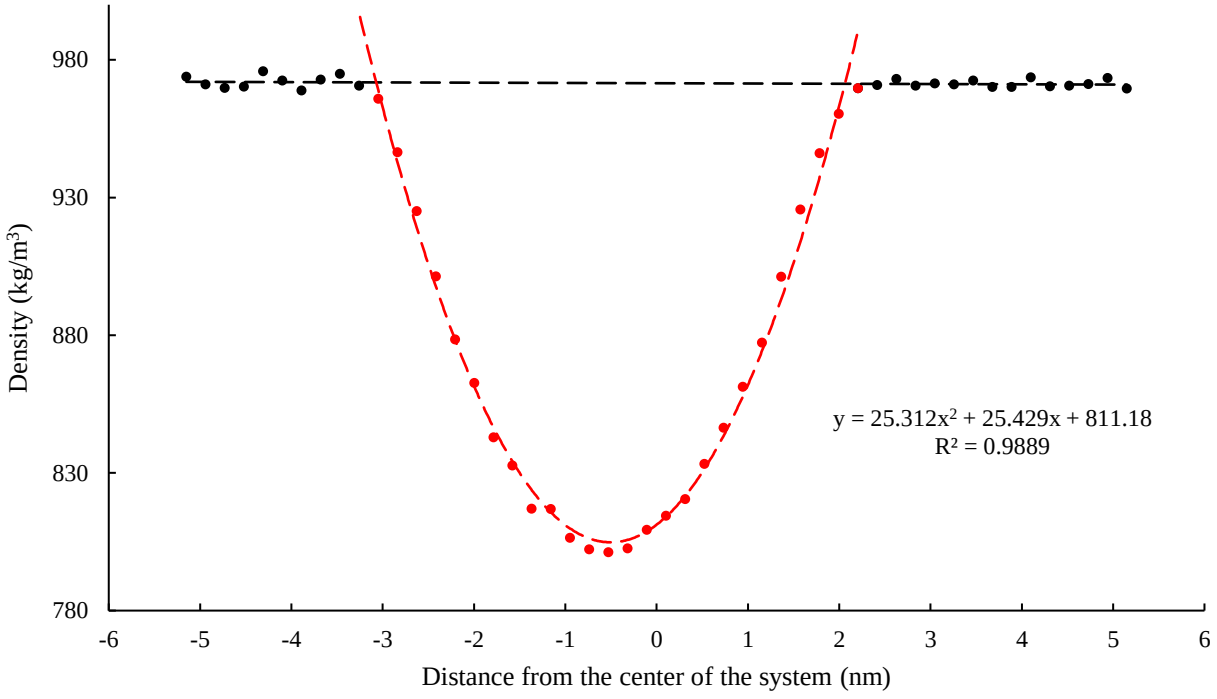

Figure 4.4: Separate trend lines for the bulk (black) and bubble (red) regions in the density profile through the x-z plane for a C1 system with a R ≈2.5 nm bubble at 1 ns where profiles have been averaged over 400 ps.

Table 4.4 includes the R^2 values obtained for different data ranges (expressed as percentage height of the parabola) for the same density profiles through the x-y, x-z, and y-z planes for a C1 system at 1 ns. Since the density profile values are not continuous, it was not always possible to truncate the data set at an exact percentage of height resulting in the merged cells in Table 4.4. The percentage height was calculated using the ratio between selected values and the difference between the highest and lowest values in each density profile.

Table 4.4: R^2 values obtained for different data ranges (expressed as percentage height of the parabola) for the same density profiles through the x-y, x-z, and y-z planes for a C1 system with a R ≈2.5 nm bubble at 1 ns.

Percentage height of the parabola	**R^2 values obtained in different planes**		
	x-y	**x-z**	**y-z**
65	0.9976	0.9978	0.9984
70	0.9985		
75	0.9986	0.998	0.999
80		0.9977	0.9991
85	0.9964	0.9958	0.9955
90	0.9911		
95	0.9829	0.9887	0.9821

From Table 4.4 we can see consistent improvement in the R^2 values until the data range reaches ~80% of the parabola height, beyond which the changes in R^2 values are insignificant. Therefore, to be consistence with all radius calculations in all systems, the parabola trend line was drawn selecting a data range of 75-80% the height of the parabola. The distance between the intercepts of the parabola trend line with the plateau of the bulk region is then taken as the diameter of the bubble. Figure 4.5 shows time average (400 ps) density profiles with trend lines plotted using the selected height (75-80%) for range of data points through the x-y, x-z and y-z planes for a C1 system with a R ≈2.5 nm bubble at 1 ns.

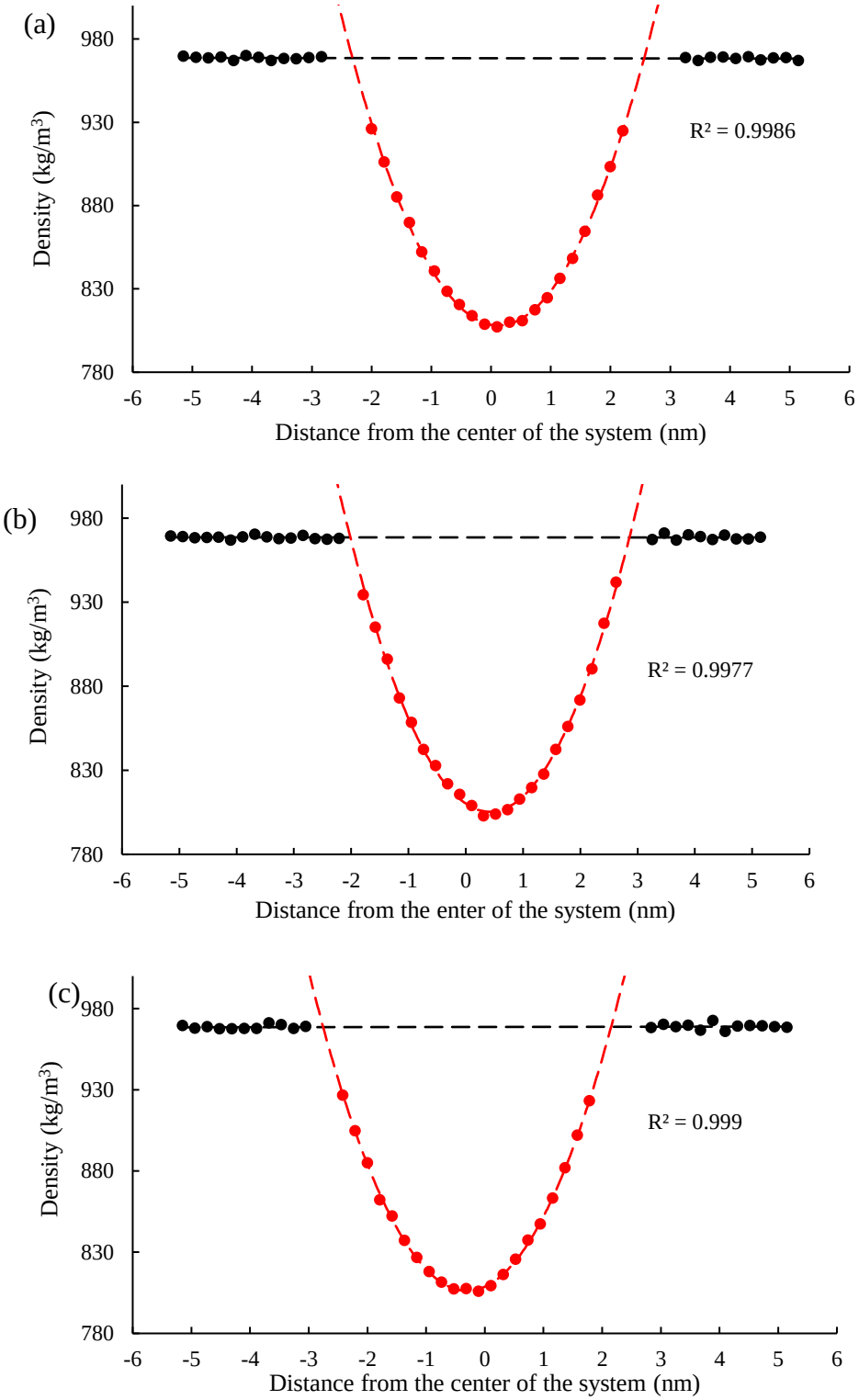

Figure 4.5: Fitted density profiles through the (a) x-y, (b) x-z and (c) y-z for a C1 system with a R ≈2.5 nm bubble at 1 ns. The density profiles have been averaged over 400 ps, with trend line fit using data points up to 75-80% of the total height of the parabola.

iii. The applicability of using parabolic width in density profiles to calculate bubble radius

Next, we wanted to confirm that our density profile's parabola agrees with the volume of layers of a sphere. To confirm the width of the parabola is equal to the diameter of the bubble, we used the radius of the bubble in each slice through the system (as shown in Figure 3.2). We also confirmed that the volume of each slice of the bubble agrees with a quadratic equation and that the diameter of the bubble can be obtained from the width of the parabola of the density profile. The details of this demonstration are given in Appendix B.

iv. Analysis on bubble size changes upon insertion

As part of our analysis of bubble size we investigated the time taken to stabilize a bubble after insertion into a pre-equilibrated water system (at 1 bar) by monitoring the bubble radius and average system pressure changes over time. We expect that if the bubble is changing (i.e., its size) there should be some indication in the pressure graph.[4–6] We determined the bubble radius by averaging over 10 ps time windows for the first 100 ps of the simulation. Figure 4.6 (a) shows how the initial R =2.8 nm bubble radius changes over the first 100 ps in a C1 system. Figure 4.6 (b) includes the instantaneous and average pressures (taken over 50 ps time windows) over the 40 ns trajectory. The initial radius was calculated considering only the first 1 ps of data, and thus may have a larger associated error. We find that there is essentially no change in bubble radius or system pressure after about 40-50 ps. Since the average pressure exhibits only fluctuation behavior after about 50 ps, this suggests that an equilibrium has been re-established in the system. However, the time required to reach equilibrium may vary somewhat with the system properties such as system size and bubble size. Therefore, to avoid possible unwanted effects from changes during this equilibration period, the first 1 ns of each simulation was ignored in radius calculations.

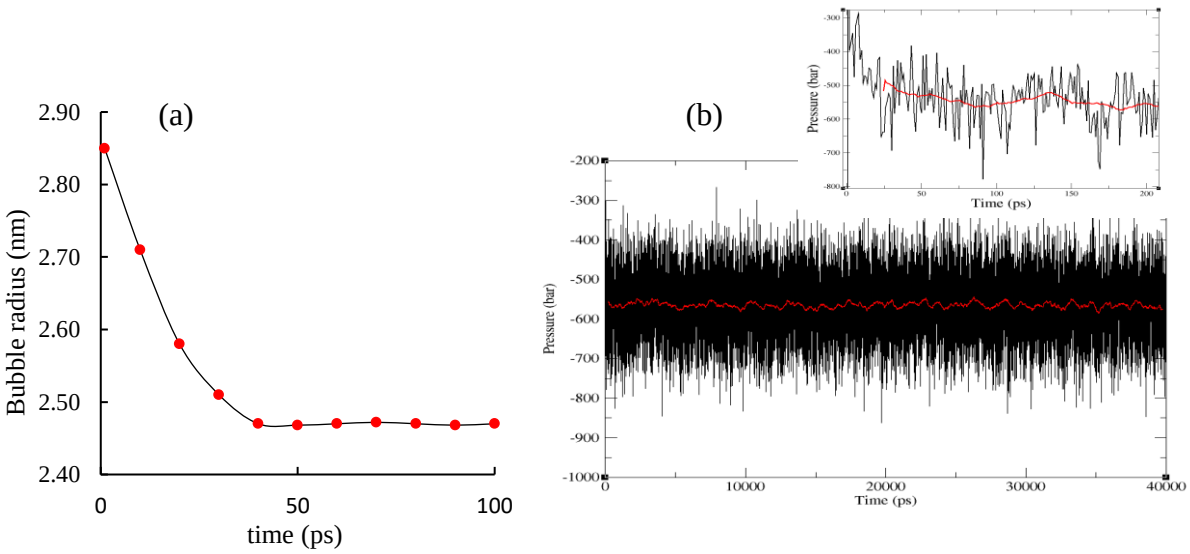

Figure 4.6:(a) Bubble radius changes during the first 100 ps of the simulation for a C1 system with a R ≈2.5 nm bubble. Data were averaged over 10 ps time windows. (b) System pressure changes over a 40 ns of the simulation for a C1 system with a R ≈2.5 nm bubble. The black graph is the instantaneous pressure, and the red line indicates the average pressure taken over 50 ps time windows.

v. Analysis of bubble size

Table 4.5 shows the radii values obtained from the width of the parabola through the x-y, x-z and y-z planes for a C1 system with a *R* ≈2.5 nm bubble at 1, 10, 20 and 30 ns, where profiles have been averaged over 400 ps, and a data range of 75 - 80 % of the height of the parabola. According to Table 4.5, as all the radii values are essentially the same our bubble is nearly a perfect sphere. Therefore, this bubble was stable under the conditions of the simulation exhibiting only small fluctuations in the values during the 30 ns trajectory. However, radius of the initial bubble inserted into the C1 system was 2.8 nm and during the 1 - 30 ns time window of the simulation we measure a bubble radius just over 2.4 nm. Recall that we inserted the bubble into equilibrated liquid water system (1 bar), and consequently the system underwent changes during re-equilibrate resulting in a reduction of the bubble radius.

Table 4.5: Bubble radii measured through the x-y, x-z, and y-z planes for a C1 system with a R ≈2.5 nm bubble at 1, 10, 20 and 30 ns using selected data height and time averaging using the PME method.

Time	**1 ns**			**10 ns**			**20 ns**			**30 ns**		
Plane	x-y	x-z	y-z	x-y	x-z	y-z	x-y	x-z	y-z	x-y	x-z	y-z
R (nm)	2.45	2.45	2.44	2.41	2.44	2.42	2.42	2.44	2.44	2.43	2.42	2.45

vi. Bubble position

During our simulations, it is important to track the position of the bubble. We used the previously discussed 200 ps time average density profiles to find the bubble positions. The center of the bubble is given by the slice which has the lowest density (largest bubble volume). The bubble positions through the x-y, x-z and y-z planes were obtained during the simulation in this manner. We can also compare the bubble position with time to get an understanding of bubble movement. Figure 4.7 shows the movement of a R ≈2.5 nm bubble in a C1 system over a 10 ns trajectory where the random displacement of the bubble is apparent. Table 4.6 includes the R ≈2.5 nm bubble positions at 0, 1, 10, 20 and 30 ns in a simulation of a C1 system. As there is no trend between positions, it is apparent the bubble is exhibiting Brownian motion.[4–6]

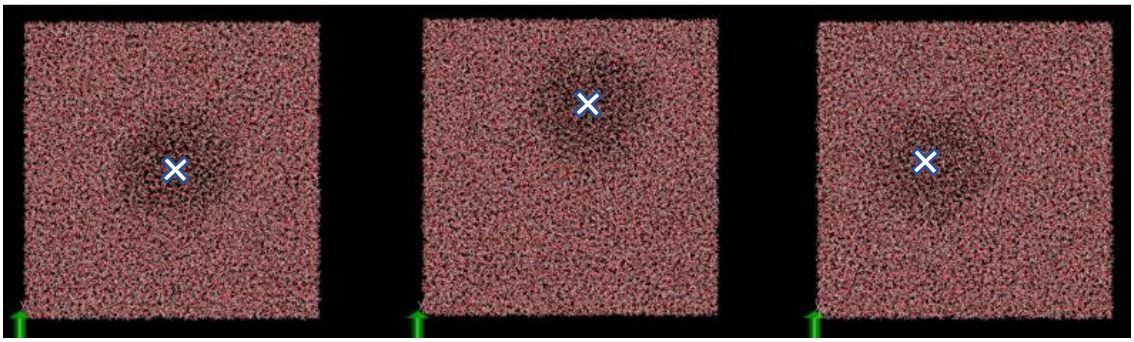

at 0 ns After 5 ns After 10 ns

Figure 4.7:Position of a R ≈2.5 nm bubble in a C1 system at the beginning, after 5 ns, and after 10 ns during an MD simulation. Cross marks show the center of the bubble at each time.

Table 4.6: Position of a R ≈2.5 nm bubble in a C1 system at 0, 1, 10, 20 and 30 ns through the x-y, x-z and y-z planes.

Plane	0 ns	1 ns	10 ns	20 ns	30 ns
	Position from the center of the system (nm)				
x-y	0.05	0.55	-1.4	-0.50	-3.80
x-z	0.25	0.30	1.25	1.20	-3.00
y-z	0.20	-0.10	0.00	0.30	-1.70

vii. Bubble radius of different systems

For each system the average bubble radius (as determined from density profiles) at 1, 3, 5, 7 and 9 ns was examined. Since there were no obvious changes in radius values, the bubbles in all systems were considered to be stable under the present conditions. The average radii and standard deviations were calculated from values at the five-time intervals and through x-y, x-z and y-z planes. Table 4.7 summarizes the calculated average bubble radii obtained for primary systems using both a 1.6 nm cut-off length and the PME method for evaluating the short-range interactions. The standard deviations for radii values are always less than 0.05 nm indicating that the uncertainty in the radius values is small. From Table 4.7 we can see that the short-range interaction method can influence the bubble size through its impact on the pressure.

Table 4.7: Average bubble radii in primary systems using a 1.6 nm cut-off length and the PME method.

System label	Average radius (nm)	
	1.6 nm cut-off length	PME
C1	2.44	2.50
C2	3.75	3.77
RD1	2.50	2.53
RD2	3.85	3.87
RD3	3.81	3.77
RD4	5.08	5.04
RD5	6.30	6.28
RD6	7.43	7.46

4.2.3 Applicability of the Laplace pressure

Since we now have the bubble radius and the average system pressure values for a range of system sizes, we can begin to examine the factors affecting the pressure of a BNB system. The first aspect to test is whether the influence of the bubble upon the system pressure is equal to the Laplace pressure, thereby confirming the applicability of the Laplace pressure to nanoscale bubbles. In Figure 4.8, the average system pressures, P_{system}, were plotted vs 1/bubble radius to investigate the applicability of the Laplace equation. We can see from Figure 4.8 that P_{system} is essentially linear in $1/R$ as predicted by the Laplace equation (see eqn. 3.4). Recall, the slope of this graph should be equal to 2γ (γ is being the surface tension), where γ of TIP4P/2005 water at 298 K and 1 bar pressure is 717 bar nm. Therefore, the expected slope is 1434 bar nm. We find that neither of the two graphs give this slope. Moreover, if the data follows the Laplace equation, it should follow a "y = mx" equation, i.e., have a zero intercept.

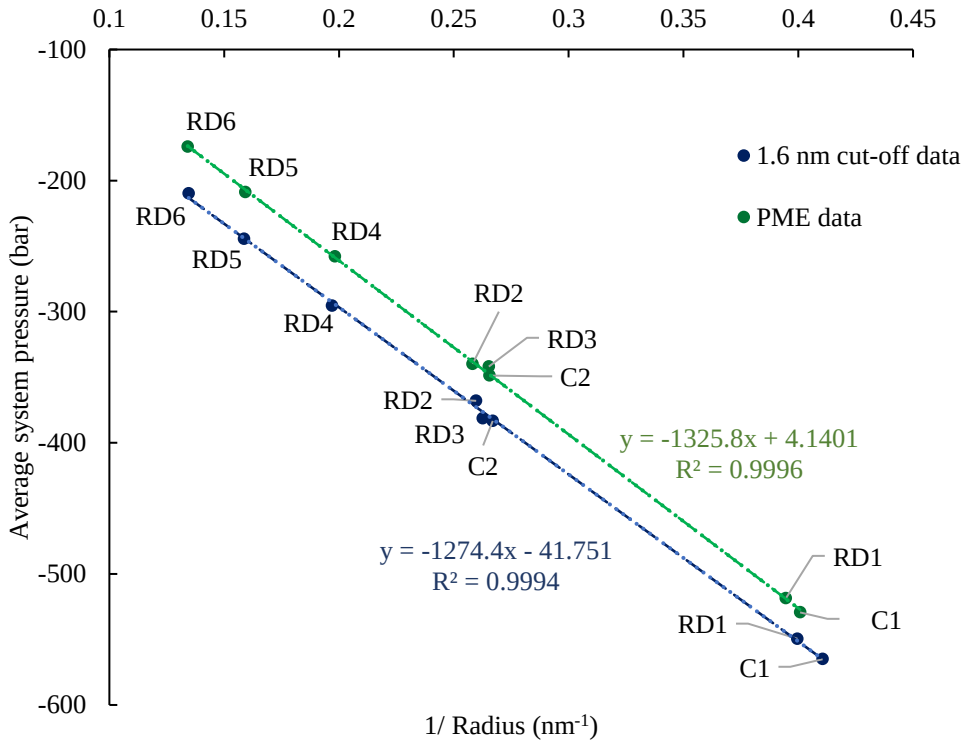

Figure 4.8: Plot of average system pressure vs 1/R from 1.6 nm cut-off length (blue) and the PME (green) data for primary systems.

To confirm a linear P_{system} vs $1/R$ relationship, we also examined the pressure × radius product. If the Laplace pressure equation holds, then $P_{system} \times R$ should give a constant, equal to -2γ, independent of bubble or system size. Table 4.8 gives results for $P_{system} \times R$ for all the primary systems from simulations using both a 1.6 nm cut-off length and the PME method. From Table 4.8, we see that $P_{system} \times R$ is not a constant for the systems, nor does it equal the expected value for -1434 bar nm. Cleary then the apparent linear behavior seen in Figure 4.8 does not confirm the Laplace equation. The results in Table 4.8 indicate that there are other factors affecting the system pressure. There will now be explored further in the next section.

Table 4.8: Values for $P_{system} \times R$ for primary systems from simulations using a 1.6 nm cut-off length and the PME method.

System label	P_{system} × Radius (bar nm)	
	1.6 nm Cut-off length	PME
C 1	-1376.3	-1320.8
C 2	-1436.0	-1312.9
RD 1	-1375.0	-1314.2
RD 2	-1417.2	-1316.0
RD 3	-1452.9	-1288.7
RD 4	-1499.7	-1301.2
RD 5	-1541.2	-1311.5
RD 6	-1560.4	-1299.1

4.3 Task 3: Investigate the existence of separation effect in the pressure for a BNB system

As we have confirmed that the pressure effect of a nanoscale bubble is not only due to the Laplace pressure, we will consider whether the surface polarization model can be used to help explain the other factors affecting the pressure.

4.3.1 Surface polarization model - factors arising

As discussed in Chapter 2, several authors have considered the possible influence of the polarization of the air-water interface on BNBs behaviour.[7–9] According to the study of Ghaani et al.[9] the polarization of the water molecules at the surface can be represented by a set of dipoles, as illustrated in Figure 4.9. Although there are only 4 molecules explicitly shown, the model assumes that the molecules in the surface all have the same average orientation depicted in Figure 4.9.

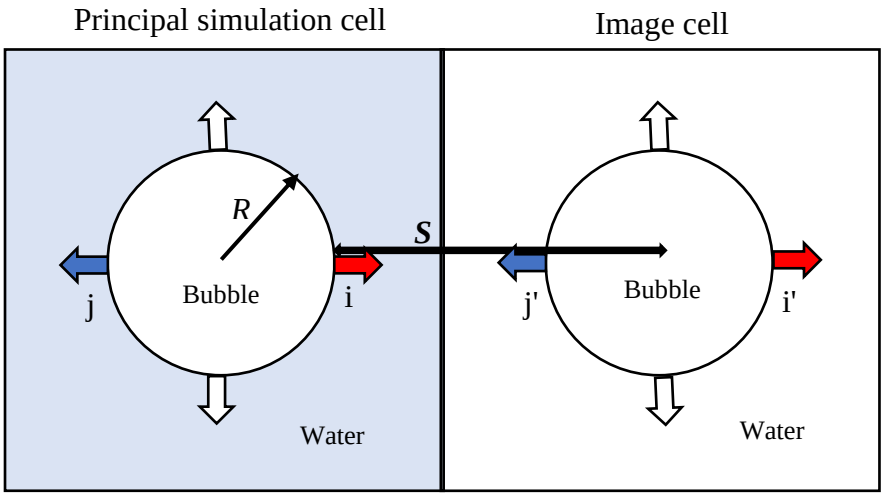

Figure 4.9: The arrangement of water molecules at the surface of a BNB in the principal simulation cell (left). Also, the arrangement is shown in an image cell (right), where the distance between molecule i and the image BNB is S.

In MD simulations of BNBs, it is important to recall that the simulation is being performed in PBC, and thus the simulation cell is surrounded by images of itself (see Figure 2.3). If L is the length of the simulation cell and S is the separation between adjacent bubbles, here taken to be the distance between center of a bubble to the interface of the next bubble in PBC, the separation will be $S = L - R$. In Figure 4.9 we can see that the red and blue dipoles in the principal simulation cell must repel, giving rise to an outward force on the red dipole labelled i. However, we can also see that there will be dipole-dipole interactions between the red dipole and those in the image cell, where the center of the image BNB is at a distance S from the dipole i. Moreover, because of the

long-range nature of dipole-dipole interactions, such interactions can be important, and particularly if S is roughly similar in value to *R*. If we consider the interaction of dipole i with the image of the blue dipole, j', we can see that while it is also repulsive, it will result in an inward force on dipole i. In the case when *R*=*S*, we can then see that the effect of dipole j and its image dipole j' will cancel. Clearly, such interactions will impact the pressure unless S is very large. To be able to correctly capture the impact of the long-range dipole-dipole interactions on BNB behaviour, one should either perform simulations where *S*>>*R*, or one must be able to identity the effect on the pressure from a set of systems with a fixed size BNB but different values for S and then correct for this dependence by extrapolating to large *S*. While both approaches will be computational challenges, second option appears to be more tractable.

It has been shown that water molecules at an air-water interface exhibit both a dipole and quadrupole polarization.[8,9] The interactions arising from these dipole and quadrupole movements can be dipole-dipole (μ-μ) or dipole-quadrupole (μ-Q) interactions.[9] It has been previously shown that the pressure contribution associate with μ-μ interactions is directly related to 1/R,

$$P_{(\mu-\mu)} \propto \frac{1}{R}. \tag{4.1}$$

Using the same mean field model, Bryant and Kusalik[10] have been able to show that the pressure contribution associate with μ-Q interactions is directly related to $1/R^2$,

$$P_{(\mu-Q)} \propto \frac{1}{R^2}. \tag{4.2}$$

Therefore, if we obtain a linear graph for $P_{system} \times R$ vs $1/R$, this may be an indication of the affect of the μ-Q interactions.

4.3.2 Evaluation of surface polarization model

To investigate the possible effect from μ-Q interactions on the pressure, plots of $P_{system} \times R$ vs $1/R$ data were examined. Figures 4.10 and 4.11 demonstrate the relationship between $P_{sysetm} \times R$ vs $1/R$ for primary systems using a 1.6 nm cut-off and the PME method, respectively. Although there is not a clear trend in Figure 4.11 with the PME method, in Figure 4.10 with a 1.6 nm cut-off there appears to be a roughly linear trend for $P_{system} \times R$ vs $1/R$. When we analyse systems which have very similar sized bubbles but giving different $P_{system} \times R$ values, (circled systems in Figure 4.10 and 4.11) these systems have different separations, S (the distance between the adjacent BNBs in their image cells).

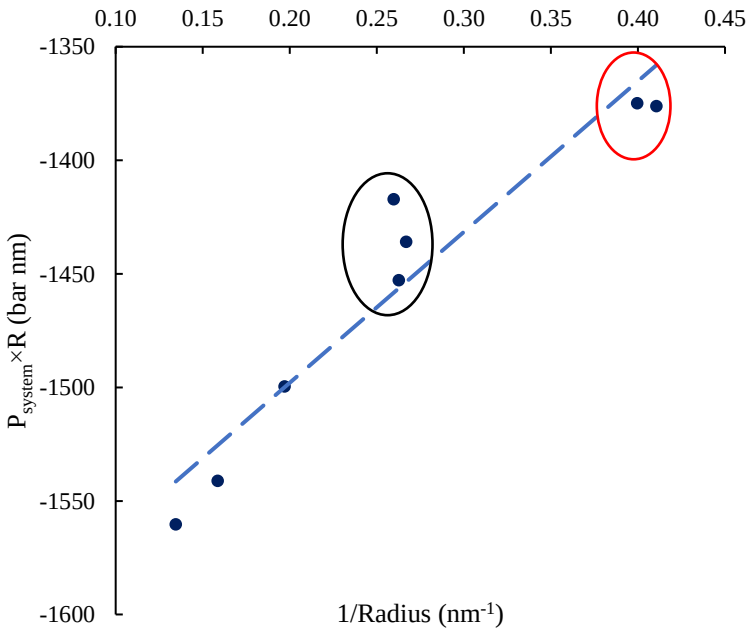

Figure 4.10: Plot of $P_{system} \times R$ vs $1/R$ for primary systems using a 1.6 nm cut-off method. Bubbles of similar size are circled (black for a $R \approx 3.75$ nm and red for $R \approx 2.5$ nm bubbles).

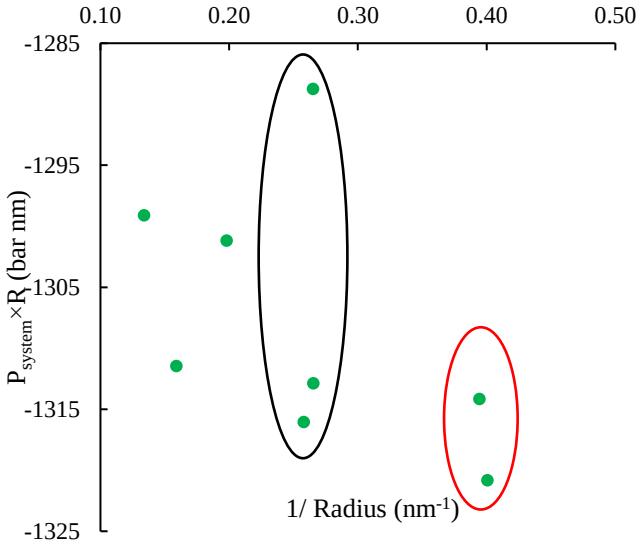

Figure 4.11: Plot of P_{system}× R vs 1/R in primary systems using the PME method. Bubbles of similar size are circled (black for a R ≈3.75 nm and red for a R ≈2.5 nm bubbles).

4.3.3 Effect of bubble separation on pressure

For the bubble separation analysis, we prepared two new sets of systems with the same bubble radius (one with ≈2.5 nm and one with ≈3.75 nm) using both a 1.6 nm cut-off and the PME method for the short-range interactions. The system preparation was somewhat challenging as we required the radius values to be essentially equal to avoid possible effects of the bubble size on pressure and bubble size cannot be exactly predicted at the start of a simulation. The desired bubble size was obtained using simply a trial and error method.

Table 4.9 reports values for bubble radii and system pressures for the systems prepared for separation analysis of a R ≈2.5 nm bubble with a 1.6 nm cut-off length. Recall, the separation was calculated as $S = L\text{-}R$. Similar simulations were performed with the PME method, and Table 4.10 includes the results obtained for separation analysis for a R ≈2.5 nm bubble with the PME method. In both sets of simulations, the standard deviations of the average pressures and radii values were less than 1 bar and 0.05 nm, respectively.

Table 4.9: Average system pressures and average radii values from separation analysis for simulations using a 1.6 nm cut-off length for R ≈2.5 nm bubbles.

System label	Average radius(nm)	Average pressure (bar)	Separation (nm)
10.5C	2.50	-554.6	8.00
11.5C	2.54	-540.7	8.96
13.5C	2.53	-553.1	10.97
16.5C	2.55	-540.3	13.95
11RD	2.51	-550.0	8.49
13RD	2.55	-544.4	10.45
15RD	2.55	-546.6	12.45
17RD	2.50	-559.9	14.50

Table 4.10: Average system pressures and radii values from separation analysis for simulations using the PME method for R ≈2.5 nm bubbles.

System label	Average radius(nm)	Average pressure (bar)	Separation (nm)
10.5C	2.56	-507.0	7.94
11.5C	2.56	-510.2	8.94
13.5C	2.57	-508.9	10.93
16.5C	2.57	-510.7	13.93
11RD	2.53	-518.6	8.47
13RD	2.52	-521.1	10.48
15RD	2.53	-519.3	12.47

Figure 4.12 shows plots of $P_{system} \times R$ vs $1/S$ obtained from the simulations using a 1.6 nm cut-off length for a R ≈2.5 nm bubble in (a) cubic and (b) RD systems. Although there is no clear linear relationship for the R ≈2.5 nm bubble in cubic systems, one is apparent for RD systems. Figure 4.13 shows plots of $P_{system} \times R$ vs $1/S$ from simulations using the PME method for a R ≈2.5 nm bubble in (a) cubic and (b) RD systems. Although we attempt to create a 17 nm RD system with a R ≈2.5 nm bubble, we were unable to obtain a stable bubble (the bubble always collapsing withing

a few picoseconds). From comparison of the plots in Figures 4.12 and 4.13 we see that $P_{system} \times R$ is apparently linear in $1/S$ in 3 of 4 cases.

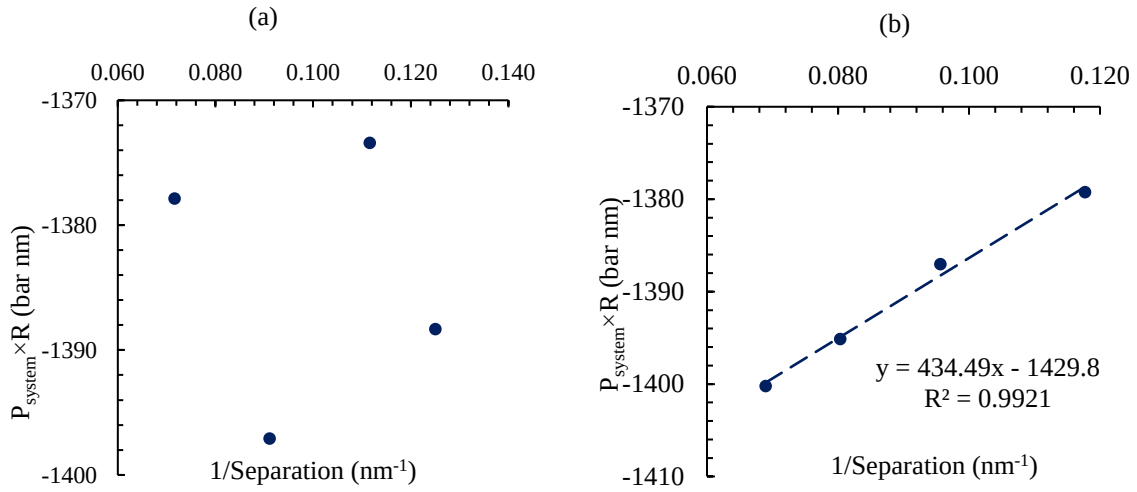

Figure 4.12: Plots of $P_{system} \times R$ vs 1/S for (a) cubic systems and (b) RD systems with a R ≈2.5 nm bubble for simulations using a 1.6 nm cut-off length.

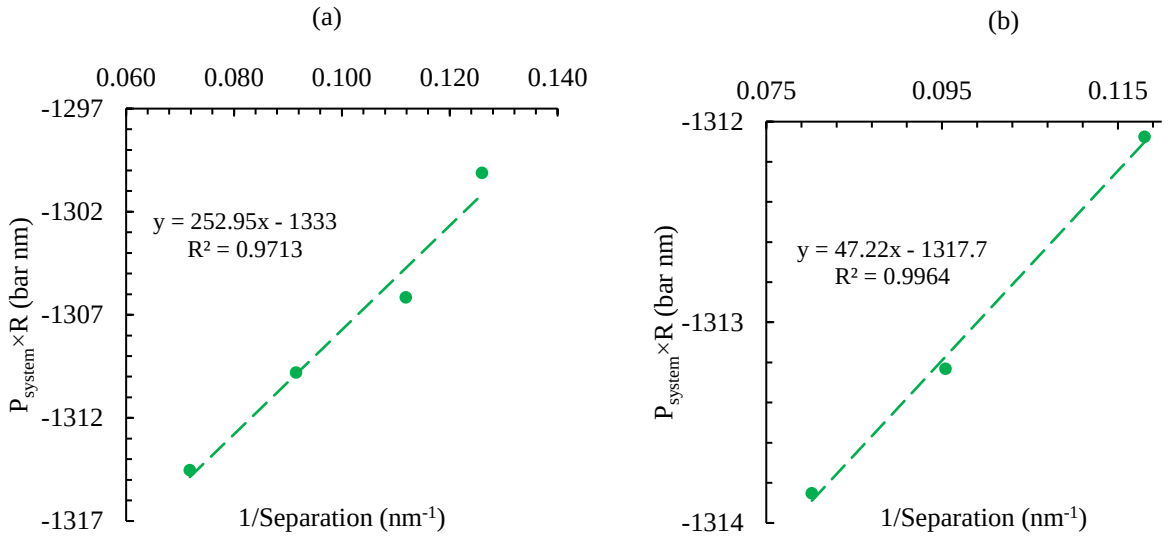

Figure 4.13: Plots of $P_{system} \times R$ vs 1/S for (a) cubic systems and (b) RD systems with a R ≈2.5 nm bubble for simulations using the PME method.

A similar approach was followed to obtain the separation dependence for R ≈3.75 nm bubble systems. Table 4.11 includes results for the separation dependence for a R ≈3.75 nm bubble with a 1.6 nm cut-off length, while Figure 4.14 shows a plot of $P_{system} \times R$ vs $1/S$ for the values from the RD systems. Table 4.12 provides results from simulations of a R ≈3.75 nm bubble using the PME method, and Figure 4.15 includes the plot of $P_{system} \times R$ vs $1/S$.

Table 4.11: Average system pressures and radii values from separation analysis for simulations using a 1.6 nm cut-off for R ≈3.75 nm bubbles.

System label	Average radius (nm)	Average pressure (bar)	Separation (nm)
13.5 C	3.76	-382.6	5.98
16.5 C	3.74	-388.3	9.02
13RD	3.79	-375.1	5.42
15RD	3.75	-381.7	7.51
17RD	3.79	-380.6	9.42
20RD	3.79	-384.7	12.42
23RD	3.74	-390.6	15.52

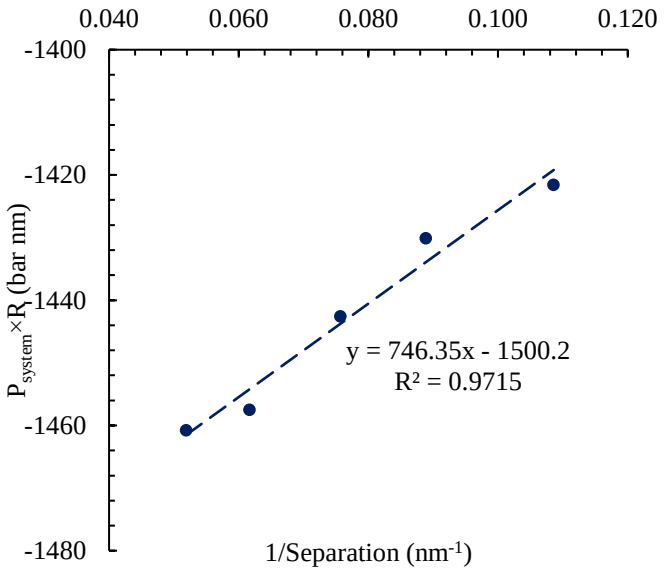

Figure 4.14: Plot of $P_{system} \times R$ vs 1/S for RD systems with a R ≈3.75 nm bubble for simulations using a 1.6 nm cut-off length.

Table 4.12: Average system pressures and radii values from separation analysis for simulations using the PME method for R ≈3.75 nm bubbles.

System label	Average radius (nm)	Average pressure (bar)	Separation (nm)
13.5C	3.77	-348.6	9.74
16.5C	3.78	-346.2	12.72
13RD	3.74	-349.7	9.26
15RD	3.77	-348.7	11.23
17RD	3.72	-354.9	13.28
20RD	3.74	-353.0	16.26

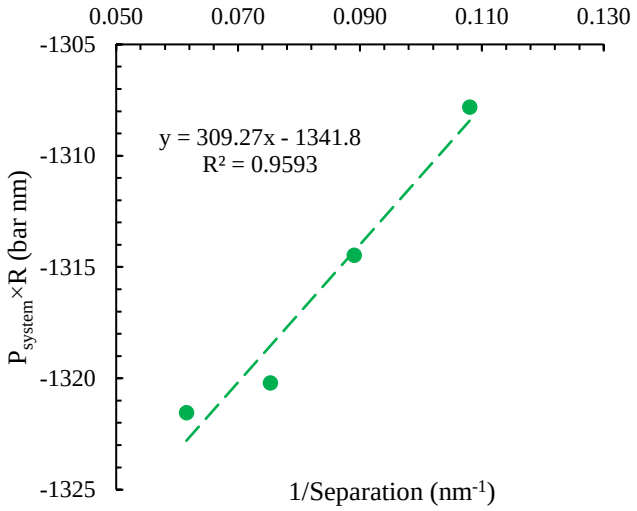

Figure 4.15: Plot of P_{system}×R vs 1/S in RD systems with a R ≈3.75 nm bubble for simulations using the PME method.

Since we were able to prepare only two cubic systems with a *R* ≈3.75 nm bubble, graphs for the cubic systems were not generated. Because of the computational cost associated with the large system simulations, this analysis was limited to *R* ≈2.5 nm and R ≈3.75 nm bubbles, although data from larger bubbles in larger system could be helpful. According to both *R* ≈2.5 nm and *R* ≈3.75 nm bubble results, there is an apparent linear relationship between P_{system}×*R* vs 1/*S* in most cases for systems with bubbles of the same size (although this was not the case for the *R* ≈2.5 nm bubbles

in cubic systems with a 1.6 nm cut-off length which may be due to additional complications arising from the cut-off length method in BNB simulation).

4.3.4 Bubble interface

In order to analyse the BNB interface thickness, radial distribution profiles from the center of the bubble (as captured by 200 ps time average density profiles) were obtained. Radial distribution profiles give the probability of finding a molecule at distance from a reference point. Figure 4.16 shows the radial distribution profiles obtained from the center of the bubbles from our primary set of systems. The profiles are zero inside the bubble as there are essentially no water molecules inside the bubble. The sloping region of the sigmoidal curve indicates the thickness of the bubble interface. According to Figure 4.16, the thickness of the bubble interface is about 1.5 - 2 nm. Values reported in the literature for the bubble interface thickness are usually about 1 nm.[5] These differences could arise because of errors associate with the bubble movement and surface fluctuations during the time window (400 ps) used for averaging the configurations.

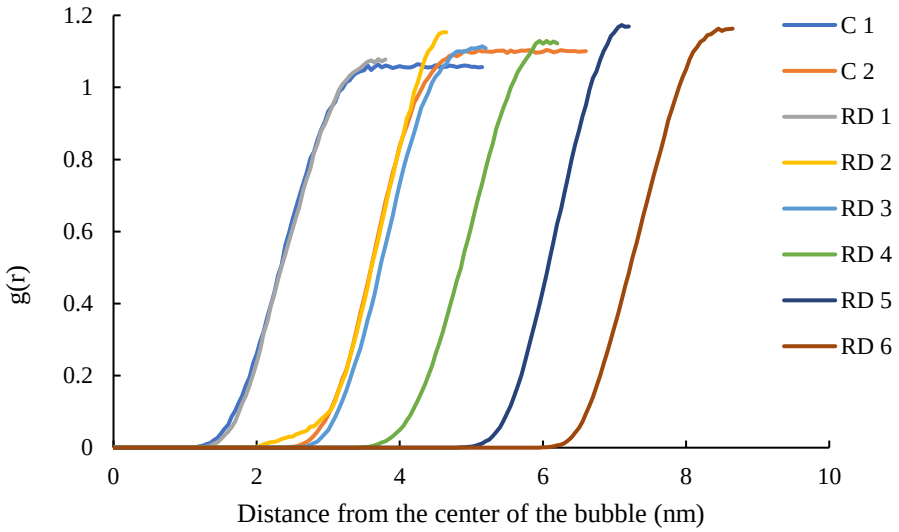

Figure 4.15: Radial distribution profiles, g(r), from the center of the bubble obtained for the primary set of systems.

To investigate whether the width of the sloping region of the sigmoidal curve is affected by the selected time average, separate radial distribution profiles were generated for same systems using different time averaging windows. Figure 4.17 presents radial distribution profiles for a R ≈3.75 nm bubble in a L=20 nm RD system obtained from averaging over 50, 100, 200 and 400 ps. Although it becomes more difficult to estimate the location of the interface from the shorter time windows, it is apparent that the length of time averaging can somewhat affect the apparent width of the interface. As the accuracy of the profile data improves with the length of the time averaging, 400 ps was used for generating the radial distribution profiles.

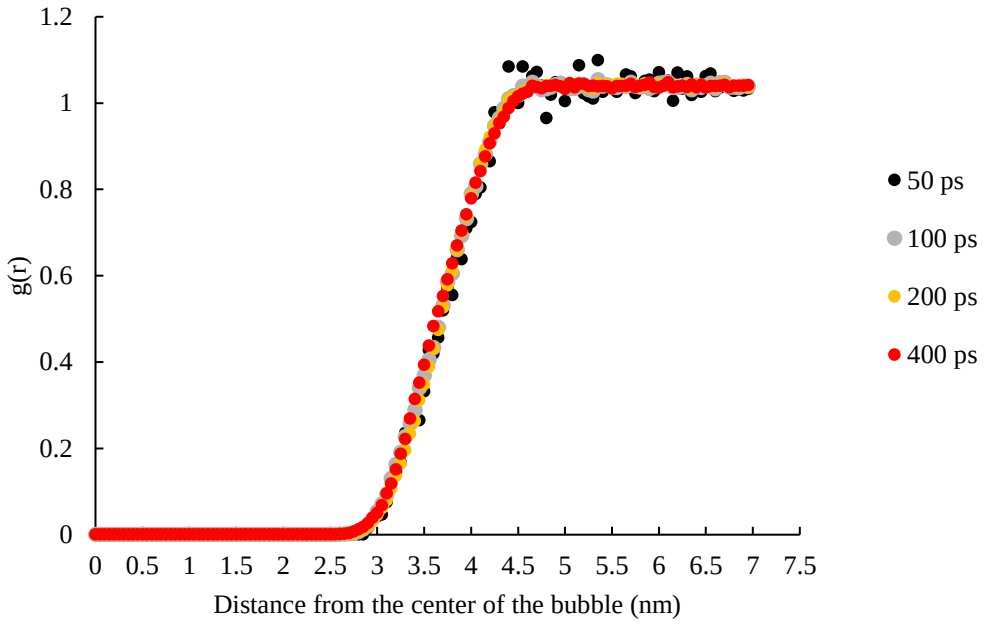

Figure 4.17: Effect of different time averages on the BNB interface width from the radial distribution profile for a R ≈3.75 nm bubble in the 20 RD system.

4.3.5 Finding the pressure associated with bulk liquid

As a final factor to consider in determination of pressure in BNB systems, we will examine the differences between the measured system pressures, P_{system}, and the pressure in the bulk liquid, P_{bulk}, as discussed in section 3.3.3. Recall, contributions to P_{system} both from molecules in the bulk liquid region of the system (water molecules away from the bubble) and surface molecules (water

molecules in the surface of the BNB) were identified. As discussed in section 3.3.3, P_{bulk} can be estimated from radial distribution profiles providing the bulk liquid density, where a sample calculation is given in Appendix C. To find the relationship between bulk liquid density and bulk liquid pressure, a L = 10.5 nm cubic bulk water system (with 38660 water molecules and without the bubble) was equilibrated at the desired pressures (i.e., -200, -300, -400, -500 and -600 bar). Table 4.13 reports the system pressures and the average system densities obtained from simulations using both a 1.6 nm cut-off and the PME method for the short-range interactions. Values for both pressure and density include 3 decimal digits to improve the accuracy of the calibration curve. From the values in Table 4.13, two calibration curves for the average density vs average pressure, shown in Figure 4.18, were obtained for simulations using (a) cut-off and (b) the PME method.

Table 4.13: Average system densities from a L=10.5 nm cubic bulk water system at different pressures using a 1.6 nm cut-off length and the PME method.

Set pressure (bar)	**1.6 nm Cut -off length**		**PME method**	
	average pressure (bar)	**average density (kg/m^3)**	**average pressure (bar)**	**average density (kg/m^3)**
-200	-198.918	987.326	-199.952	987.479
-300	-299.623	982.513	-299.849	982.638
-400	-399.434	977.599	-400.157	977.714
-500	-499.212	972.592	-500.072	972.74
-600	-599.384	967.408	-600.133	967.557

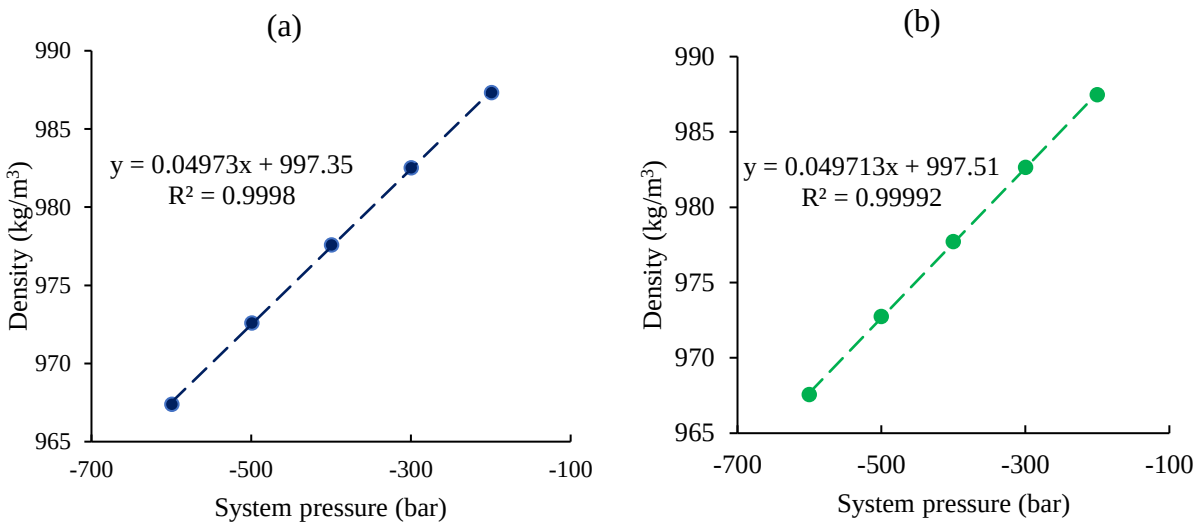

Figure 4.18: Average density vs pressure calibration curves from a L= 10.5 nm cubic bulk water system at different pressure conditions using (a) a 1.6 nm cut-off length and (b) the PME method.

As the systems in these simulations contained only water, the average system density should be the average bulk liquid density for each pressure. For both the cut-off and the PME data, the bulk liquid density is found to depend linearly on the bulk liquid pressure. Therefore, if we can determine the average bulk liquid density in a BNB system, we can easily obtain the average bulk liquid pressure (i.e., the value for P_{bulk} required for our analysis of contributions to P_{system}). To accurately determine the average bulk liquid density, additional BNB systems were generated and used to obtain radial distribution profiles from the center of the bubble. The systems in Figure 4.16 are not useful as their plateau regions are relatively small and hence can not provide precise values. To avoid unwanted pressure changes in this analysis due to changes in bubble size, sets of systems with bubbles of the same size with considerably longer plateau regions were used. We focused on $R \approx 2.5$ nm systems to help to reduce computational costs. Figure 4.19 shows examples of the radial distribution profiles for a $R \approx 2.5$ nm bubble in different cubic (C) and RD systems (see Table 3.7). Average values for the plateau region were determined for each system for 10 data sets obtained at 1 - 10 ns. The standard deviations for the plateau averages were also calculated. Nine decimal

digits were retained in the values to ensure no loss of accuracy. Table 4.14 summaries the average plateau values and the standard deviations for each system. The total volume of the system is the value reported by the simulation software. Using the number density and total volume of each system, the density of the bulk liquid was calculated (Appendix C). Once the bulk liquid density was obtained, the bulk pressure was obtained for each system from the appropriate calibration curve.

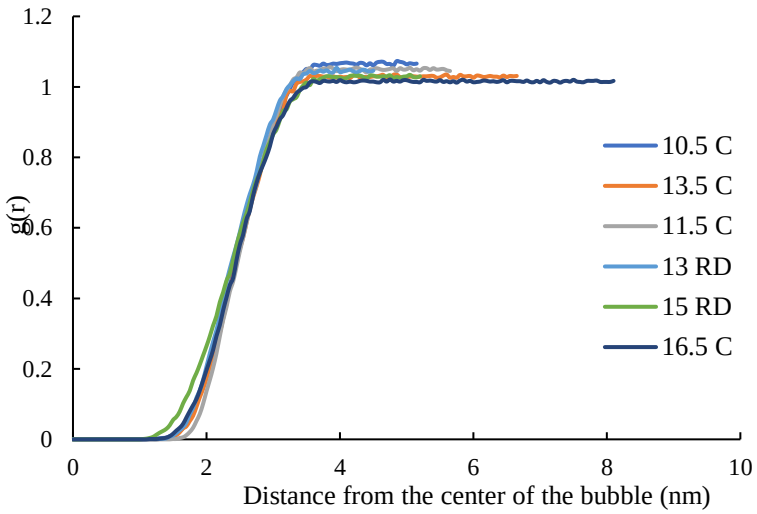

Figure 4.19: Radial distribution profiles from the center of the bubble for a R ≈2.5 nm bubble in L=10.5, 11.5, 13.5, 16.5 nm cubic and 13 and 15 nm RD systems.

Table 4.14: System properties (volume and number density, N/V) and the plateau averages and standard deviations (stdev.) from the radial distribution profiles.

System label	Volume (nm^3)	Number density (molecules/nm^3)	Plateau average	Stdev. of plateau
10.5C	1160.58	30.38	1.06681	0.00083
11.5C	1520.88	30.97	1.04898	0.00048
13.5C	2460.38	31.54	1.03008	0.00083
16.5C	4492.12	31.97	1.01615	0.00057
13RD	1553.15	31.09	1.04380	0.00116
15RD	2386.48	31.57	1.02818	0.00057

Table 4.15 summarizes key values for the analysis of the bulk liquid pressure. In Table 4.15, V_{water} is the total water volume calculated from the bubble volume and the total system volume, δP is the pressure difference between the system and bulk pressures (see eqn. 3.13), and the length of the plateau is the region of the radial distribution profile for each system corresponding to the bulk liquid. We remark that special care was taken to select only the data points in the plateau region and to avoid points that might be in the sloping region and hence influenced by the interface.

Table 4.15: Results for the analysis of bulk liquid pressure. System pressure errors are the values reported by the software.

System label	**Bulk pressure (bar)**	**System pressure (bar)**	**System pressure error (bar)**	V_{water} **(nm^3)**	δP **(bar)**	$V_{water} \times \delta P$ **(bar nm^3)**	**Length of the plateau (nm)**
10.5C	-565.2	-507.0	0.42	1090.0	58.1	63400	1.35
11.5C	-516.3	-510.2	0.99	1450.6	6.1	8890	1.95
13.5C	-516.0	-508.9	0.83	2389.0	7.1	17020	2.70
16.5C	-515.2	-510.7	2.20	4421.0	4.5	20034	3.80
13RD	-535.9	-521.1	0.63	1486.1	14.7	21900	0.85
15RD	-533.4	-519.3	0.92	2331.9	14.1	32800	1.50
				Average $V_{water} \times \delta P$		21500	

While the focus here was to obtain values for $P_{bulk,}$ we noted that the errors associate with the P_{bulk} values are non-negligible, estimated to be at least ±5 bar. Therefore, we did not used the P_{bulk} values directly, but rather looked to determine them from $P_{system.}$ According to the analysis in section 3.3.3, for bubbles of the same size, the product of $V_{water} \times \delta P$ should be a constant. We see from Table 4.15 that there is considerable variation in this product. In order to reduce the errors in these results, the average of the product of $V_{water} \times \delta P$ across the different systems was determined. In Table 4.15, since the product of $V_{water} \times \delta P$ for the 10.5C and 11.5C systems are apparently

outliers compared to the values from other systems, they were ignored in the calculation of the average $V_{water} \times \delta P$.

According to eqn.3.17 in section 3.2.3 ($P_{surface}$ - P_{bulk}) can be obtained from,

$$\left(P_{system} - P_{bulk}\right) = \delta P = \alpha \times A \times \frac{P_{surface} - P_{bulk}}{V_{water}}, \tag{4.3}$$

where constant α is the interface thickness (see eqn.3.15). The average bubble interface width and bubble radius were determined by averaging over all the system values (see Table 4.16). From eqn. 3.15 and 3.16, the bubble interface volume was calculated using the average interface thickness (1.9 nm) and average bubble radius (2.55 nm) from Table 4.16. Then using the average for δP, the value for ($P_{surface} - P_{bulk}$) was found to be 138 bar. Finally, the estimated bulk liquid pressure, P^*_{bulk}, was calculated by rearranged eqn. 4.3 as,

$$P^*_{bulk} = P_{system} - \frac{V_{surface} \times 138\ bar}{V_{water}}\ . \tag{4.4}$$

This estimate allows P^*_{bulk} to be obtained directly from (more reliable) P_{system} values, thereby helping to reduce its uncertainty. Table 4.16 includes the estimated bulk pressure values calculated according to this approach.

Table 4.16: Bubble radius, separation and interface thickness of the systems used for bulk liquid pressure analysis. The values for P^*_{bulk} are estimated from eqn. 4.4.

System label	Average radius (nm)	Separation (nm)	Interface width (nm)	P^*_{bulk} (bar)
10.5C	2.56	5.37	2.0	-529.2
11.5C	2.56	6.38	1.9	-526.8
13.5C	2.57	8.35	1.8	-519.0
16.5C	2.57	11.36	1.9	-516.2
13RD	2.52	7.96	1.9	-537.3
15RD	2.52	9.96	1.8	-529.6
Average bubble radius = **2.55**		Average interface width = **1.9**		

Results for P^*_{bulk} are plotted vs 1/S in Figure 4.20. Interestingly, we find an apparent linear relationship with different slopes for cubic and RD systems. This different slope can be seen to arise because of the different number of neighbouring cells in the cubic (6) and RD (12) systems. This behaviour is then consistent with the behaviour predicted by the surface polarization model[9] discussed in section 4.3.1. We also find that the two data sets appear to share a common y-intercept. As 1/S = 0 represents the limit of infinite separation, this common point of extrapolation helps provide further confirmation of the separation effect in the pressure for BNB systems. These results predicted that for a bubble at infinite bubble separation, the bulk liquid pressure will be about -503 bar at 298 K, independent of system shape. Therefore, from the present results and this analysis, we have confirmed the pressure in BNB systems is affected by the bubble separation.

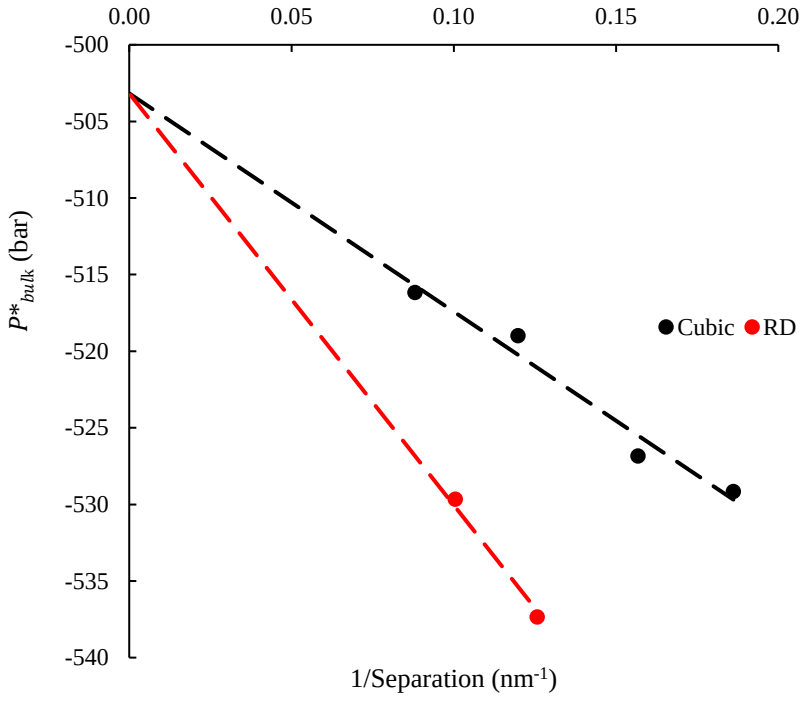

Figure 4.20: Effect of separation on bulk liquid pressure (estimated) in cubic (black) and RD (red) systems with a R ≈2.55 nm bubble. Here the black line is the best fit curve to the data points, while the red line was drawn as a best fit to the two data points while being constrained to share the same intercept as the black line.

4.4. Summary

This chapter discussed the various simulation results obtained for each of the approaches described in Chapter 3. Starting from finding the average system pressure, bubble radius, bubble position, and interface thickness, it also examined and evaluated different pressure contributions for BNB systems. Finally, we confirmed that the separation between the bubbles impacts the pressure in a BNB system which can directly affect the stability of BNBs.

4.5 References

1. Abraham, M. J.; Gready, J. E. Optimization of Parameters for Molecular Dynamics Simulation Using Smooth Particle-Mesh Ewald in GROMACS 4.5. *J Comput Chem* **2011**, *32* (9), 2031–2040. https://doi.org/10.1002/jcc.21773.

2. Petersen, H. G. Accuracy and Efficiency of the Particle Mesh Ewald Method. *J Chem Phys* **1995**, *103* (9), 3668–3679. https://doi.org/10.1063/1.470043.

3. Abraham, M. J.; Murtola, T.; Schulz, R.; Páll, S.; Smith, J. C.; Hess, B.; Lindah, E. Gromacs: High Performance Molecular Simulations through Multi-Level Parallelism from Laptops to Supercomputers. *SoftwareX* **2015**, *1–2*, 19–25. https://doi.org/10.1016/j.softx.2015.06.001.

4. Lu, Y.; Yang, L.; Kuang, Y.; Song, Y.; Zhao, J.; Sum, A. K. Molecular Simulations on the Stability and Dynamics of Bulk Nanobubbles in Aqueous Environments. *Physical Chemistry Chemical Physics* **2021**, *23* (48), 27533–27542. https://doi.org/10.1039/d1cp03325e.

5. MATSUMOTO, M. Surface Tension and Stability of a Nanobubble in Water: Molecular Simulation. *Journal of Fluid Science and Technology* **2008**, *3* (8), 922–929. https://doi.org/10.1299/jfst.3.922.

6. Hong, S. N.; Choe, S. H.; Jong, U. G.; Pak, M. S.; Yu, C. J. The Maximum Interbubble Distance in Relation to the Radius of Spherical Stable Nanobubble in Liquid Water: A Molecular Dynamics Study. *Fluid Phase Equilib* **2019**, *487*, 45–51. https://doi.org/10.1016/j.fluid.2019.01.014.

7. Matyushov, D. v. Electrophoretic Mobility without Charge Driven by Polarisation of the Nanoparticle-Water Interface. Mol Phys 2014, 112 (15), 2029–2039. https://doi.org/10.1080/00268976.2014.882521.

8. Martins-Costa, M. T. C.; Ruiz-Lopez, M. F. Solvation Effects on Electronic Polarization and Reactivity Indices at the Air–Water Interface: Insights from a Theoretical Study of Cyanophenols. Theor Chem Acc 2015, 134 (2). https://doi.org/10.1007/s00214-014-1609-z.

9. Ghaani, M. R.; Kusalik, P. G.; English, N. J. Massive Generation of Metastable Bulk Nanobubbles in Water by External Electric Fields. Sci Adv 2020, 6 (14). https://doi.org/10.1126/sciadv.aaz0094.

10. Bryant R.; Kusalik P.G. Unpublished Work.

APPENDIX

Appendix A: Calculation of number of water molecules in each system

The calculation used to find the number of water molecules in initial systems and number of water molecules after the bubble insertion in Chapter 3, Table 3.1 is given below.

Volume of a cubic system = L^3 (nm^3) . (A1)

Density of water at 298 K is 33.4 molecules/nm^3.[1] Therefore,

Total water molecules in the system $= 33.4 \frac{\text{molecules}}{\text{nm}^3} \times L^3$ (nm^3). (A2)

For an example, calculation for cubic system with L=10.5 nm,

Volume of the systems = $(10.5)^3$ nm^3

= 1157.6 nm^3

Total number of water molecules in initial system = 1157.6 × 33.4 molecules

= 38,664 molecules

Rounding off, 38,660 water molecules were filled to the cubic system with L=10.5 nm.

Number of water molecules in each system after the bubble insertion can be calculated using $R_{in.}$ and eqn. A3, A4 and A5. Recall, R_{in} is the initial radius of the bubble.

Volume of a sphere with R_{in} radius $= \frac{4}{3}\pi R_{in}^3$. (A3)

Number of water molecules in the water sphere = $33.4 \times \frac{4}{3}\pi R_{in}^3$ molecules . (A4)

Therefore, water molecules remaining in the systems after the bubble insertion, from eqn. A3 and A4,

$$= (L^3 - \frac{4}{3}\pi R_{in}^3) \times 33.4 \text{ molecules} \ . \qquad \text{(A5)}$$

For cubic system with L=10.5 nm and R_{in}= 2.8 nm,

Number of water molecules in the bubble $= 33.4 \times \frac{4}{3}\pi(2.8)^3$

$= 3070$ molecules.

Therefore, water molecules in cubic system with L=10.5 nm after the bubble insertion,

$= 38660 - 3070$

$= 35590$ molecules.

By rounding off, 35600 molecules were settled with R_{in} =2.8 nm bubble in cubic system with L=10.5 nm.

It is worth mentioning that during the NPT simulation, the lengths of some systems changed by less than 0.01 nm. To avoid errors caused by these changes in volume, the final volume obtained from the software was used in the NVT equilibrium. Additionally, filling the exact number of calculated water molecules in the system can sometimes result in errors during the energy minimization step. To mitigate these errors, the number of water molecules was rounded off, avoiding overlapping of molecules.

Appendix B: Applicability of using parabolic width in density profiles to calculate bubble radius

As described in section 3.2.2, the width of the parabola in the density profiles was used to determine the bubble diameter. To confirm the applicability of this method, the following study was conducted to a cubic system with L= 10.5 nm and R ≈2.5 nm bubble.

1. Slicing through the system and finding the center of the bubble: Slices were taken through the entire system (refer to Figures 3.2 and 3.3) as illustrated in Figure B1 (a). The center was found by selecting the position with the lowest density in density profile. Note that the bubble moves during the simulation, so the center of the system may not always be the same as the center of the bubble.

2. Determining the radii of the slices: In Figure B1 (b), the radius of the overall bubble is represented as R (which is equal to the half of the width of the density profile parabola - Figure 3.4) and the distance from the center of the bubble to the selected slice is designated as D. The radius of the selected bubble slice is labeled as R_1. The value of D can be easily extracted from the position data in the density profile.

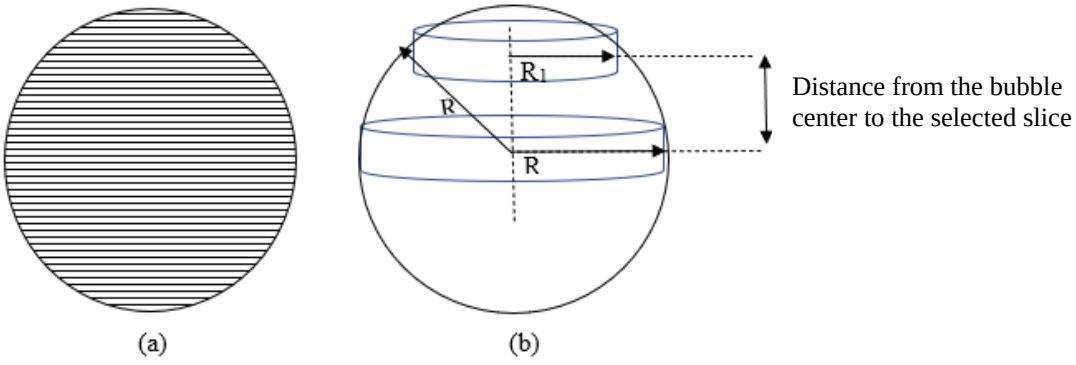

Figure B.1:(a) Slices through the bubble (b) radius of the bubble is R , radius of the selected bubble slice R_1 and distance from the bubble center to the selected slice D is shown.

3. Determining the radii of the slices:

Using the Pythagorean theorem, R_1 could be calculated as eqn. B1:

$$R_1 = \sqrt{R^2 - D^2} \ . \quad \text{(B1)}$$

Note that with the selected slice, D changes, and hence R_1 values for each slice can be calculated.

4. Calculating the volume of each slice: Assuming each slice is cylindrical, the volume of each slice could be calculated using eqn. B2, where d is the thickness of the slice: (d = 0.2 nm was selected for all density profiles to balance precision and computational time.).

$$v = \pi \times R_1^2 \times d \ . \quad \text{(B2)}$$

Substituting R_1 from eqn. B1,

$$v = \pi \times (R^2 - D^2) \times d \ , \quad \text{(B3)}$$

$$= \pi d R^2 - \pi d D^2 \ . \quad \text{(B4)}$$

Eqn. B4 is a quadratic in D, which give a parabolic graph similar to parabola in density profiles. This confirmed the feasibility of using density profiles for determining the bubble diameter. However, it was noted that the assumption of a cylindrical shape might not be entirely accurate for slices at the edge of the sphere, which tend to have a more cap-like shape. To improve the precision of the measurement, data points from the edge were excluded when plotting the parabolic fit, and the R^2 value of the fit was taken into consideration.

Appendix C: Calculation of bulk liquid density from radial distribution profiles

The bulk liquid density in each system was calculated using the average g(r) values from the plateau region in Chapter 4, Figure 4.19, with the aid of eqns. C1 and C2. The plateau region g(r) represents the likelihood of finding a water molecule in the bulk liquid region.

$$Bulk\ liquid\ density\ = Plateau\ average \times\ conversion\ factor\ \times \left(\frac{N}{V}\right)\ . \qquad \text{(C1)}$$

A conversion factor was applied to convert the number of water molecules into a mass density. The value of (N/V) in eqn. C2 was calculated by dividing the number of water molecules in the system after bubble insertion by the volume of the bulk liquid region, which was obtained from the software.

$$Conversion\ factor = \frac{molecular\ weight\ of water\ (kgmol^{-1})}{Avergadro\ number(mol^{-1})} \times 10^{-27} m^{-3}\ , \qquad \text{(C2)}$$

$$= \frac{18.01528\times10^{-3}\ kgmol^{-1}}{6.022\times10^{-23}\ mol^{-1}} 10^{-27} m^{-3}\ . \qquad \text{(C3)}$$

The conversion factor is 29.91577549 kgm^{-3}.

Appendix D: Data files used for simulations

The topology file for the smallest cubic system, along with the MD parameter files for energy minimization (em.mdp), NPT simulation for 1 ns, and NVT simulation for 40 ns using a 1.6 nm cut-off length and PME method, are provided. Additionally, the input file used for Packmol to insert the R_{in} = 2.8 nm bubble is also included. Further, all the Gromacs and Packmol files required can be downloaded from GitHub.[2,3]

Topology file for TIP4P/2005 water model with 38660 water molecules

```
[ defaults ]
; nbfunc comb-rule          gen-pairs            fudgeLJ fudgeQQ
  1                 2                    no                  1.0        1.0
[atomtypes]
;name     mass      charge   ptype    sigma       epsilon
IW     0          0.000       D   0.0          0.0
OWT4   15.9994       0.000       A   0.31589      0.77490
HW      1.0079       0.000       A   0.00000E+00   0.00000E+00

[moleculetype]
; name nrexcl
water  1

[atoms]
; nr type resnr residu atom cgnr charge
1     OWT4 1     water  OW1  1     0       15.9994
2     HW   1     water  HW2  1     0.5564    1.0079
3     HW   1     water  HW3  1     0.5564    1.0079
4     IW   1     water  MW4  1    -1.1128    0.0

[constraints]
;i j funct doh  dhh
1       2       1       0.09572
1       3       1       0.09572
2       3       1       0.15139

[exclusions]
1       2       3       4
2       1       3       4
3       1       2       4
4       1       2       3

; The position of the dummy is computed as follows:
;
;                     O
;
;                     D
;
;           H                   H
;
; const = distance (OD) / [ cos (angle(DOH))             * distance (OH) ]
;             0.01546 nm       / [ cos (52.26 deg)             * 0.09572 nm       ]

; Dummy pos x4 = x1 + a*(x2-x1) + b*(x3-x1)

[dummies3]
; Dummy from                          funct      a                    b
4       1       2       3       1       0.13193828      0.13193828

[system]
```

water tip4p/2005
[molecules]
water 38660

em.mdp file used in energy minimization

```
; minim.mdp - used as input into grompp to generate em.tpr
; Parameters describing what to do, when to stop and what to save
integrator  = steep         ; Algorithm (steep = steepest descent minimization)
emtol       = 1000.0        ; Stop minimization when the maximum force < 1000.0 kJ/mol/nm
emstep      = 0.01          ; Minimization step size
nsteps      = 50000         ; Maximum number of (minimization) steps to perform

; Parameters describing how to find the neighbors of each atom and how to calculate the interactions
nstlist         = 1         ; Frequency to update the neighbor list and long range forces
cutoff-scheme   = Verlet    ; Buffered neighbor searching
ns_type         = grid      ; Method to determine neighbor list (simple, grid)
coulombtype     = PME       ; Treatment of long range electrostatic interactions
rcoulomb        = 1.0       ; Short-range electrostatic cut-off
rvdw            = 1.0       ; Short-range Van der Waals cut-off
pbc             = xyz       ; Periodic Boundary Conditions in all 3 dimensions
```

npt.mdp file used in NPT simulation for 1 ns

```
define          = -DPOSRES      ; npt
; Run parameters
integrator      = md            ; leap-frog integrator
nsteps          = 500000            ; 2 * 500000 = 1000 ps
dt              = 0.002         ; 2 fs
; Output control
nstxout         = 500           ; save coordinates every 1.0 ps
nstvout         = 500           ; save velocities every 1.0 ps
nstenergy       = 500           ; save energies every 1.0 ps
nstlog          = 500           ; update log file every 1.0 ps
; Bond parameters
continuation            = no            ; Restarting after NVT
constraint_algorithm    = lincs     ; holonomic constraints
constraints             = all-bonds ; all bonds (even heavy atom-H bonds) constrained
lincs_iter              = 1             ; accuracy of LINCS
lincs_order             = 4             ; also related to accuracy
; Neighborsearching
cutoff-scheme   = Verlet
ns_type             = grid              ; search neighboring grid cells
nstlist             = 10            ; 20 fs, largely irrelevant with Verlet scheme
rcoulomb            = 1.6               ; short-range electrostatic cutoff (in nm)
rvdw                = 1.6               ; short-range van der Waals cutoff (in nm)
; Electrostatics
coulombtype         = PME               ; Particle Mesh Ewald for long-range electrostatics
pme_order           = 4             ; cubic interpolation
fourierspacing  = 0.16          ; grid spacing for FFT
; Temperature coupling is on
tcoupl          = V-rescale             ; modified Berendsen thermostat
```

```
tc-grps        = system       ; two coupling groups - more accurate
tau_t          = 0.1          ; time constant, in ps
ref_t          = 298          ; reference temperature, one for each group, in K
; Pressure coupling is on
pcoupl              = Berendsen        ; Pressure coupling on in NPT
pcoupltype          = isotropic              ; uniform scaling of box vectors
tau_p               = 2.0                    ; time constant, in ps
ref_p               = 1.0                    ; reference pressure, in bar
compressibility     = 4.5e-5                 ; isothermal compressibility of water, bar^-1
refcoord_scaling    = com
; Periodic boundary conditions
pbc            = xyz          ; 3-D PBC
; Dispersion correction
DispCorr       = EnerPres     ; account for cut-off vdW scheme
; Velocity generation
gen_vel        = no           ; Velocity generation is off
```

nvt.mdp file used in NVT simulation for 40 ns using a 1.6 nm cut-off length method

```
title               = tip4p/2005 NVT equilibration
define              = -DPOSRES  ;
; Run parameters
integrator          = md       ; leap-frog integrator
nsteps              = 20000000     ; 2 * 200000 = 40000 ps
dt                  = 0.002    ; 2 fs
; Output control
nstxout             = 500      ; save coordinates every 1.0 ps
nstvout             = 500      ; save velocities every 1.0 ps
nstenergy           = 500      ; save energies every 1.0 ps
nstlog              = 500      ; update log file every 1.0 ps
; Bond parameters
continuation        = no       ; first dynamics run
constraint_algorithm    = lincs     ; holonomic constraints
constraints         = none
lincs_iter          = 1        ; accuracy of LINCS
lincs_order         = 4        ; also related to accuracy
; Nonbonded settings
cutoff-scheme       = Verlet    ; Buffered neighbor searching
ns_type             = grid     ; search neighboring grid cells
nstlist             = 10       ; 20 fs, largely irrelevant with Verlet
rcoulomb            = 1.6      ; short-range electrostatic cutoff (in nm)
rvdw                = 1.6      ; short-range van der Waals cutoff (in nm)
DispCorr            = EnerPres  ; account for cut-off vdW scheme
; Electrostatics
coulombtype         = PME      ; Particle Mesh Ewald for long-range electrostatics
pme_order           = 4        ; cubic interpolation
fourierspacing      = 0.16     ; grid spacing for FFT
; Temperature coupling is on
tcoupl              = Nose-Hoover
tc-grps             = System   ; two coupling groups - more accurate
tau_t               = 0.4            ; time constant, in ps
ref_t               = 298            ; reference temperature, one for each group, in K
; Pressure coupling is off
```

```
pcoupl              = no       ; no pressure coupling in NVT
; Periodic boundary conditions
pbc                 = xyz      ; 3-D PBC
```

nvt.mdp file used in NVT simulation for 40 ns using the PME method

```
title               = tip4p/2005 NVT equilibration
define              = -DPOSRES  ;
; Run parameters
integrator          = md       ; leap-frog integrator
nsteps              = 20000000     ; 2 * 200000 = 40000 ps
dt                  = 0.002    ; 2 fs
; Output control
nstxout             = 500      ; save coordinates every 1.0 ps
nstvout             = 500      ; save velocities every 1.0 ps
nstenergy           = 500      ; save energies every 1.0 ps
nstlog              = 500      ; update log file every 1.0 ps
; Bond parameters
continuation        = no       ; first dynamics run
constraint_algorithm    = lincs     ; holonomic constraints
constraints         = none
lincs_iter          = 1        ; accuracy of LINCS
lincs_order         = 4        ; also related to accuracy
; Nonbonded settings
cutoff-scheme       = Verlet    ; Buffered neighbor searching
ns_type             = grid     ; search neighboring grid cells
nstlist             = 10       ; 20 fs, largely irrelevant with Verlet
rcoulomb            = 1.2      ; short-range electrostatic cutoff (in nm)
rvdw                = 1.2      ; short-range van der Waals cutoff (in nm)
DispCorr            = No  ; account for cut-off vdW scheme
; Electrostatics
coulombtype         = PME      ; Particle Mesh Ewald for long-range electrostatics
pme_order           = 4        ; cubic interpolation
fourierspacing      = 0.12     ; grid spacing for FFT
;Van der Waals
vdwtype             = PME
ewald-rtol-lj       = 10e-5
; Temperature coupling is on
tcoupl              = Nose-Hoover
tc-grps             = System   ; two coupling groups - more accurate
tau_t               = 0.4          ; time constant, in ps
ref_t               = 298          ; reference temperature, one for each group, in K
; Pressure coupling is off
pcoupl              = no       ; no pressure coupling in NVT
; Periodic boundary conditions
pbc                 = xyz      ; 3-D PBC
```

Note that although we used a relaxation time (tau_t) of 0.4 ps in this study, it is recommended to use a larger tau_t (>2 ps) if there is no specific need for strong temperature coupling. The use of a smaller tau_t may cause artifacts during the simulation due to its strong coupling.

Packmol input file used for bubble insertion

```
#
# water
#
tolerance 2.0
filetype pdb
output C1_bubble.pdb  ⬅ name of the out-put fie we used

structure npt.pdb  ⬅ resulted configuration file from NPT simulation
  number 35600  ⬅ final water molecules in the system
  inside box 0. 0. 0. 105.0  105.0  105.0  ⬅ L of the system in x, y, and z direction in Å units
  outside sphere  105.0  105.0  105.0 28.0  ⬅ initial bubble radius
end structure
```

Note that although Gromacs and VMD software uses nanometers as the unit of lengths/distances, Packmol software uses Angstrom unit.

References

1. *Scaling in Density Introduction*. https://www.astro.princeton.edu/~dns/teachersguide/ScDensInt.html (accessed 2023-02-11).
2. *Gromacs · GitHub*. https://github.com/gromacs (accessed 2023-02-15).
3. *Packmol - Initial configurations for Molecular Dynamics*. https://m3g.github.io/packmol/ (accessed 2023-02-15).